ABSTRACT

Title of Document: FACTORS INFLUENCING SURFACE ATMOSPHERE EXCHANGE OF GASEOUS ELEMENTAL MERCURY IN WESTERN MARYLAND

Christopher Warren Moore,
Doctor of Philosophy, 2011

Directed By: Dr. Mark S. Castro
Program of Marine, Estuarine, and Environmental Science

The purpose of this study was to examine the dynamics of the surface – atmosphere exchange of gaseous elemental mercury (GEM) in western Maryland. The site studied was the Piney Reservoir Ambient Air Monitoring Station (PRAAMS) in Garrett County. I used several different techniques to quantify the exchange, including a soil pore air sampling system that I developed, dynamic flux chambers, and the modified Bowen ratio (MBR) technique. I found that GEM exchange dynamics vary widely from the small scale (< 1 m^2) of the flux chambers to the large scale of the MBR technique. When I scaled the flux chamber measurements up to the annual time scale, I predicted a net GEM emission of 2.0 to 5.3 $\mu g\ m^2\ yr^{-1}$ to the atmosphere from PRAAMS, while with the MBR technique I estimated a GEM deposition of 3.3 $\mu g\ m^2\ y^{-1}$. The differences in these estimates highlight the

difficulties with measuring the exchange of a substance that can be both deposited to and emitted from soils. It also shows how uncertain the current estimates of this exchange can be. On the other hand, I was able to quantify soil redox potential as an important driver of GEM fluxes and soil pore total gaseous mercury (TGM) concentrations. This had not been previously reported. I was also able to show the importance of soil organic matter (SOM) and soil pore TGM concentration gradients on the surface –atmosphere exchange of GEM. This work opens the door for other studies on the dynamics of GEM fluxes in all sites with background concentrations of GEM.

FACTORS INFLUENCING SURFACE ATMOSPHERE EXCHANGE OF GASEOUS ELEMENTAL MERCURY IN WESTERN MARYLAND

By

Christopher Warren Moore

Dissertation submitted to the Faculty of the Graduate School of the
University of Maryland, College Park, in partial fulfillment
of the requirements for the degree of
Doctor of Philosophy
2011

Advisory Committee:
Dr Mark Castro, Chair
Dr. Steven Brooks
Dr. Robert Gardner
Dr. Andrew Heyes
Dr. John Ondov
Dr. John Sherwell

Dedication

I would like to dedicate this work to my wonderful wife Michelle Flanary-Moore and my parents, Darrell and Terri Moore. They have given me the support to accomplish my dreams. I will never be able to thank them enough.

Acknowledgements

I would like to thank my committee for all of the support they have given me throughout the entire process. My advisor Mark Castro was instrumental in my completing this work. Without him, the work would not have been completed. Steve Brooks gave me invaluable field experience and sent to me locations such as Summit, Greenland and Guiyang, China, places that I will never forget. Bob Gardner had an unbelievable gift to make valuable informed suggestions on a project that was outside his area of expertise. Bob was also always there to offer his expertise and advice on any topic that I was unsure about. Andrew Heyes brought a unique, unequalled knowledge of biogeochemical cycling of many different constituents. It was that knowledge that led me to focus on soil redox potential, one of the more important findings of my work. John Sherwell was always there with advice and a vast knowledge of the mercury pollution problem as a whole and the difficulties facing regulators and funding agencies. John Ondov always brought fresh alternative ideas and perspectives to the project and for that I am grateful. It was John who suggested I look at the diffusion of mercury from soil pore air and from that the soil pore air TGM section of my dissertation was born. Thank you all!

Table of Contents

Dedication ii
Acknowledgements iii
Table of Contents iv
List of Tables vi
List of Figures vii
Chapter 1: Introduction 1
Chapter 2: A Simple and Accurate Method to Measure Total Gaseous Mercury Concentrations in Unsaturated Soils 4
2.1 Abstract 4
2.2 Introduction 5
2.3 Methods 6
2.3.1 Study Site 6
2.3.2 Equipment and Materials 7
2.3.3 Collection of Soil TGM Samples 12
2.4 Results and Discussion 14
2.4.1 Precision 14
2.4.2 Accuracy 16
2.4.3 Sample Collection Efficiency 18
2.5 Conclusions 18
Chapter 3: Total Gaseous Mercury Dynamics in Background Soils 20
3.1 Abstract 20
3.2 Introduction 20
3.3 Methods 24
3.3.1 Study Site 24
3.3.2 Soil Pore [TGM] 25
3.3.3 Soil Eh 26
3.3.4 Soil Temperature, Moisture, Bound Total Mercury, and Organic Matter 26
3.3.5 Statistical Procedures 27
3.4 Results and Discussion 28
3.4.1 Soil Pore Air [TGM] at All Depths 28
3.4.1 Soil Pore [TGM] at the Forest Oe – A Interface 31
Chapter 4: Factors Influencing Gaseous Mercury Fluxes in Background Soils of Western Maryland 35
4.1 Abstract 35
4.2 Introduction 36
4.3 Methods 39
4.3.1 Site Description 39
4.3.2 Soil GEM Fluxes 42
4.3.3 Soil Temperature and Moisture 44
4.3.4 Soil Eh 44
4.3.5 Soil Pore [TGM] 45
4.3.6 QA/QC 46

4.3.7 Statistical Procedures 47
4.4 Results and Discussion 47
4.4.1 Soil GEM flux 47
4.4.2 Predicted Annual GEM Flux 54
4.5 Conclusions 56
Chapter 5: Modified Bowen Ratio Fluxes of Gaseous Elemental Mercury in Western Maryland 58
5.1 Abstract 58
5.2 Introduction 59
5.3 Methods 61
5.3.1 Study Site 61
5.3.2 Modified Bowen Ratio 63
5.3.3 QA/QC 65
5.3.4 Flux Footprint 66
5.3.5 Statistical Analysis 67
5.4 Results and Discussion 68
5.4.1 GEM Flux Validation 68
5.4.2 GEM Fluxes 71
5.4.3 GEM Emission and Deposition 76
5.4.4 Comparison with other measurements at PRAAMS 79
5.5 Conclusions 81
Chapter 6: Conclusions 83
Appendix 1: Supporting Information for Chapter 3 88
Appendix 2: Soil Redox Probe Construction 92
Appendix 3: Soil Moisture Probe Calibration 103
Appendix 4: Total Mercury Inputs to PRAAMS 109
Bibliography 111

List of Tables

2.1……..17
2.2……..18
4.1……..48
4.2……..49
4.3……..50
5.1……..62
5.2……..66
5.3……..73
5.4……..77
A1.1……...89
A2.1…….101

List of Figures

1.1……..2
2.1……..8
2.2……..10
2.3……..13
2.4……..15
3.1……..29
3.2……..30
3.3……..32
4.1……..39
4.2……..48
4.3……..52
4.4……..53
5.1……..61
5.2……..70
5.3……..72
6.1……..85
A1.1……..90
A1.2……..90
A1.3……..91
A2.1……..93
A2.2……..93
A2.3……..95
A2.4……..96
A2.5……..96
A2.6……..97
A2.7……..97
A2.8……..98
A2.9……..99
A3.1……106
A3.2……106
A3.3……107
A3.4……107
A3.5……108
A3.6……108

Chapter 1: Introduction

High levels of mercury contamination in humans can harm the brain, heart, kidneys, lungs, and immune system of people of all ages. The toxicity of mercury has made all forms mercury a focus of research for many years. The primary anthropogenic source of mercury to the atmosphere is coal fired power plants. The emission of mercury from coal fired power plants has drawn the attention of the US EPA, which on March 16, 2011 introduced Mercury and Air Toxics Standards. Once the mercury enters the atmosphere it can move to soils and other surfaces, making its way to wetlands and sediments. Once in the wetlands and sediments the mercury can be methylated, then bioconcentrate as it moves up the aquatic food chain, and ultimately ending up in fish. Humans eat the fish and suffer the effects of mercury poisoning. We must understand how much mercury moves through the environment and what controls that movement to measure the benefits of regulations like the Mercury and Air Toxic Standards.

The focus of my research was on one compartment of the mercury biogeochemical cycle, the surface atmosphere exchange of gaseous elemental mercury (GEM). Atmospheric mercury consists of gaseous elemental mercury (GEM, Hg^0), gaseous oxidized mercury (GOM, Hg^{2+}), and fine (< 2.5 μm) particulate bound mercury (FPM) (Poissant et al., 2005; Schroeder and Munthe, 1998). GEM is the dominant form in the atmosphere, accounting for up to 98% of the atmospheric mercury burden. Several components of mercury deposition in western Maryland have been quantified by other studies (Figure 1.1). Since GEM is volatile, it can undergo a constant bi-directional movement between the surface and atmosphere.

This bi-directional movement of GEM means that the net exchange of GEM between the surface and atmosphere (emission or deposition?) is not known.

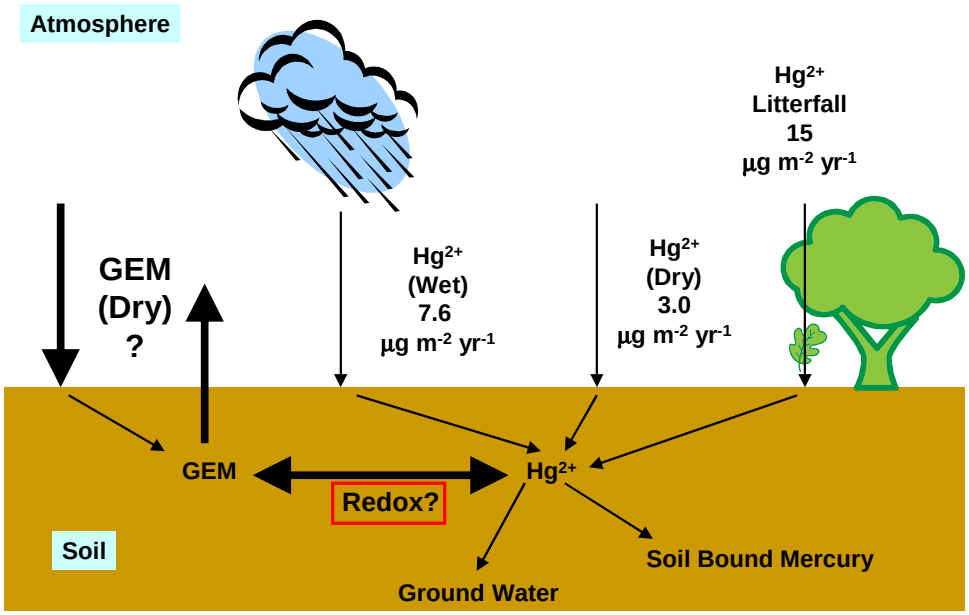

Figure 1.1. The surface atmosphere exchange of mercury in western Maryland. Several components of mercury deposition have been quantified by other projects. Several unknowns surrounding the controls and quantities of GEM surface atmosphere exchange were unknown before this study.

Another compartment of the mercury biogeochemical cycle that has rarely been studied but could be quite important to the surface atmosphere exchange is the pool of soil mercury contained in soil pore air. The size and controlling factors of this pool of mercury are not known. In particular, does soil redox potential (Eh) influence the dynamics of this pool of mercury (Figure 1.1)? The many uncertainties

with the surface atmosphere exchange and the soil pore air mercury pool prompted me to develop two main objectives for the study:

1) Determine if soil characteristics along an environmental gradient (forest vs. grass area) affect the soil GEM concentrations and atmospheric exchanges.

2) Identify atmospheric and ecosystem conditions that drive the exchange of gaseous elemental mercury between the atmosphere and soils at the Piney Reservoir Ambient Air Monitoring Station (PRAAMS).

The following chapters are arranged as four manuscripts that have been submitted for publication. Chapters 2, 3, and 4 address Objective 1. Chapter 2 focuses on the method development of a technique to measure soil pore total gaseous mercury (TGM) concentrations. This technique was used in Chapter 3 to evaluate the dynamics of the soil TGM pool in the forest and grass areas at the Piney Reservoir Ambient Air Monitoring Station (PRAAMS) in Garrett County, MD. The technique was also used in Chapter 4 along with dynamic flux chamber techniques to evaluate the fine scale ($< 1\ m^2$) surface atmosphere exchange of GEM in the two areas at PRAAMS.

Chapter 5 is focused on Objective 2. In this chapter I used micrometeorological techniques to measure the large scale (100s of meters) variation of the GEM fluxes at PRAAMS. Along with these fluxes I measured several other environmental parameters. I wanted to determine if any of the environmental parameters were influencing the larger scale GEM fluxes.

Chapter 2: A Simple and Accurate Method to Measure Total Gaseous Mercury Concentrations in Unsaturated Soils

2.1 Abstract

The goal of this project was to develop a method to measure the total gaseous mercury (TGM) concentrations in unsaturated soils. Existing methods did not allow for easy replication, were costly, and were more suited for other gases, such as CO_2, that do not react with collection surfaces. To overcome these problems, I developed a method that simultaneously collects up to ten soil pore air samples. I used a single mass flow controller, one pump, and two banks of rotameters to draw soil air out of the ground at 25 smL min^{-1} onto gold coated quartz traps. Analysis of the gold traps was performed with a Tekran 2500 CVAFS mercury detector. The system was field tested at the Piney Reservoir Ambient Air Monitoring Station (PRAAMS) in western Maryland. My system was relatively precise and accurate. For example, replicate TGM concentrations differed by less than 25% and recovery of known amounts of mercury were greater than 95%. Field measurements showed that the maximum soil pore air TGM concentrations, between 3 and 4 ng m^{-3}, occurred at the Oe - A soil horizon interface. At all other depths, the total mercury concentrations were lower than the ambient air concentrations of 1.8 ng m^{-3}. I believe my new method can be used to precisely and accurately measure the TGM concentrations in unsaturated soils at multiple locations simultaneously.

2.2 Introduction

Many uncertainties remain in our understanding of TGM exchanges between the atmosphere and background soils. For example, gaseous elemental mercury may be in a constant bi-directional flux between soils and the atmosphere, making it difficult to determine net deposition or emission at a site (Bash 2010; Dastoor and Larocque 2004; Cohen et al. 2004). Several factors, such as UV radiation, temperature, soil moisture and ozone concentrations have been shown to influence this flux (e.g. Moore and Carpi 2005; Ericksen et al. 2006; Engle et al. 2005) Another important factor that is likely to affect this flux is the TGM pool in background soils (Sigler and Lee 2006; Wallschläger et al. 2002; Johnson et al. 2003; Kromer et al. 1981). This TGM pool may ultimately control the emission of TGM to the atmosphere.

There have been a few studies that have examined the TGM concentrations in unsaturated soils (Sigler and Lee 2006; Wallschläger et al. 2002; Johnson et al. 2003; Kromer et al. 1981). These previous studies had several limitations caused by the measurement methods. Kromer et al. (1981) developed a stationary system that used an oven and a gold trap attached to a spectrometer. This early system had a high detection limit (200 ng m^{-3}) and did not allow multiple samples to be collected. Wallschläger et al. (2002) used a custom made stainless steel probe through which soil pore air was drawn out of the ground via a Tekran 2537A Mercury Vapor Analyzer at 1.5 L min^{-1}. Unfortunately, drawing soil pore air at a rate above 30 mL min^{-1} can cause ambient air to be introduced into the sample (Sigler and Lee 2006).

However, 30 mL min^{-1} is below the minimum flow rate (500 mL min^{-1}) of the Tekran 2537A.

Since soil pore air cannot be sampled directly by an automated Tekran 2537A analyzer, Johnson et al. (2003) and Sigler and Lee (2006) attempted to determine the TGM concentrations in a known volume. Johnson et al. (2003) withdrew 50 mL soil gas samples with gas-tight glass syringes. Sigler and Lee (2006) collected soil pore air in 1 L Teflon flasks. Total mercury concentrations in these syringes and flasks were determined using a Tekran 2537A. Some of the problems associated with these collection methods include: interaction with the walls of containment vessels (e.g. Carpi et al. 2007), leakage, inaccurate flow rate measurements, and lack of replication. Previous methods were also labor intensive and expensive. Most importantly, however, previous methods provide only a single un-replicated snapshot of the mercury concentration in the soil profile. There is clearly a need for improvements in our approaches to measure the TGM concentrations in soil air. Therefore, the goal of the current project was to develop and test a new method to quantify the TGM concentrations in background soils. In this paper, I describe a new method and present results from laboratory and field tests.

2.3 Methods

2.3.1 Study Site

Field measurements were made at PRAAMS in Garrett county Maryland. Atmospheric mercury measurements have been made at PRAAMS since 1997 and it is the measurement site for a suite of atmospheric chemistry and meteorological

parameters. Soils at PRAAMS are well drained Dekalb-Gilpin very stony loams with a depth to bedrock of 50 to 101 cm (USDA 2010). The ambient air monitoring equipment is located in a clearing, surrounded by deciduous forest.

2.3.2 Equipment and Materials

All materials in contact with the soil pore air sample were PFA Teflon and Pyrex. Soil gases were collected using a fluted Pyrex^{TM} glass funnel that had a top diameter of 100 mm and a 100 mm stem length (Fisher Scientific, Inc. Part Number: 10-329D). Each funnel was buried top down at each sampling depth (Figure 2.1).

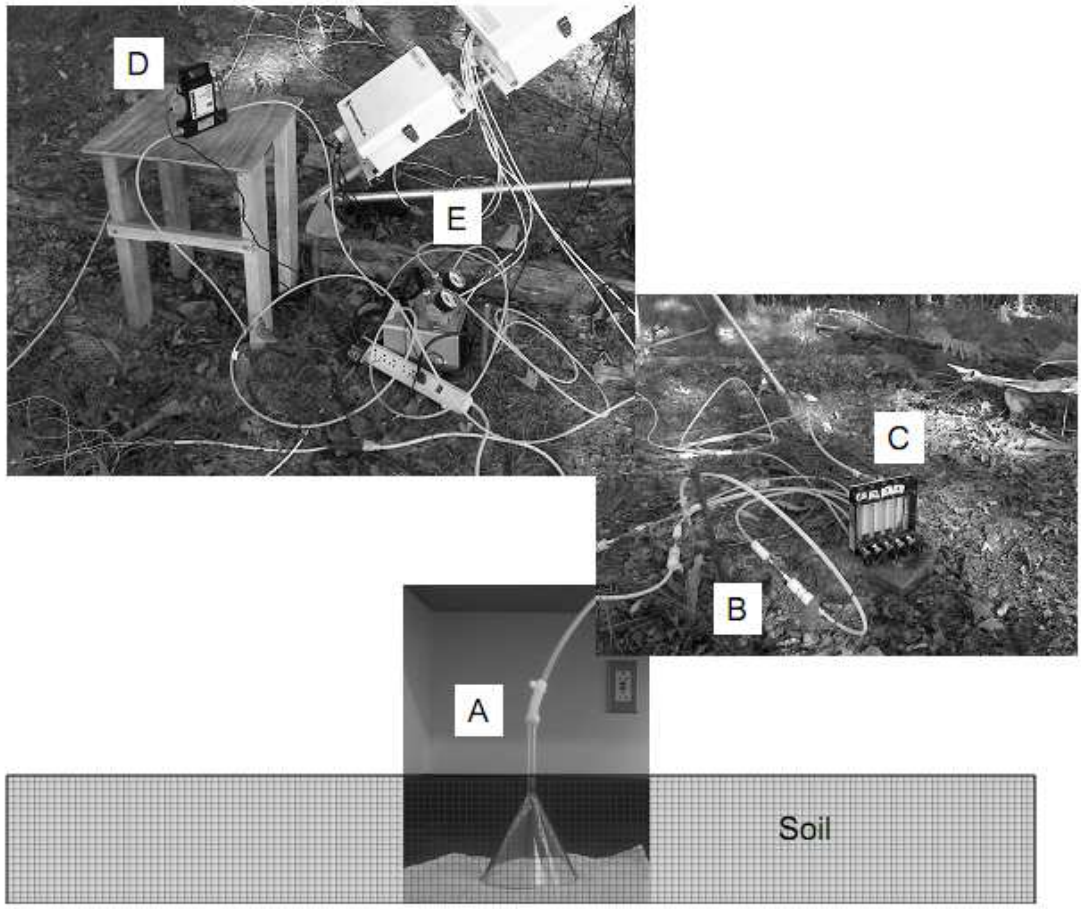

Figure 2.1. The soil TGM system. A is the 100 mm Pyrex glass funnel inverted in the ground. B is the gold quartz trap, C is a bank of rotameters, D is the gas flow controller, and E is the vacuum pump. The flow direction is A to E. A is connected to B with 1/4" Teflon tubing, the rest of the system is attached with 1/4" polyethylene tubing.

Attached to the glass stem was a 65 cm length of 1/4" O.D. x 1/8" ID Teflon tubing (Jensen Inert Products, TTH0108-063) that was custom fit to the stem of the funnel. Previous studies used Teflon funnels, which were expensive and structurally

weak. The preliminary test with Teflon funnels showed that they were crushed by the overlying soil. The Pyrex™ glass funnel was more rigid, could withstand the weight of the soil, could be acid cleaned prior to installation, and did not alter the TGM concentrations.

Precautions were taken to create air-tight seals in all sampling equipment. For example, the Teflon tubing was placed in a lathe and the last 5 cm was "shaved" to produce a custom fit for each funnel. To shave the Teflon, a stainless steel rod was inserted into each 65 cm length of tubing for rigidity. After the tubing was shave it was inserted into the funnel and rubber tubing was placed over the joint between glass stem and Teflon tubing. The rubber tubing was secured with cable ties (Figure 2.1). Ultra high purity argon was passed through the funnel and tubing to check for leaks and no leaks were found. In addition, each funnel and tubing assembly was attached to a Tekran 2537A to sample lab air (Figure 2.2).

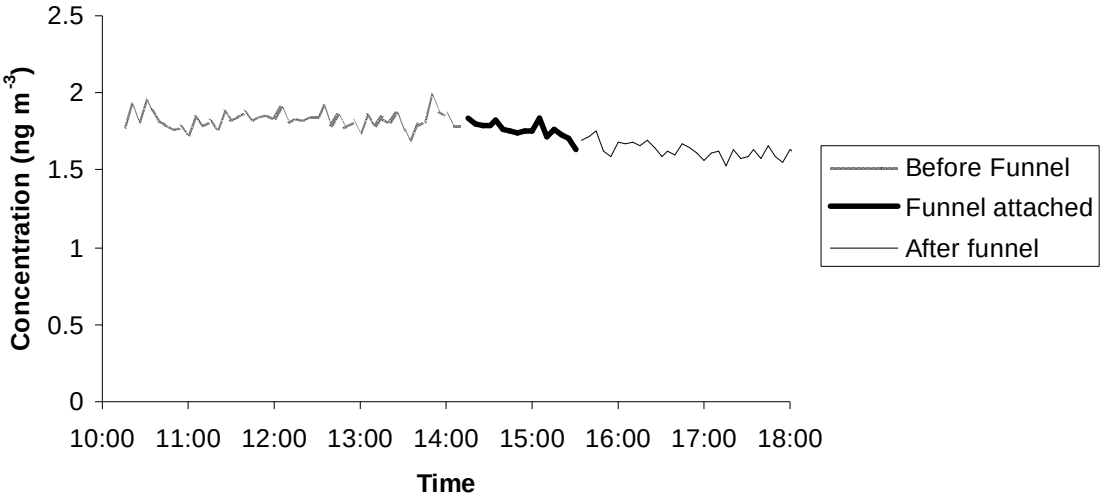

Figure 2.2. Concentrations in ambient lab air before, during, and after attaching a funnel to the 2537A. No difference could be seen between the period that the funnel and tubing assembly were attached and the period that they were not attached

Measured concentrations were not affected by the sampling system. Prior to deployment, all tubing and funnels were soaked for 8 hours in a 10% HCl bath, rinsed with D.I. water, dried in a particle free hood and then double bagged for transport to PRAAMS.

In early June 2009, one funnel was installed at each of four depths: Oe – A soil horizon interface (3 - 7 cm depth), the A - E soil horizon interface (9 – 15 cm depth), 5 cm into the E soil horizon (13 – 20 cm depth), and 10 cm into the E soil horizon (18 – 25 cm depth) in three sampling plots in the deciduous forest. Funnels were separated at least 20 cm laterally to minimize disturbance during installation and reduce the risk of depleting the TGM pool in the soil (Sigler and Lee 2006). Soil was

carefully removed with a small plastic trowel at a diameter slightly larger than the 100 mm funnel diameter to the specified soil depth. The area where the funnel contacted the soil was scraped until it was smooth. The funnel was then inserted top down and pressed to make a seal between the soil and funnel. The removed soil was then carefully placed back on top of the funnel, to attempt to preserve the pre-disturbance soil bulk density and soil horizons. The trowel was cleaned with deionized water and dried with a lint-free wipe between installations. After burial, the sampling system was allowed to equilibrate for several weeks before the September 2009 sampling.

Tekran Inc. gold coated quartz traps were used to collect TGM in the soil pore air (Figure 2.1). These gold traps had been used extensively to measure TGM in ambient air (Brosset 1987; Munthe et al. 2001; Keeler and Barres 1999) and water (USEPA 2002). The gold quartz traps collected all species of gaseous mercury in the sample stream. The gold traps were connected to the Teflon tubing (attached to the buried funnel) via a 1/4" PFA straight union compression fitting (Cole Parmer, R-31320-22). The downstream end of the trap was connected to polyethylene tubing (1/4" O.D. x 0.170" ID Lowes, Item: 15275), which was connected to the rest of the system using 1/4" nylon straight union compression fittings (Cole Parmer, R-06382-11).

Soil air was carefully and slowly (25 smL min^{-1}) drawn through each funnel using precise and accurate flow meters (± 0.125 smL min^{-1}). I used two banks of five rotameters, which allowed us to collect up to 10 samples simultaneously (Cole Parmer, frame: EW-03214-64, vials: R-32047-19, 50 mL min^{-1}, valves: R-03218-72).

Flow to the two banks of rotameters was controlled by a single Aalborg compact gas mass flow controller (Cole Parmer, R-32660-19). The vacuum pump (Gast Group, DOA-P104-AA) had regulators to adjust the flows, which allowed the flow controller and rotameter to be very stable (Figure 2.1). Polyethylene tubing was used downstream of the gold quartz traps, to connect the pump, gas flow controller, and rotameters. The two banks of rotameters were connected to the gas flow controller via a "T" compression fitting (Lowes, Item: 25184, Model: A-12). A single 47 mm diameter 0.2 µm filter was placed between the "T" fitting and the gas flow controller to prevent moisture from damaging the flow controller.

2.3.3 Collection of Soil TGM Samples

Upon arrival at the sampling plots, the mass flow controller was plugged in and allowed to equilibrate until the reading was 0.00 smL min^{-1}. At this point, the valve on the mass flow controller opened and I turned the pump on. For approximately one hour, ambient air was drawn through both banks of rotameters, without being attached to the sampling funnels. This allowed the system to equilibrate. After the hour, a Bios Definer 220 was used to set the flows for each of the outlets from the bank of rotameters at 25 smL min^{-1}. This flow rate corresponds to a calculated vertical wind speed across the sampling funnel of ~0.5 mm s^{-1} which would not disturb the soil gas profile (Fang and Moncrieff 1998; Sigler and Lee 2006).

Once the flows were stable at 25 smL min^{-1}, the rotameters were connected to the funnels in two plots (total of eight funnels) with a piece of polyethylene tubing in

place of the gold trap, and the funnels were flushed for 30 minutes. This allowed the 235 mL funnel volume to be flushed ~3 times. After 30 minutes, the short piece of polyethylene tubing was replaced with a gold quartz trap and sampled at 25 smL min^{-1}. All eight soil funnels were sampled simultaneously with ambient air. Once the samples were collected, the gold traps were placed in two Ziploc® bags and transported back to the laboratory for analysis the same day.

In the laboratory, I used a Tekran 2500 CVAFS to analyze each trap separately. Calibration of the 2500 was performed with a Tekran 2505 mercury vapor calibration unit and a digital syringe (Hamilton, Series 1700, 25µL) (Keeler and Barres 1999). The calibration curve was generated from three replicate injections of 5 µL, 10 µL, and 15 µL of mercury vapor. These volumes corresponded to ~43.5, ~87.0, and ~130.4 pg of TGM. Blanks were also incorporated into the calibration to form a four point calibration curve (Figure 2.3).

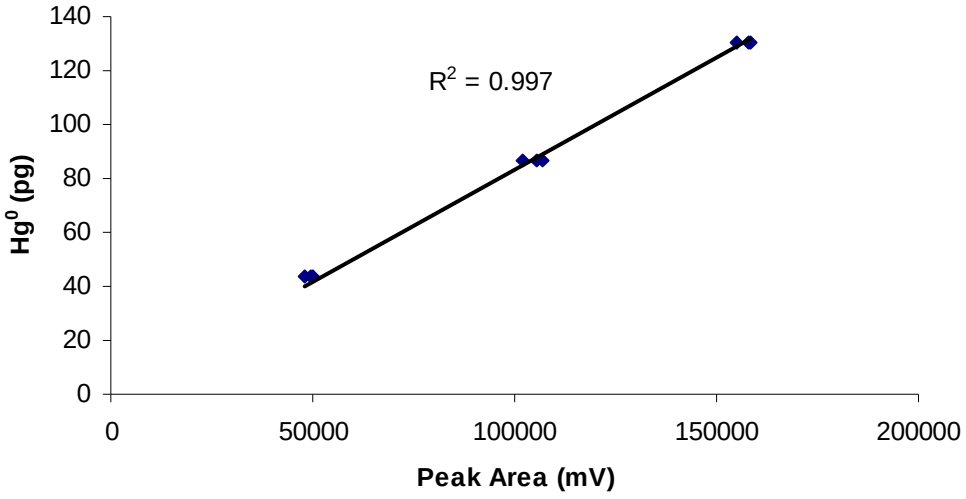

Figure 2.3. Example calibration curve from the 9/16/2009 sampling generated from three replicate injections of 43.5, 87.0, and 130.4 pg of TGM (n = 9).

The curve was forced through zero because the samples were lower than my lowest standard (Figure 2.3) (Keeler and Barres 1999). The analysis proceeded only if the r^2 of the calibration curve was >0.99. From the calibration curve, I could determine the mass of mercury released by the sample traps upon desorption. All samples analyzed (except blanks) were above the 0.1 pg detection limit of the Tekran 2500 (Tekran Corporation), which corresponded to a detection limit of 0.02 ng m^{-3}. Each sample trap was placed in a coiled nicrome wire heater and heated for 3 minutes in a stream of ultra-high purity argon (Keeler and Barres 1999). The TGM peak (which was the only peak seen in the samples) was released from the trap at ~2 minutes. Once the trap was analyzed, the concentration of TGM (C_{TGM}, ng m^{-3}) in soil pore air was determined with the equation:

$$C_{TGM} = \frac{m_{TGM}}{F * t_{sampled}}$$

where m_{TGM} is the mass (ng) of mercury on the gold trap, F is the flow rate (smL min^{-1}) through the gold trap, and $t_{sampled}$ is the sampling time (min).

2.4 Results and Discussion

2.4.1 Precision

To evaluate the precision of the soil gas TGM system, 9 traps were used to simultaneously sample ambient air. Flows through the traps were set at 25 smL min^{-1} and ambient air was sampled for three hours. The mean ambient air concentration was 1.79 ± 0.44 ng m^{-3} (C.V. 24.5%). This variation was slightly higher than the

~15% reported in Method IO-5 for manual sampling of ambient air (Keeler and Barres 1999). The higher variation may be from differences in the flows controlled by the rotameters and/or differences in the individual gold traps.

Field tests showed that the soil gas TGM system had a precision of better than 25% (Figure 2.4). For two days of sampling, I obtained two replicates per sampling

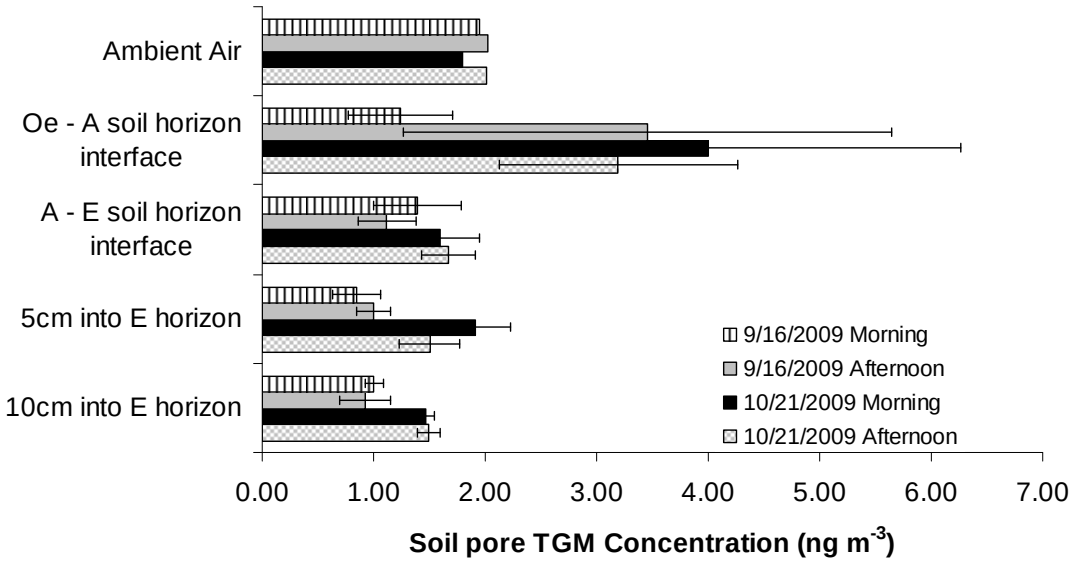

Figure 2.4. Soil pore TGM concentrations from four depths in September and October 2009. Each column represents the mean of two replicates with the error bars indicating one standard deviation above and below the mean.

depth for the four sampling periods. Concentrations ranged from 0.85 to 4.01 ng m^{-3}. Standard deviations ranged from 0.08 to 2.26 ng m^{-3}. The mean coefficient of variation for replicate samples was 24.8%, similar to that observed for the ambient air measurements. The highest concentrations (>3.0 ng m^{-3}) and largest coefficients of variation were at the Oe – A soil horizon interface (Figure 2.4). The Oe – A soil

horizon interface was in a constant exchange with the atmosphere, therefore was expected to be more variable than the lower depths (Sigler and Lee 2006). Lower coefficients of variation were obtained for all concentrations at the three deeper depths (Figure 2.4). The soil pore air mercury concentrations at deeper depths may not have been as heavily influenced by surface – atmosphere exchange and was expected to vary less than the Oe – A soil horizon interface. The lowest standard deviation at the deepest depth further demonstrated the precision of the measurement technique. Based on previous studies, soil TGM concentrations can vary by more than 1000%, between the deeper and upper layers of the soil profile (Sigler and Lee 2006). This indicates that the precision of the technique was well within the expected variation of soil TGM concentrations.

2.4.2 Accuracy

The accuracy of each gold coated quartz sand trap was determined by injecting each trap with the same amount of TGM (43.425 pg) generated by the Tekran 2505 mercury vapor calibration unit. I calibrated the Tekran 2500 mercury analyzer using independent mercury sources, specifically, water standards that were bubbled onto gold quartz traps as described in USEPA Method 1631 (USEPA 2002). The mean recovered amount of mercury for the twenty traps was 42.78 pg (C.V. 4.8%), with a mean percent difference (between injection amount and recovered amount) of 3.9% (Table 2.1). The largest difference was 8.7% which is substantially

Table 2.1. Recovery of injected amounts of mercury by the 20 gold coated quartz sand traps used in this study.

Trap	Hg^0 Injection (pg)	Hg^0 Recovered (pg)	Percent difference (%)
1	43.42	45.41	4.48
2	43.43	41.78	3.87
3	43.42	39.80	8.70
4	43.43	41.46	4.63
5	43.43	43.43	0.00
6	43.42	40.46	7.07
7	43.42	43.42	0.01
8	43.43	43.27	0.36
9	43.43	47.40	8.75
10	43.42	45.26	4.16
11	43.42	44.82	3.17
12	43.42	43.10	0.74
13	43.43	40.07	8.05
14	43.42	43.48	0.14
15	43.42	40.68	6.52
16	43.43	43.09	0.78
17	43.43	41.04	5.66
18	43.42	43.93	1.18
19	43.43	43.82	0.92
20	43.42	39.99	8.23

lower than the 15% variation reported in Keeler and Barres (1999), indicating better than expected accuracy for the gold traps. Therefore, I believe this technique can accurately measure TGM concentrations in unsaturated soils.

2.4.3 Sample Collection Efficiency

To verify the collection efficiency of the gold quartz traps, two traps were connected in sequence and ambient lab air was sampled for 3 to 6 hours. For the four samples, there was no detectable TGM on the second trap (Table 2.2). For the 6 hour sample, 24.3 pg of TGM was collected by the first trap without break through. Soil pore air samples had a mean of 6.95 pg of TGM and only one field sample collected more than 24.3 pg of TGM. Therefore, I am confident that the gold traps are 100% effective at collecting TGM in soil air.

Table 2.2. QA/QC test to verify that all mercury in the soils were collected by the gold quartz traps. TGM concentrations were below detection limits of 0.1 pg for every second trap in the back to back sampling train.

Sample Hours	3	4.5	5	6
pg of Hg on sample trap	12.2	13.9	14.6	24.3
pg of Hg on 2nd trap	BDL	BDL	BDL	BDL

2.5 Conclusions

My new system had several advantages and strengths. It allowed the sampling of multiple depths simultaneously, it was portable allowing movement between plots, it eliminated collection/container interaction problems, and it did not need to sample large volumes of soil gas. The system was relatively precise and accurate, could be used in a variety of weather conditions and had a low detection limit. However, the system had some weaknesses. The system worked only in

unsaturated soils. Trying to pump soil air from saturated soils would flood the gold traps with soil water, ruining the air samples and, possibly, the gold traps. During times of heavy rain, snow melt or saturated conditions, the system was not useful. Another weakness was the fragility of both the gold traps and the stems of the funnels. Since these were both made of glass they could be easily broken. Finally, the rotameters took time to calibrate initially but, when coupled with the gas flow controller, were stable throughout the sample collection.

Based on laboratory tests and field measurements, my new soil gas sampling system can be used to precisely and accurately measure TGM concentrations in unsaturated soils. The new system directly collects the TGM on gold quartz traps at low flow rates, which do not alter the soil gas profile. In addition, the system allows us to collect ten samples simultaneously, which are analyzed using a Tekran 2500 CVAFS. I am confident that the new system could be used to study the TGM pools and dynamics in unsaturated soils.

Chapter 3: Total Gaseous Mercury Dynamics in Background Soils

3.1 Abstract

The purpose of the study was to determine the effects of temperature, moisture, redox potential (Eh) and organic matter content on the total gaseous mercury concentrations ([TGM], $Hg^0 + Hg^{2+}$) in background soils. The measurements were made in a grass area and adjacent deciduous forest at the Piney Reservoir Ambient Air Monitoring Station (PRAAMS) in western Maryland. Three plots in each area were sampled at the Oe – A soil horizon interface, the A – E soil horizon interface, and 5 and 10 cm into the E soil horizon every third week from July 2009 to June 2010. Mean soil pore [TGM] over all depths in the forest (2.27 ± 2.20 ng m^{-3}) was significantly higher than the mean soil pore [TGM] in the grass area (1.52 ± 1.91 ng m^{-3}). The soil pore [TGM] was highest and most variable at the forest area Oe – A soil horizon interface (4.11 ± 2.04 ng m^{-3}), ranging from 1.5 to 8.36 ng m^{-3}. This soil horizon interface also had 11 to 26% more organic matter and the Eh was 100 to 400 mV lower than the other soil depths. These two factors were important because soil organic matter (SOM) can retain Hg^{2+} and act as an electron donor for the reduction of Hg^{2+} to Hg^0. The results suggest that soil Eh and SOM are significant factors in the retention and formation of TGM in background soils.

3.2 Introduction

The size and dynamics of the gaseous mercury pool in soils may influence the exchange of mercury between soils and the atmosphere (Johnson and Lindberg, 1995;

Moore et al., 2011b; Sigler and Lee, 2006; Zhang and Lindberg, 1999). For example, soils with [TGM] higher than ambient air may be a source of TGM to the atmosphere (Moore et al., 2011b; Sigler and Lee, 2006). Examining these soil gas mercury pools and dynamics is operationally and analytically challenging because sampling methods must not alter the natural soil gas profiles but must collect a large enough volume of soil air to obtain detectable concentrations. Typically [TGM] in background soils approach the limits of most analytical methods. To accurately quantify variations in soil pore TGM concentrations often requires the development of new equipment and methods (Johnson et al., 2003; Kromer et al., 1981; Moore et al., 2011a; Sigler and Lee, 2006; Wallschläger et al., 2002). Regardless of these measurement issues, a few studies have examined variations of soil pore [TGM] (Johnson et al., 2003; Johnson and Lindberg, 1995; Kromer et al., 1981; Sigler and Lee, 2006; Wallschläger et al., 2002). These studies have shown that [TGM] are influenced by soil temperature, soil moisture, and organic matter content (Johnson and Lindberg, 1995; Sigler and Lee, 2006). Other studies reported that soil Eh is an important factor influencing soil gaseous mercury dynamics (Obrist et al., 2010; Zhang and Lindberg, 1999) but soil Eh and soil [TGM] have not been quantified together.

Higher ambient soil temperatures can increase soil pore [TGM] by increasing the volatilization of gaseous elemental mercury (Hg^0) (Bahlmann and Ebinghaus, 2003; Carpi and Lindberg, 1998; Choi and Holsen, 2009a; Choi and Holsen, 2009b; Edwards et al., 2001; Ericksen et al., 2006; Gillis and Miller, 2000; Gustin et al., 2004; Gustin et al., 1997; Lin et al., 2010; Obrist et al., 2005; Scholtz et al., 2003; Sigler and Lee, 2006; Tsiros, 2002). At higher temperatures, more Hg^0 can be

volatilized into soil pore air and increase the [TGM] (Gabriel and Williamson, 2004). Hg^0 is only semi-volatile at ambient temperatures and the volatility is an exponential function of temperature (Sigler and Lee, 2006). Also at higher temperatures, it is possible that microbial activity is stimulated which can increase the reduction of Hg^{2+} to Hg^0 (Baldi, 1997; Fritsche et al., 2008a; Kritee et al., 2008).

Soil organic matter (SOM) has been shown to have a strong affinity for Hg^{2+} and forest soils with higher SOM content have higher amounts of total mercury bound to them (Akerblom et al., 2008; Andersson, 1979; Demers et al., 2007; Gabriel and Williamson, 2004; Grigal, 2003; Johansson et al., 1991; Meili, 1991; Obrist et al., 2009; Obrist et al., 2011; Sigler and Lee, 2006; Yin et al., 1997). The organic matter provides binding sites for Hg^{2+}, and the primary source of organic matter to forest soils is litterfall. The primary sources of Hg^{2+} to soils are direct wet and dry deposition and leaf litter decomposition. The various forms of Hg^{2+} deposition make it the form with the highest total deposition to soils and surfaces. Due to the relatively high inputs of Hg^{2+} (compared with GEM exchange) and the high organic matter, the shallow soil layers, such as the Oi and Oe horizons, can play an important role in the sequestration and release of Hg^{2+} (Obrist et al., 2011). In turn, the high Hg^{2+} that is bound to SOM may increase soil pore [TGM] if reduced to Hg^0 by changing soil Eh conditions that causes the release of the Hg^{2+} from the binding sites in the SOM (Andersson, 1979; Skogerboe and Wilson, 1981).

Soil Eh can affect soil [TGM] by affecting the availability of electrons for the oxidation of Hg^{2+} to Hg^0 (Andersson, 1979; Gabriel and Williamson, 2004; Obrist et al., 2009; Schuster, 1991; Zhang and Lindberg, 1999). Under low soil Eh conditions,

the Hg^{2+} contained in SOM can be more readily reduced to Hg^0 (Andersson, 1979). This reduction can lead to higher [TGM] and emissions into the atmosphere. At higher Eh, Hg^0 can be oxidized to Hg^{2+} which can lower the soil pore [TGM] due to the stronger affinity of SOM to bind Hg^{2+} or the Hg^{2+} being dissolved in soil water (Andersson, 1979; Schuster, 1991).

Increases in soil moisture can cause movement of TGM between compartments of the mercury biogeochemical cycle. This effect may be indirect because soil moisture alters soil Eh, which can directly affect TGM dynamics in soils (Ponnamperum, 1972; Zarate-Valdez et al., 2006). Increases in soil water will often decrease soil Eh, which can increase the rate of reduction of Hg^{2+} to Hg^0 (Ponnamperum, 1972; Zarate-Valdez et al., 2006). Others have reported that the more polar water molecule out competes the mercury for binding sites and the mercury is subsequently released to the atmosphere (Gustin and Stamenkovic, 2005).

Despite the potential importance of the soil pore TGM pool in overall mercury cycling, no studies have simultaneously measured the combined and complimentary effects of soil Eh and soil moisture on soil pore [TGM]. Also, little information exists on the spatial and temporal dynamics of the soil pore TGM pool. Therefore, the purpose of this study was to determine the effects of temperature, moisture, redox potential (Eh) and organic matter content on the total gaseous mercury concentrations ([TGM]) in backgrounds soils.

3.3 Methods

3.3.1 Study Site

Measurements were made at PRAAMS in Garrett county Maryland (elevation: 781 m) (39°42'21.29"N, 79° 0'43.21"W). In 2004, the deciduous forest at PRAAMS was selectively harvested in order to establish a large open area for an atmospheric monitoring station. There is currently a suite of atmospheric trace gases, aerosols, and meteorological parameters measured at PRAAMS. Since this disturbance, PRAAMS has been mowed and small trees have been cut to keep the site open. A variety of native grasses, thorns, and flowers now cover the open area.(Moore et al., 2011b) For this study, I established three 3 m by 2m sampling plots in the open grass area and three in the adjacent intact deciduous forest stand.

Soils at PRAAMS were classified as a Dekalb and Gilpin very stony loam (USDA, 2009). The O horizon was the only soil depth that was considerably different between the two areas. The forest O horizon consisted of large sticks, rocks, decomposed and un-decomposed litter extending to a depth of 7 cm. In the grass area, the O horizon was shallower (4 cm) with fewer large sticks and rocks. The A horizon in the two areas was black and 6 to 10 cm thick. The E horizon in the two areas usually started at 10 cm below the surface and was light brown. Soil pH for all depths was significantly lower in the forest (3.99 ± 0.14) than the grass area (4.43 ± 0.17). In the forest area, the top 25 cm of soil had a mean bulk density of 0.83 g cm^3. The mean bulk density for the top 25cm of soil in the grass area was 1.01 g cm^{-3}. The mean bound total mercury concentration in the top 25 cm of soil in the forest area and grass area was 0.07 and 0.04 μg g^{-1}, respectively.

3.3.2 Soil Pore [TGM]

Soil pore [TGM] was measured every third week from July 2009 through June 2010 with my own system described in chapter 2 (Moore et al., 2011a). Samples were collected twice throughout the day (for 1.5 to 3 hours depending on weather). The measurements represent only the daytime periods. Diurnal and nighttime variation was not examined. I collected samples from inverted Pyrex glass installed at the Oe – A soil horizon interface (3 - 7 cm depth), the A - E soil horizon interface (9 – 15 cm depth), 5 cm into the E soil horizon (13 – 20 cm depth), and 10 cm into the E soil horizon (18 – 25 cm depth) in each plot (Appendix 1).

Mercury in soil pore air was collected directly onto gold coated quartz sand traps by pumping air out of the ground at 25 mL min^{-1}. This flow rate was used to eliminate entrainment of ambient air and to avoid creating an artificial soil pore [TGM] gradient (Fang and Moncrieff, 1998; Sigler and Lee, 2006). I determined the mass of total mercury collected on the traps (m_{Hg}) by thermally desorbing into a Tekran 2500 CVAFS mercury detector. All analyses except on 7/22/2009 in the grass area and 7/28/2009 in forest were performed on the day of sample collection. The detector was calibrated with a Tekran 2505 mercury vapor calibration unit and a digital syringe (1702RN, 25 µL, Hamilton Co.) (Moore et al., 2011a). The soil pore [TGM] was determined with the equation: [TGM] (ng m^{-3}) = m_{Hg} (ng) / Flow rate (m^3 min^{-1}) / time sampled (min).

3.3.3 Soil Eh

Soil Eh probes were constructed from 10 gauge copper and 0.5 mm 99.997% platinum wires (Appendix 2) (Moore et al., 2011b; Rabenhorst et al., 2009; van Bochove et al., 2002; Wafer et al., 2004). Initially, five Eh probes were deployed at the A – E soil horizon interface, 5 cm into the E soil horizon and 10 cm into the E soil horizon in all plots. The signal from these probes was compared to that from a Ag/AgCl half cell reference electrode (Rabenhorst et al., 2009). The probes were monitored every 10 minutes with a Campbell Scientific CR10X datalogger. After the 10/21/2009 sampling, I realized that the highest and most variable soil pore air [TGM] was at the Oe – A soil horizon interface. On 11/9/2009, I deployed 10 soil Eh probes at this interface. These 10 probes were deployed on the day of sampling, then removed and redeployed on the next sampling date. The Oe – A horizon probes were monitored with a separate CR10 datalogger and Ag/AgCl reference electrode. Soil Eh was not measured at the lower three depths in the forest area on 11/9/2009 due to datalogger problems. On 1/6/2010 in the forest and 1/9/2010 and 1/29/2010 in the grass area soil Eh was not measured to keep the reference electrode from freezing.

3.3.4 Soil Temperature, Moisture, Bound Total Mercury, and Organic Matter

Soil temperature and soil moisture was measured with 5 cm long Decagon Devices 5TE probes (Appendix 3) (Decagon Devices, Inc., Pullman, WA, USA). One sensor was installed at the Oe – A soil horizon interface, A – E soil horizon interface, and 5 and 10 cm into the E horizon in each plot for both areas.

To determine soil bound total mercury concentrations ([THg]) and SOM content, 0.5 kg soil samples were collected from each depth in each plot on 7/8/2010. Soil samples were collected within 2 m of the funnels, immediately after the soil gas sampling was completed for the year. SOM content was determined by the loss on ignition technique (LOI) (Nelson and Sommers, 1996). For soil bound total mercury determination, I measured 1 g sub-samples into 40 mL Teflon digestion vials. The sub-samples were digested in 10 mL of cold Aqua Regia followed by dilution (25 and 50 µL in 50 mL of DI water) and oxidation with BrCl (USEPA, 2002). The 50 mL sample was analyzed with USEPA Method 1631 on a Tekran 2600 Automated Total Mercury Analyzer (USEPA, 2002).

3.3.5 Statistical Procedures

Daily means of the 10 minute soil temperature, moisture, and Eh measurements at each depth were calculated only for the times that soil pore [TGM] samples were collected. All plots (N = 3) for each area were combined to calculate a single mean for each depth on each sampling day. A student's t-test was used to determine if differences existed between the early and late samplings within a day. An ANOVA was used to determine if differences existed among depths, plots, or seasons. All differences in means were deemed significant at the $\alpha = 0.05$ level. Also all means are reported with ± one standard deviation from the mean.

3.4 Results and Discussion

3.4.1 Soil Pore Air [TGM] at All Depths

Mean soil pore [TGM] for all depths was significantly (df = 184, t = -2.27, p = 0.003) higher in the forest (2.27 ± 2.20 ng m^{-3}) than in the grass area (1.52 ± 1.91 ng m^{-3}) (Figure 3.1). These concentrations were low compared to sites enriched with mercury but were in the range of other background soils (Appendix 1 Table A1.1). In the forest, mean soil pore [TGM] for all depths in summer (2.47 ± 2.37 ng m^{-3}) and spring (2.52 ± 2.68 ng m^{-3}) were significantly higher than fall (1.73 ± 1.08 ng m^{-3}) and winter (1.31 ± 1.06 ng m^{-3}). In the grass area, summer (1.84 ± 1.46 ng m^{-3}) and spring (1.63 ± 1.05 ng m^{-3}) were also significantly higher than fall (0.87 ± 2.37 ng m^{-3}) and winter (0.86 ± 0.57 ng m^{-3}). This seasonal variation was consistent with the variations throughout the year in a red maple, white pine, and oak forest sites at Coventry, Connecticut (Sigler and Lee, 2006). Collectively, these seasonal variations appear to be driven by seasonal variations in soil temperature (Figure 3.2). Higher summer and spring temperature may have increased the volatilization of Hg^0 from the soil matrix into the soil pore air or increased production of Hg^0 in these soils (Ericksen et al., 2006; Kim et al., 1995; Sigler and Lee, 2006).

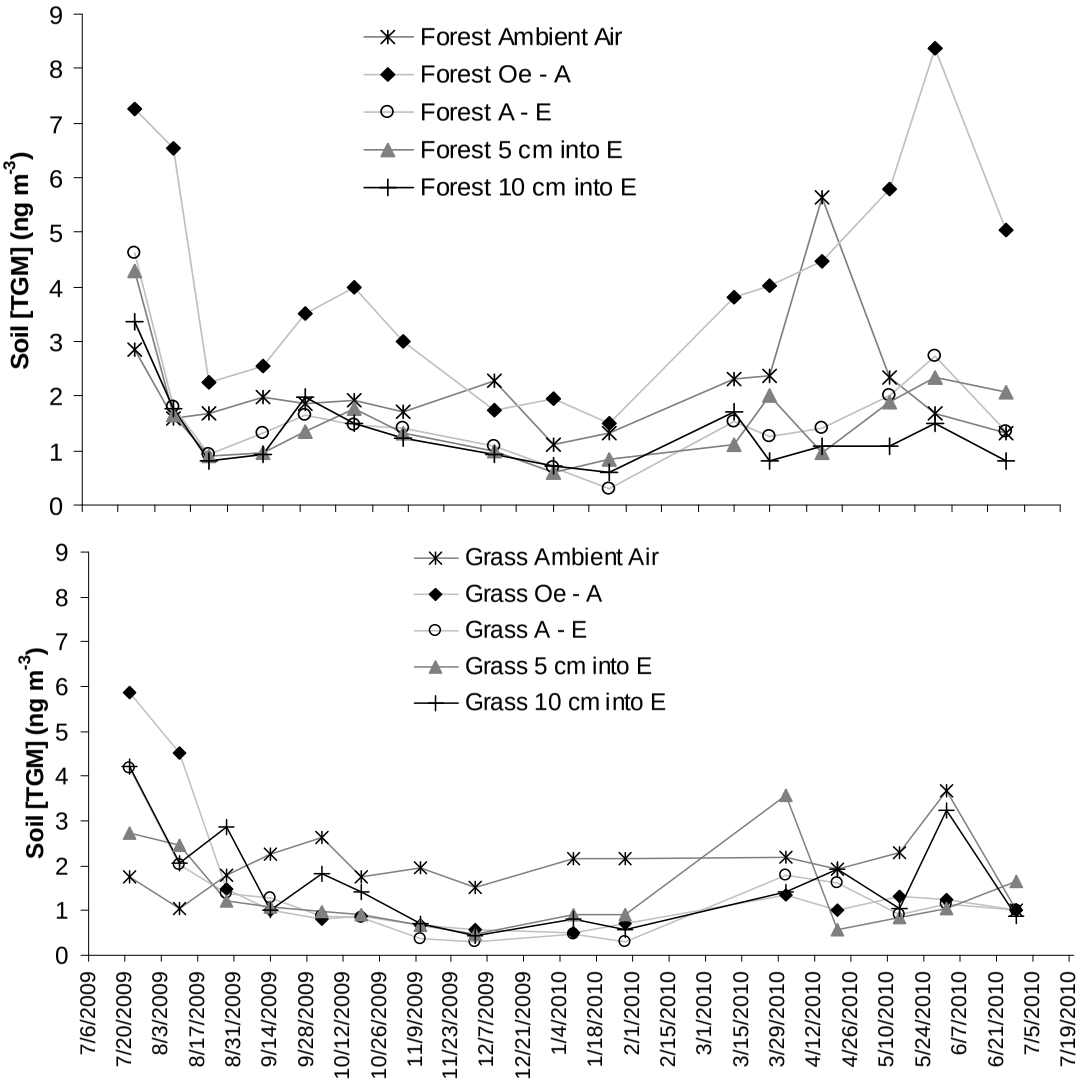

Figure 3.1. Mean daily soil pore [TGM] and ambient [TGM] at the Oe – A and A – E soil horizon interfaces and 5 and 10 cm into the E horizon in the forest (top) and grass (bottom) areas.

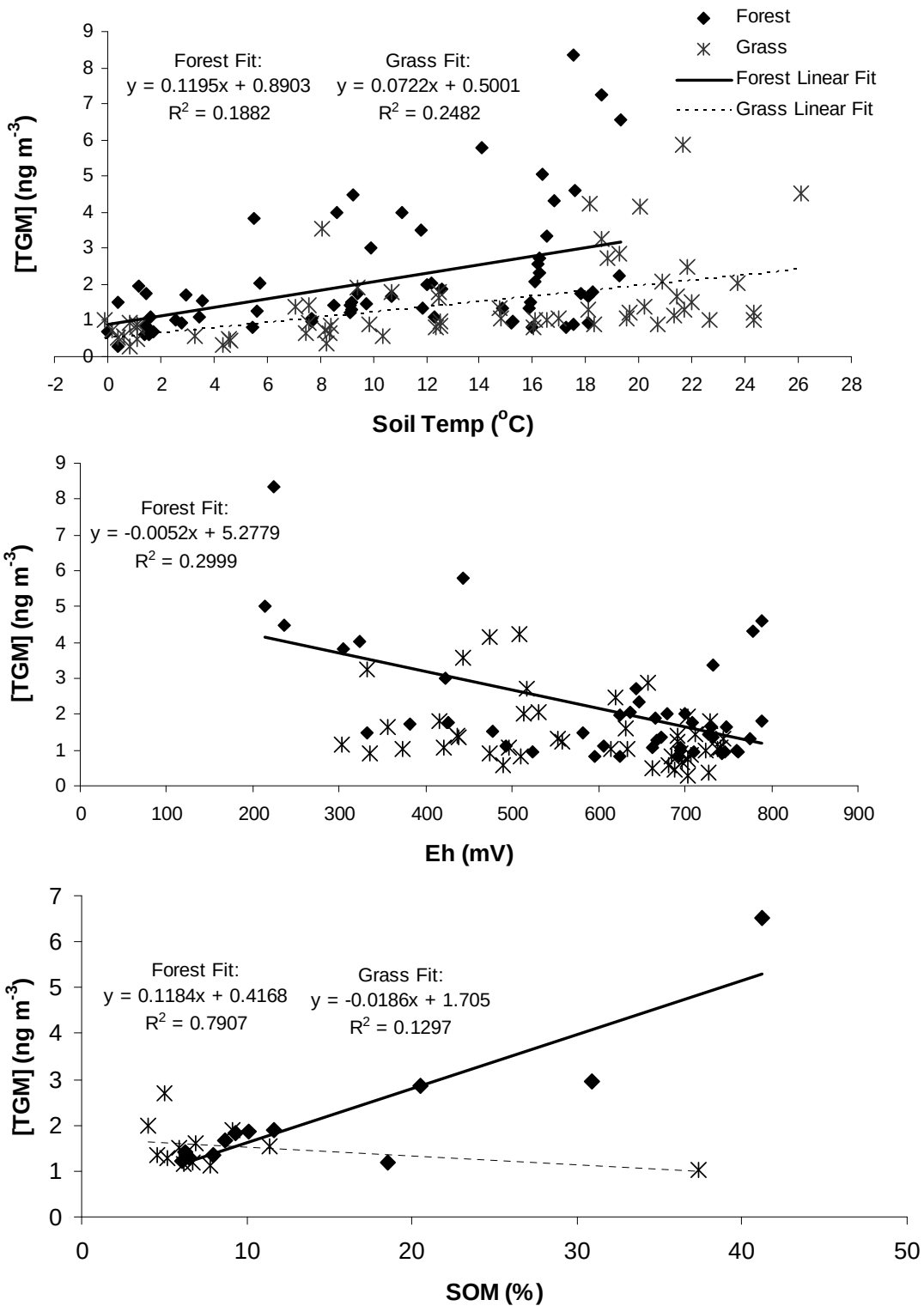

Figure 3.2. Soil pore air [TGM} vs. soil temperature (top), soil Eh (middle), and SOM (bottom) on soil pore air [TGM]. Each data point on the top and middle panels

represents a daily mean for each plot. The bottom panel shows soil pore [TGM] means at each depth in each plot vs. the mean soil organic matter content at that depth.

3.4.1 Soil Pore [TGM] at the Forest Oe – A Interface

Soil pore [TGM] at the forest Oe – A interface was significantly higher and more variable throughout the year than the other soil depths in either area (Figure 3.1). Soil temperature and moisture were not significantly different between this interface and the other soil layers. As a result, other factors were responsible for the distinct soil pore [TGM] dynamics at the Oe - A interface.

One of the parameters that were different at the Oe – A interface compared to the other depths was that soil Eh. Throughout the sampling period, soil Eh at the forest Oe – A interface remained at or below 400 mV, while the other depths in the forest area were above 400 mV (Figure 3.3). This was similar to one of the soils in Norrstrom (1994). Also during this period, soil moisture at the Oe – A interface was not correlated

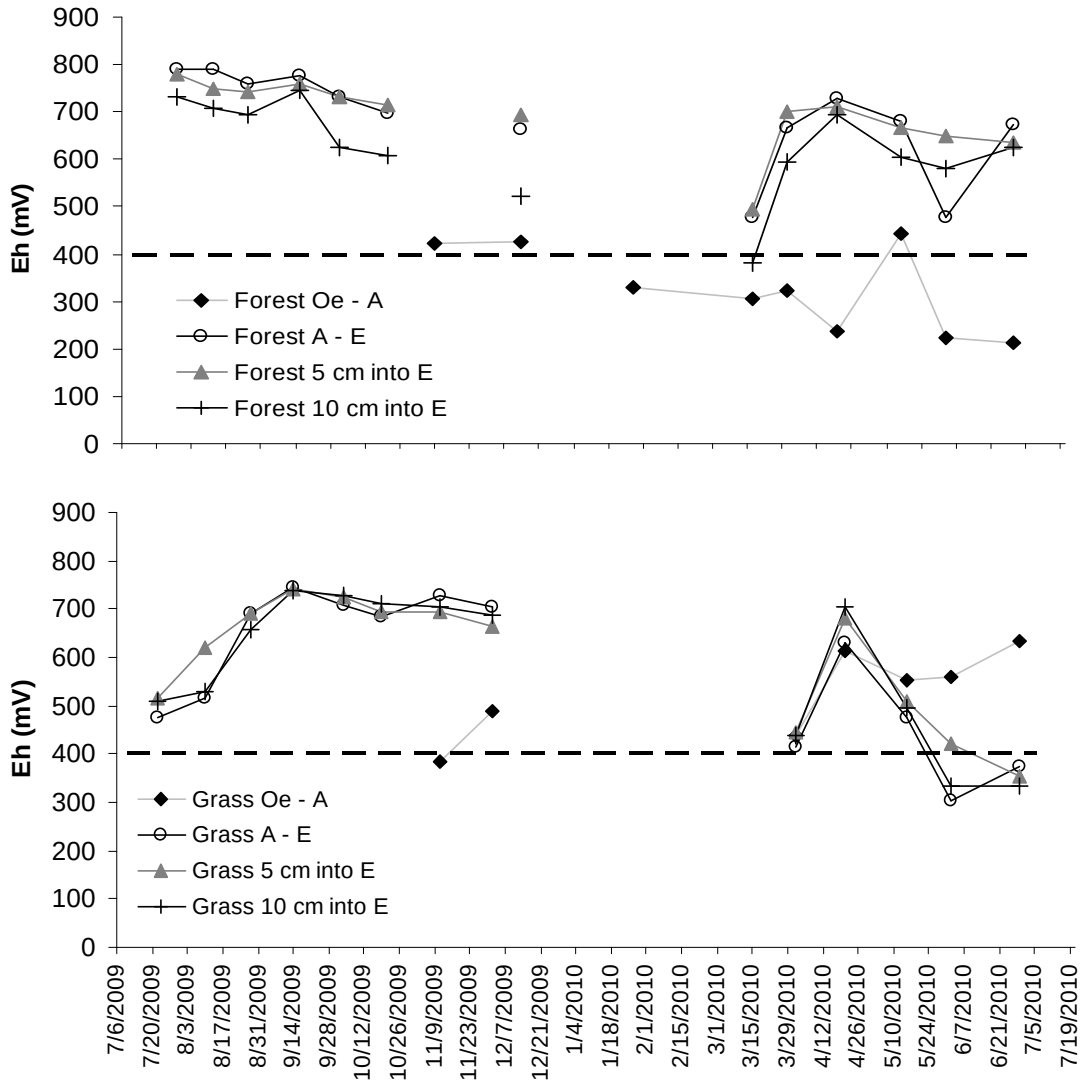

Figure 3.3. Mean soil Eh at the Oe – A and A – E soil horizon interfaces and 5 and 10 cm into the E horizon in the forest (top) and grass (bottom) areas during the times of soil pore air [TGM] sampling at PRAAMS. The dotted line on both panels indicates 400 mV.

with soil Eh or soil pore [TGM]. Due to this lack of correlation, I suspect that soil Eh was the main driver of soil pore [TGM] in this horizon. It appears that at a soil Eh below 400 mV, soil bound Hg^{2+} is reduced to Hg^{0}, which was volatilized into the soil

pore air. This was consistent with other soil studies who reported that below 400 mV and below a soil pH of 7, the most stable species of mercury was Hg^0 (Andersson, 1979; Schuster, 1991). While above a soil Eh of 400 mV and below a soil pH of 7, the most stable mercury species was Hg^{2+} (Andersson, 1979; Schuster, 1991). This transition was also evident in the grass area. When soil Eh dropped below 400 mV on 6/2/2010, the soil pore [TGM] at 10 cm into the E horizon rose to 3.24 ng m^{-3}, the highest at that depth for the entire measurement period (Figures 3.1 and 3.3).

SOM was also likely playing an important role in the TGM dynamics. Mean SOM at all depths in both areas, except the Oe – A soil horizon interfaces, was below 15%. At the Oe – A interface in the grass area, the mean SOM was 19.3 ± 15.7%, but was 30.9 ± 10.3% at the Oe – A interface in the forest. The higher SOM content in the forest could be explained by litterfall input from the overstory deciduous trees. Total mercury associated with litterfall was approximately 15 μg m^{-2} y^{-1}, twice the wet deposition input of mercury (NADP, 2010; USGS, 2010). This litterfall was the reason that the forest area Oe – A soil horizon interface had the highest SOM and highest soil matrix bound [THg] (Appendix 1 Figures A1.1 and A1.2). The increased mercury after litterfall was consistent with results from other studies (Andersson, 1979; Grigal, 2003; Meili, 1991; Obrist et al., 2009; Obrist et al., 2011). The lower soil matrix bound THg concentration at the other soil depths meant there was less Hg^{2+} available to be reduced to Hg^0. Based on these observations, I suggest that the upper soil horizons in forests with high litterfall inputs and low soil Eh are important sites for the formation of TGM.

Seasonal variations in soil pore [TGM] in both grass and forest were influenced by temperature. Soil [TGM] increased as soil temperature increased. One soil layer, the forest Oe – A soil horizon interface, had very different TGM dynamics. This layer consistently had a soil Eh below 400 mV, higher SOM content (30.9%) and elevated [TGM]. The results suggest that shallow soil surface layers in forests play an important role in mercury cycling in background soils at PRAAMS and may be important sources of mercury to the atmosphere.

Chapter 4: Factors Influencing Gaseous Mercury Fluxes in Background Soils of Western Maryland

4.1 Abstract

The purpose of the study was to examine the effects of soil temperature, moisture, redox potential (Eh) and pore air total gaseous mercury (TGM, $Hg^0 + Hg^{2+}$) dynamics on the surface – atmosphere exchange of gaseous elemental mercury (GEM) in western Maryland. I made the measurements in a deciduous forest stand and an adjacent cleared grass field. I quantified the GEM fluxes with dynamic flux chambers. The measurements were made every third week from July 2009 through June 2010. Mean GEM fluxes in the forest were -0.09 ± 0.37 ng m^{-2} h^{-1} in the summer, 0.38 ± 1.08 ng m^{-1} h^{-1} in the fall, 1.41 ± 1.48 ng m^{-2} h^{-1} in the winter and 1.02 ± 0.91 ng m^{-2} h^{-1} in the spring. Mean GEM fluxes in the grass area were -0.52 ± 1.53 ng m^{-2} h^{-1} in the summer, -0.22 ± 0.69m^{-2} h^{-1} in the fall, 0.67 ± 0.50 ng m^{-2} h^{-1} in the winter and 2.04 ± 1.03 ng m^{-2} h^{-1} in the spring. GEM fluxes were negatively correlated with soil temperature and soil Eh and positively correlated with soil moisture in the forest area. In the grass area, GEM fluxes were negatively correlated with soil Eh only and positively correlated with soil moisture. GEM fluxes in the forest area were also often in the opposite direction of the soil pore [TGM] concentration gradients between soil depths and ambient air. When I scaled the measurements to the annual time scale, I estimated a net daytime GEM flux of 2.0 to

5.3 µg m^{-2} y^{-1}. The results suggest that on the scale of flux chambers the soils at PRAAMS are net sources of mercury to the atmosphere.

4.2 Introduction

Surface - atmosphere cycling of GEM can be significant to the overall biogeochemical cycling of mercury at sites with background (low) soil mercury concentrations (Bash and Miller, 2009; Ericksen et al., 2006; Gustin and Jaffe, 2010; Gustin et al., 2006; Hartman et al., 2009; Kuiken et al., 2008). Quantifying the net GEM flux is a challenging task because of the bi-directional movement of the predominant atmospheric mercury species, gaseous elemental mercury (GEM, Hg^0) (Gustin and Jaffe, 2010; Lindberg et al., 2007; Poissant and Casimir, 1998). On the other hand, the other species of atmospheric mercury, gaseous oxidized (Hg^{2+}) and fine particulate bound mercury tend to be dry deposited and not re-emitted (Gustin and Jaffe, 2010 and references therein). Although several studies have examined GEM surface atmosphere exchange, an important aspect of the mercury biogeochemical cycle in background soils, few attempts have been made to measure in all seasons throughout the year..

Measurement and modeling studies for background areas suggest that soil temperature and soil moisture can be important factors influencing GEM fluxes (Bahlmann and Ebinghaus, 2003; Bash et al., 2004; Carpi and Lindberg, 1998; Choi and Holsen, 2009a; Choi and Holsen, 2009b; Edwards et al., 2001; Ericksen et al., 2006; Gillis and Miller, 2000; Gustin and Stamenkovic, 2005; Lindberg et al., 1999; Poissant et al., 2004; Scholtz et al., 2003; Song and Van Heyst, 2005; Zhang et al.,

2001). Soil Eh and the [TGM] (GEM + Hg^{2+}) in soil pore spaces are two other controls, which are thought to influence GEM fluxes. These two controls are not often measured in most field studies because they are difficult to accurately measure (Johnson et al., 2003; Obrist et al., 2010; Sigler and Lee, 2006; Zhang and Lindberg, 1999). Several studies have recommended that long term measurement campaigns are required to understand how these controlling factors change throughout the year (Choi and Holsen, 2009b; Gustin et al., 2006; Kuiken et al., 2008; Lin et al., 2010).

Increases in temperature are believed to increase the volatilization of gaseous elemental mercury (Bahlmann and Ebinghaus, 2003; Carpi and Lindberg, 1998; Choi and Holsen, 2009a; Choi and Holsen, 2009b; Edwards et al., 2001; Gillis and Miller, 2000; Gustin et al., 2006; Poissant et al., 2004; Zhang et al., 2001). This relationship has been shown to be an exponential Arrhenius type equation at ambient background temperatures with GEM flux increasing at higher temperatures (Bahlmann and Ebinghaus, 2003; Zhang et al., 2001). Higher temperatures can also increase microbial activity (Fritsche et al., 2008a; Obrist et al., 2010), which, in turn, may increase the reduction of Hg^{2+} to GEM (Baldi, 1997). Since the GEM is more volatile than the Hg^{2+}, this tends to also increase the GEM fluxes at higher ambient temperatures.

GEM fluxes have been shown to increase with increaseing soil moisture content (Ericksen et al., 2006; Gustin and Stamenkovic, 2005; Lin et al., 2010; Lindberg et al., 1999; Song and Van Heyst, 2005). However, changes in GEM fluxes with increasing soil moisture may caused by the associated decreases soil Eh (Ponnamperum, 1972; Zarate-Valdez et al., 2006). Another possibility is that the

more polar water molecules out competes the Hg^{2+} molecules for the soil binding sites (Gustin and Stamenkovic, 2005).

Soil Eh may cause the simultaneous reduction of Hg^{2+} and the oxidation of Hg^0 (Gabriel and Williamson, 2004; Johnson and Lindberg, 1995; Obrist et al., 2010; Zhang and Lindberg, 1999). Although the direct relationship between soil GEM fluxes and soil Eh has not been quantified, lower soil Eh conditions are expected to result in the reduction of more Hg^{2+} to Hg^0. This reduction can lead to the emission of Hg^0 into the atmosphere. At higher Eh, there is less reduction of Hg^{2+} leaving more Hg^{2+} that can more readily become bound to soil particles or dissolved in pore water. As a result, I would expect higher GEM emissions from soils with lower soil Eh (Zhang and Lindberg, 1999).

Soil pore air [TGM] may also be influencing GEM fluxes by affecting the [TGM] gradient between soils and the atmosphere (Johnson et al., 2003; Sigler and Lee, 2006; Wallschläger et al., 2002; Zhang and Lindberg, 1999). I know that soil pore [TGM] can be greater than the ambient air [TGM] (Sigler and Lee, 2006). The difference in concentration can create a diffusion gradient, which can promote the emission of GEM into the atmosphere. Thus, soil pore [TGM] dynamics are likely to be important drivers of the atmospheric GEM fluxes, but these dynamics have been rarely studied in background soils**.**

The purpose of the study was to increase our understanding of factors that influence soil-atmosphere GEM exchanges in background soils. In particular, I wanted to explore the possibility that soil Eh and soil pore [TGM] were important controllers of GEM fluxes. In addition, I wanted to determine the net annual daytime

flux of GEM for background soils in forests and grass areas, two land-cover classes that dominant the landscape of western Maryland.

4.3 Methods

4.3.1 Site Description

This study was conducted at the Piney Reservoir Ambient Air Monitoring Station (PRAAMS) in Garrett county Maryland (39°42'21.29"N, 79° 0'43.21"W) (Figure 4.1). PRAAMS is located on a relatively flat, high elevation ridge top (781 m) adjacent to the Piney Creek Reservoir. Measurements of mercury in wet

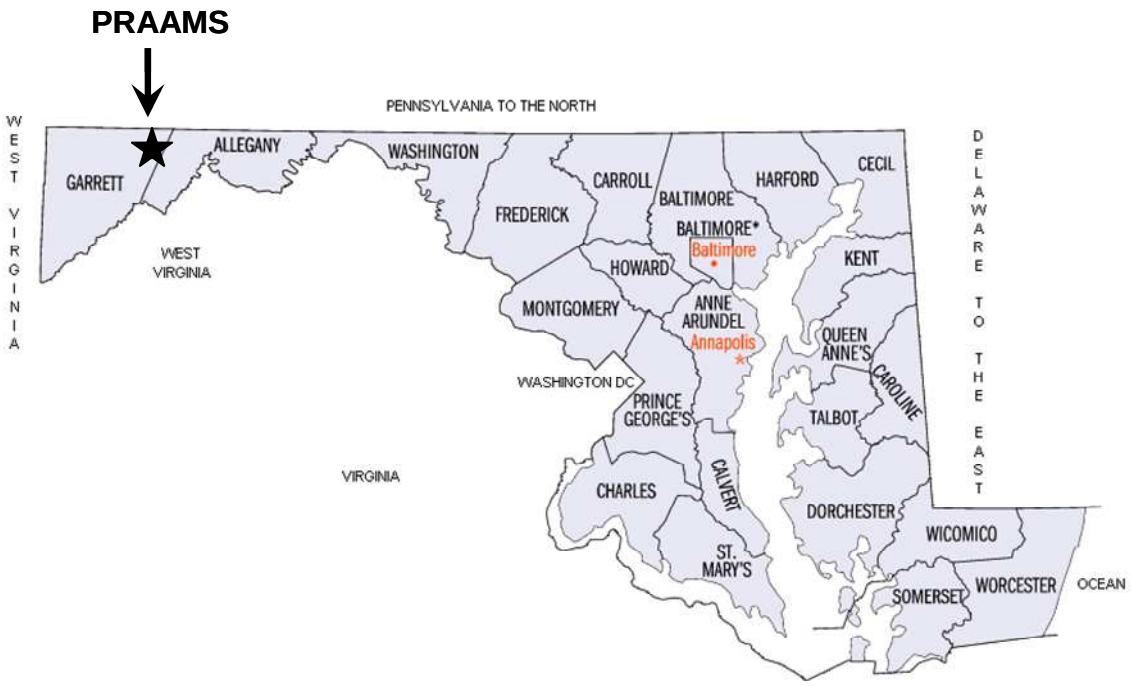

Figure 4.1. The location of PRAAMS within Maryland (http://www.censusfinder.com/mapmd.htm).

deposition were started here in 1997 (Mason et al., 2000). In 2004, the ridge top was cleared to expand the measurement program. A diverse suite of atmospheric gases, aerosols and meteorological parameters are now measured at the site. The cleared area has since re-established as a grass field with a mix of thorns (*Rubus spp.*), orchard grass (*Dactylis glomerata*), flowers (*Aster spp.*), Virginia creeper (*Parthenocissus quinquefolin*), black locust (*Robinia pseudoacacia*), and black cherry (*Prunis serotina*). This grass area is surrounded by deciduous forests dominated by Northern Red Oak (*Quercus rubra),* white oak (*Quercus alba),* sugar maple (*Acer saccharum),* and shag bark hickory (*Cayra laciniosa)* with an understory of marginal woodfern (*Dryopteris marginalis*) and christmas fern (*Polystichum acrostichoides*). PRAAMS is also the location of MD08, a monitoring station in the National Atmospheric Deposition Program National Trends Network, Mercury Deposition Network and Atmospheric Mercury Network. Annual wet deposition of total mercury measured in the open area at PRAAMS ranges between 5.5 and 10.2 $\mu g\ m^{-2}\ y^{-1}$ with a mean of 7.6 $\mu g\ m^{-2}\ y^{-1}$ from 2004 to 2009 (NADP, 2009).

Mean annual air temperature for the entire campaign was 8.5^{o}C, roughly equal to the long term (1972 – 2010) annual temperature of 8.8^{o}C (SERCC, 2010). For the measurement period, precipitation was 136.0 cm, the 5th highest since 1972 and snowfall was 260.9 cm, the 13th highest since 1972 (SERCC, 2010). PRAAMS was at least partially snow covered from 12/20/2009 to 3/25/2010. The snowpack melted twice. The first melt began on 1/16/2010 when soil temperatures increased to 1.5^{o}C during the day. As a result, this first melt occurred relatively slowly but most of the 20 cm snow pack had melted by 1/29/2010. The next snowfall of 70 cm occurred

from 2/5 to 2/7/2010. Snow then continued to fall in February, creating a 90 cm snow pack. This 90 cm snow pack started to melt on 3/7/2010. By 3/24/2010, all of the snow had melted at PRAAMS.

The measurements were made at three permanent study plots in both the cleared grass area and adjacent forest stand. I created the three 3 m by 2 m plots in each area in early June 2009. Soils in both areas had a mean total mercury concentration of 0.05 µg of mercury per g of soil (µg g^{-1}). According to Lindberg et al. (1999), background soils contain less than 0.5 µg g^{-1}. Soils were classified as Dekalb and Gilpin very stony loams (USDA, 2009). Depth to bedrock was 50 to 101 cm (USDA, 2009). The O horizon in the forest was 7 cm thick and 4 cm thick in the grass area. The forest O horizon contained large sticks, rocks, decomposed and undecomposed litter. In the grass area, the O horizon had fewer large sticks and rocks than the forest. The A horizon in both areas was 6 to 10 cm thick. The E horizon in both areas was light brown and usually started at least 10 cm below the surface. In the grass area, the mean soil pH over all depths was 4.43 ± 0.17. The mean soil pH for the forest was 3.99 ± 0.14 over all depths. Mean bulk density of the forest O horizon was 0.55 ± 0.12 g cm^{-3} and was 0.60 ± 0.14 g cm^{-3} in the grass area. Mean bulk density in the A horizons was 0.74 ± 0.15 g cm^{-3} in the forest and 1.08 ± 0.13 g cm^{-3} in the grass area. The highest mean bulk densities were in the E-horizon: 1.20 ± 0.16 g cm^{-3} in the forest and 1.32 ± 0.14 g cm^{-3} in the grass area. Mean loss on ignition (LOI) for all depths in was 15% ± 11% in the forest and was highest at the Oe – A soil horizon interface (31% ± 10%). Mean LOI for all depths in the grass area was 9% ± 9% and was also highest at the Oe – A soil horizon interface (19% ± 16%).

4.3.2 Soil GEM Fluxes

I measured GEM fluxes every third week from 7/22/2009 to 6/30/2010 with a 10.0 L (29 cm diameter) polycarbonate dynamic flux chamber. The chamber was attached to a Tekran 2537A (2537A) Mercury Vapor Analyzer. The 2537A had a 0.2 μm filter in the sample line that allowed only GEM to enter the analyzer. The 2537A was set up the day before sampling and allowed to sample ambient air overnight. The analyzer was calibrated immediately before sampling. Fluxes were measured only if the channels differed by less than 5%. The chamber was inert to Hg^0, had no memory effects and low blanks (Lindberg and Zhang, 2000; Southworth et al., 2007). Blank chamber tests were performed in the lab by sealing the bottom of the chamber with cleaned polyethylene. By sealing the bottom of the chamber it drew air only through the holes in the side through which ambient air is drawn during deployment on the soil. There was no significant difference between periods when lab air was sampled with clean Teflon tubing and periods when lab air was sampled with the flux chamber sealed with polyethylene. GEM fluxes and the soil pore air [TGM] were measured simultaneously in order to link the surface GEM fluxes to the soil TGM pools. However, the GEM fluxes were measured at least 1 m away from the pore [TGM] concentration measurements to avoid creating artificial gradients in [TGM] with the flux chamber.

Each sampling week consisted of two days of field measurements made during daylight hours. On day one of each sampling period, I measured the forested or grass plots then the next day I sampled the plots in the other area. For each

sampling period, I changed the sampling area and plot order to prevent time and temperature biases. On each sampling day, two plots were sampled in the morning for up to three hours. Each afternoon, one of the plots sampled in the morning was re-sampled along with the third plot. During the 1.5 to 3 hour soil gas samplings, our flux chamber was rotated between the two plots being sampled.

Several efforts were made to standardize the flux measurement technique. For instance, the 1.5 L min^{-1} flow of air being removed from the top of the chamber was controlled by the mass flow controller in the 2537A. I used polycarbonate chamber bases permanently driven into the ground to create an airtight fit between the soil and chamber. The bases also allowed us to sample the same location for the duration of the study. The chamber top was rotated between the bases in the two plots being sampled for soil pore air [TGM] every hour. Before the chamber was placed on a base in a new plot, it was positioned on its side for 20 min to sample ambient air directly through the chamber. Also to verify that there were no blank effects of the polycarbonate bases, the chamber was placed on a base that was sealed with of clean polyethylene once every sampling day.

After the initial 20 minute blanking period, the chamber was placed on a polycarbonate base and weighted down with 5 kg of rocks to assure an airtight fit. The chamber was left on the base for 30 to 45 minutes before rotating to the next plot. I calculated GEM flux with Equation 4.1:

$$F_{TGM} = Q \times \frac{(C_{out} - C_{in})}{A}$$

where Q was the air flow through the chamber (1.5 L min^{-1}) and C_{out} was the [GEM] of air being removed from the top of the chamber. C_{in} was the 20 minute mean

ambient air [GEM] immediately before the chamber was placed on the base, and A was the area of the surface covered by the chamber (660.5 cm^2). With this method I calculated a flux in ng m^{-2} h^{-1} for every 5 minute period that the chamber was on the base. I took the mean of all 5 minute fluxes to determine a mean daytime flux for each day sampled.

4.3.3 Soil Temperature and Moisture

I measured soil temperature and soil moisture with 5 cm long Decagon Devices 5TE soil moisture, soil temperature and electrical conductivity probes (Decagon Devices, Inc., Pullman, WA, USA). Temperature and electrical conductivity were factory calibrated for all soil types (Decagon Devices, Inc). For soil moisture, I calibrated the sensors for each depth at both sites using the procedures recommended by Decagon Devices, Inc. One sensor was installed at the Oe – A soil horizon interface, A – E soil horizon interface, and 5 and 10 cm into the E horizon in each plot of both areas. This made a total of 3 probes per depth in each area.

4.3.4 Soil Eh

I constructed soil Eh probes from 10 gauge copper and 0.5 mm 99.997% platinum wires (Rabenhorst et al., 2009; van Bochove et al., 2002; Wafer et al., 2004). I crimped the platinum wire into a small hole in the end of a 25 to 36 cm length of the copper wire. Epoxy was applied at the junction of the copper and platinum wires until the copper was completely covered and 5 mm of platinum wire was exposed. The epoxy was then covered with heat shrink tubing. Probes were

tested in Light solution (Light, 1972) then saturated quinhydrone solution before deployment. The probes varied by ± 1 mV in the heavily poised Light solution and by ± 20 mV in the less poised saturated quinhydrone solution. Five Eh probes were deployed at the A – E soil horizon interface (9 to 15 cm depths), 5 cm into the E soil horizon (13 to 20 cm depths) and 10 cm into the E soil horizon (18 to 25 cm depths) in each plot. This made a total of 15 Eh probes per depth in both the grass and forest areas. The probes were monitored continuously with a Campbell CR10X, a multiplexer and a single Ag/AgCl half cell reference electrode in each area (Rabenhorst et al., 2009). After the 10/21/2009 sampling, I determined that the highest soil pore air [TGM] was at the Oe – A soil horizon interface (3 – 7 cm depth). Beginning 11/9/2009, I deployed 10 soil Eh probes at this interface for each of the remaining sampling dates. These probes were deployed on the day of sampling, then removed and redeployed on the next sampling date. These probes were monitored with a separate CR10 datalogger and Ag/AgCl reference electrode. Soil Eh was not measured when temperatures were below 0^{o}C because the filling solution in the reference electrode would freeze.

4.3.5 Soil Pore [TGM]

I measured soil pore air [TGM] on the days that GEM fluxes were samples with a new system described in Moore et al. 2010. This system did not have a 0.2 μm Teflon filter to prevent other forms of mercury being collected by the gold trap. Therefore, it was reported as TGM. I collected the mercury in soil air by slowly passing the air through gold coated quartz sand traps. The traps were connected to

Pyrex® funnels permanently installed at the same depths as the soil temperature and soil moisture probes in each sampling plot. This made a total of three funnels per depth in each area. The funnels were installed eight weeks before measurements began. I used a single vacuum pump and mass flow controller to draw air from the funnels. Flow was equally distributed to the funnels using two banks of five rotameters. This technique allowed us to simultaneously collect samples from eight funnels and ambient air for three hour sampling periods. Soil pore air was sampled at 25 mL min^{-1} to prevent changes in the [TGM] gradients (Fang and Moncrieff, 1998). Gold traps were sealed, individually double bagged, and transported to the Appalachian Laboratory for analysis on the same day they were collected. Traps were thermally desorbed into a Tekran 2500 CVAFS mercury detector that had been calibrated using a Tekran 2505 mercury vapor calibration unit and three replicate injections each of 43.0, 87.5, and 130.4 pg of TGM. Analysis of gold traps proceeded only if the R^2 of the nine point calibration curve was greater than 0.99 (Moore et al., 2010).

4.3.6 QA/QC

Soil pore [TGM] concentrations were not significantly different between morning (1st sampling) and afternoon (2nd sampling) for either area. This allowed us to conclude that I was not altering soil [TGM] with the sampling technique. Also, the shallow Oe – A forest soil interface had significantly higher soil pore [TGM] concentrations than other layers. Therefore, I concluded that I had minimal entrainment of ambient air into the soil pore air samples.

4.3.7 Statistical Procedures

I used R Project (version: 2.10.1) to perform all statistical tests. I calculated daily means for soil temperature, moisture content, and Eh only during the times that GEM fluxes were measured on each sampling day. I used Welch's t-tests to determine differences in GEM flux between the forest and grass area. I used Pearson product moment correlations to evaluate relationships among soil GEM flux, soil temperatures, moisture content, Eh, and soil pore [TGM]. I used an ANOVA to test for seasonal differences. To determine pairwise differences among seasons for both areas, I used a Tukey's HSD test at the $\alpha = 0.05$ level. For the multiple linear regression (MLR) modeling I used the GEM flux, soil Eh, temperature, and soil moisture content data collected every ten minutes.

4.4 Results and Discussion

4.4.1 Soil GEM flux

GEM fluxes exhibited strong seasonal variation over the one year sampling period (Table 4.1). Both study areas had similar seasonal patterns, but the magnitude and direction of the fluxes were sometimes different (Figure 4.2). Depending on the

Table 4.1. Seasonal summary of GEM fluxes in the measurement areas at PRAAMS.

	Forest	Grass
Units	ng m^{-2} h^{-1}	ng m^{-2} hr^{-1}
Summer		
Mean	-0.09 ± 0.37	-0.52 ± 1.53
Max	2.27	3.17
Min	-1.00	-3.39
Fall		
Mean	0.38 ± 1.08	-0.22 ± 0.69
Max	4.31	1.33
Min	-2.55	-2.03
Winter		
Mean	1.41 ± 1.48	0.67 ±0.50
Max	6.36	1.90
Min	-0.13	0.08
Spring		
Mean	1.02 ± 0.91	2.04 ± 1.03
Max	3.56	4.16
Min	-0.32	-0.16

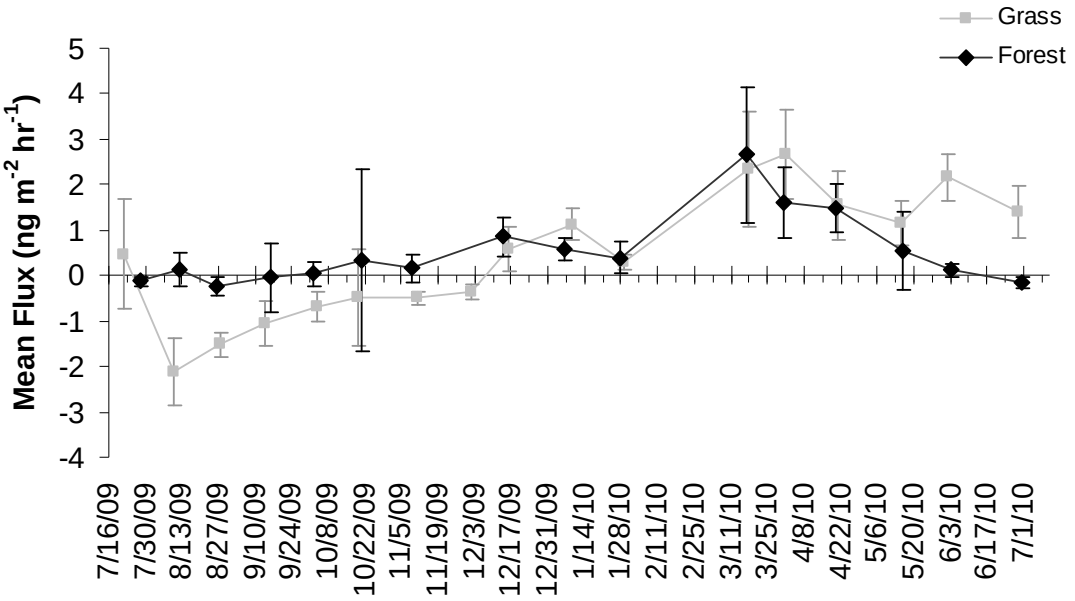

Figure 4.2. Mean daytime GEM flux for the measurement period. Error bars indicate one standard deviation from the mean.

season, soils could be strong sinks or sources of mercury. However, the mean GEM flux for both areas over the entire sampling period was not significantly different ($t = 0.28$, $df = 31$, $p = 0.78$) (Table 4.2). The annual mean fluxes were at the low end of

Table 4.2. Soil GEM fluxes at PRAAMS and other sites. NR indicates not reported values.

Mean TGM Flux (ng m^{-2} hr^{-1})	Max Flux (ng m^{-2} hr^{-1})	Min Flux (ng m^{-2} hr^{-1})	Time of Year	Ecosystem	Study
PRAAMS:					
0.53 ± 1.11	6.36	-2.55	All Seasons	Deciduous Forest	This Study
0.51 ± 1.53	4.16	-3.39	All Seasons	Grass Field	This Study
Other Studies:					
2.3 ± 0.95	3.7	0.6	June	Mixed Forest	Zhang et al. 2001
2.2 ± 5.2	43	-0.5	May - October	Mixed Forest	Sigler and Lee 2006
1.5 ± 0.18	3.8	-0.3	Summer	Mixed Forest	Ericksen et al. 2006
1.0	-1.4	3.8	July - August	Hemlock Forest	Boudala et al. 2000
1.55 ± 2.98	27.1	-2.49	Spring	Deciduous Forest	Choi and Holsen 2009
1.46 ± 1.06	5.26	-1.34	Summer	Deciduous Forest	Choi and Holsen 2009
0.82 ± 0.97	4.12	-1.92	Fall	Deciduous Forest	Choi and Holsen 2009
0.19 ± 0.95	1.94	-0.70	Winter	Deciduous Forest	Choi and Holsen 2009
7.6 ± 1.7	10.2	5	June	Open Grass Field	Zhang et al. 2001
2.95 ± 2.15	8.29	0.62	Summer	Open Grass Field	Poissant and Casimir 1998
1.9	-0.15	4.3	June	Open Grass Field	Boudala et al. 2000
1.4 ± 0.4	NR	NR	August	Open Grass Field	Schroeder et al. 1989
1.12 ± 0.10	9.7	-0.9	Summer	Grasslands	Ericksen et al. 2006

the 0.3 to 7.6 ng m^{-2} h^{-1} range of values reported in previous studies (Table 4.2). The findings were also consistent with previous studies that showed similar mean flux rates in forests and grasslands (Table 4.2).

Forest area mean soil temperatures at all depths during GEM flux sampling were significantly correlated with mean daily GEM fluxes (Table 4.3). As

Table 4.3. Correlations coefficients (r) between mean daily GEM flux and measured soil parameters at each depth.

Soil Depth	Temperature		Moisture		Eh		Pore [TGM]	
	r	p value	r	p value	r	p value	r	p value
Forest								
Oe - A interface	**-0.54**	0.0296	**0.56**	0.0249	-0.02	0.9571	-0.14	0.6126
A - E interface	**-0.65**	0.0082	**0.5**	0.0489	**-0.75**	0.005	-0.21	0.4445
5 cm into E horizon	**-0.65**	0.0069	0.48	0.0606	**-0.67**	0.0164	-0.25	0.3427
10 cm into E horizon	**-0.66**	0.005	0.49	0.0543	**-0.71**	0.0098	-0.12	0.6554
Grass								
Oe - A interface	0.13	0.6498	0.48	0.0733	0.59	0.1642	-0.21	0.4429
A - E interface	-0.11	0.7003	**0.62**	0.0141	**-0.69**	0.0096	0.04	0.8971
5 cm into E horizon	-0.18	0.5287	-0.21	0.4567	**-0.73**	0.0047	0.19	0.5072
10 cm into E horizon	-0.21	0.4501	**0.53**	0.0404	**-0.62**	0.0236	0.01	0.9579

temperature increased, GEM flux decreased. In the grass area GEM flux was not correlated with soil temperature at any depth (Table 4.3). Several other studies found that GEM fluxes increased as temperature increased (e.g. Bahlmann and Ebinghaus, 2003; Bash et al., 2004; Choi and Holsen, 2009a; Choi and Holsen, 2009b; Ericksen et al., 2006; Gillis and Miller, 2000; Gustin et al., 2006; Xiao et al., 1991; Zhang et al., 2001). The negative relationship in the forest was the opposite reported by other studies. This relationship in the forest and the lack of a significant relationship with temperature in the grass area indicated that other factors were driving the GEM fluxes at PRAAMS.

Forest daily mean GEM flux was correlated with daily mean soil moisture content at the Oe – A and A – E soil interfaces (Table 4.3). Grass area GEM flux was correlated with soil moisture at the A – E soil interface and 10 cm in the E horizon (Table 4.3). In both areas, GEM flux increased as soil moisture increased. This relationship was consistent with the findings of others (e.g. Bahlmann and Ebinghaus,

2003; Gustin et al., 2004; Gustin and Stamenkovic, 2005; Wallschlager et al., 2000). Since soil moisture and soil Eh were correlated at all depths except the Oe – A soil interface in both areas, this relationship could indicate that increased soil water indirectly affected the GEM flux by lowering the soil Eh.

In both areas, GEM flux increased as soil Eh at the A – E soil horizon interface and 5 and 10 cm into the E soil horizon decreased (Table 4.3). This pattern was consistent with the findings of others that in a simple soil system with an Eh above 400 mV and a pH below 7, the most stable form of mercury was $HgCl_2$ (Andersson, 1979; Schuster, 1991). Those studies also found that in soils below 400 mV and pH of 7, Hg^0 was the most stable mercury species (Andersson, 1979; Schuster, 1991). Since Hg^0 is more volatile than Hg^{2+} higher fluxes were expected at lower soil Eh values. In PRAAMS soils, the transition from sink to source occurred at 601 mV for the A – E soil horizon in the grass area rather than 400 mV (Figure 4.3). In the forest, where the soil Eh was higher, and inputs of mercury through

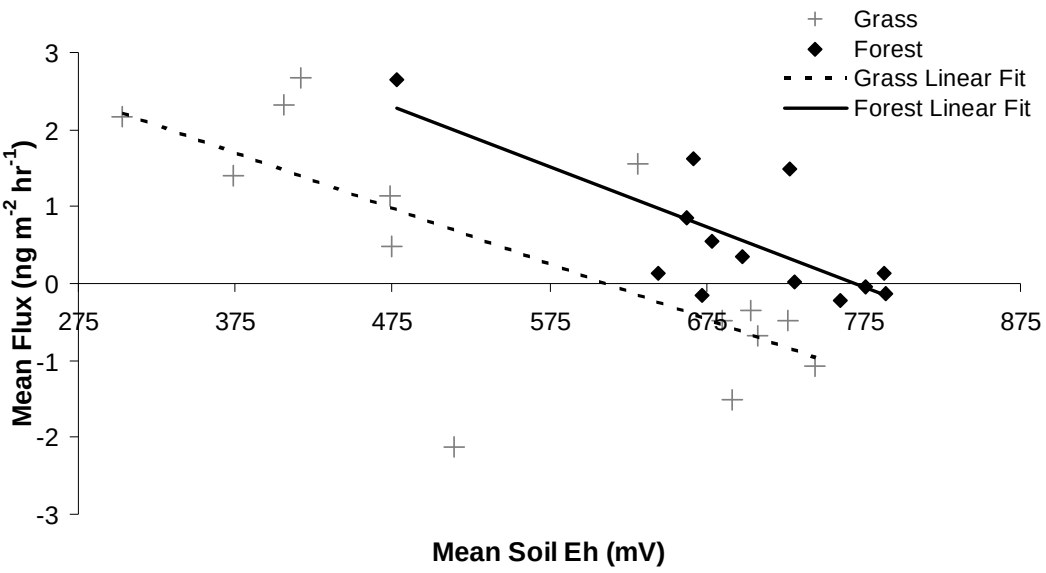

Figure 4.3. Mean daily GEM flux v. mean daily soil redox at the A – E soil horizon. The linear fit equation in the grass area was Flux = -0.0072*Soil Eh + 4.3873 (R^2 = 0.48) and Flux = -0.0078*Soil Eh + 6.0122 (R^2 = 0.56) in the forest area.

litterfall were different, the transition for A – E soil horizon occurred at 773 mV (Figure 4.3). At 5 cm into the E horizon the transition from source to sink occurred at 769 mV in the forest and 620 mV in the grass area. At 10 cm into the E horizon it occurred at 717 mV and 620 mV respectively.

GEM fluxes were not correlated with soil pore [TGM] at any depth. To determine the influence of soil pore [TGM], I examined the [TGM] gradients between soil depths and ambient air. To do this I subtracted the [TGM] at each soil depth from the ambient air concentration measured 2 cm above the surface with the soil pore air sampling system. I found significant negative relationships between the flux and [TGM] gradient for all depths in the forest area but not the grass area (Figure 4.4).

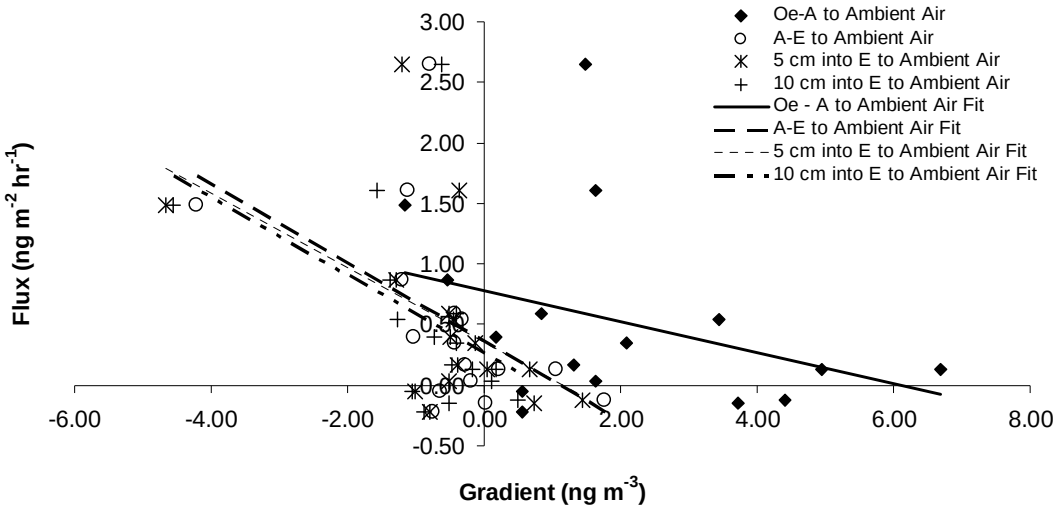

Figure 4.4. The GEM flux v. the change in [TGM] between the soil layers and ambient in the forest area. The linear relationships for the Oe – A interface to ambient air was GEM flux = -0.1272*Δ[TGM] + 0.776 (R^2 = 0.1189), for the A – E interface to ambient air was GEM flux = -0.326*Δ[TGM] + 0.3541 (R^2 = 0.2723), for 5 cm into the E horizon to ambient air was GEM flux = -0.3085*Δ[TGM] + 0.3527 (R^2 = 0.2673), and for 10 cm into the E horizon to ambient air was GEM flux = -0.3212*Δ[TGM] + 0.2593 (R^2 = 0.2202).

The negative relationships between the GEM flux and [TGM] concentration gradients could indicate that the different time scales of the two measurement techniques was limiting my ability to evaluate the relationship between soil pore [TGM] and GEM fluxes. The soil pore [TGM] may have been changing with the GEM flux throughout the day. However, I was not able to capture the short term

variation of soil pore [TGM] with my cumulative collection of TGM on the gold traps.

4.4.2 Predicted Annual GEM Flux

To estimate the net annual daytime GEM flux, I used the linear relationship between soil Eh at the A – E soil interface and GEM fluxes for both areas (Figure 4.3). I used soil Eh measurements at the A – E soil interface due to the lack of continuous measurements at the Oe – A soil interface. For days during the year that did not have soil Eh measurements, I used the relationship between soil moisture and soil Eh at the A – E interface to estimate hourly soil Eh values with equations 4.2 and 4.3:

$$Eh_{Forest} = -3.327SM_{Forest} + 813.6 \ : (R^2 = 0.38)$$

$$Eh_{Grass} = -7.423SM_{Grass} + 807.9 \quad (R^2 = 0.25)$$

Where Eh_{Forest} and Eh_{Grass} were the hourly soil Eh at the A – E soil interface in the forest and grass areas respectively. SM_{Forest} and SM_{Grass} were the hourly soil moisture contents at the A – E interface (% moisture) in the forest and grass areas, respectively. I then calculated hourly soil Eh values for the daylight hours of each day and used that data in the model to calculate hourly soil TGM fluxes for daytime periods. To get the net annual daytime flux I summed all hourly daytime fluxes for the year. With this approach, I estimated a net emission of 2.1 $\mu g\ m^{-2}\ y^{-1}$ from the forest soil and 2.0 $\mu g\ m^{-2}\ y^{-1}$ from the grass area.

I also used multiple linear regression (MLR) modeling for a second estimate of annual net GEM flux. The regression models were based on the daytime GEM

flux, soil temperature, moisture, and Eh measured every ten minutes on sampling days. The best (highest R^2) MLR model for the forest soils used soil Eh and soil temperature at the A – E soil interface. The MLR model explained 42.4% of the variation in the GEM fluxes. Soil moisture content was not statistically significant. In the grass area, the best MLR model contained soil Eh, soil temperature, and soil moisture content at the A – E soil interface. This model explained 39.7% of the variation in the GEM fluxes in the grass area. I estimated hourly soil Eh for periods when data was missing with Equations 4.2 and 4.3. For the forest area I used equation 4.4:

$$F_{TGM} = -0.0025Eh_{Forest} - 0.094T_{Forest} + 4.11$$

and for the grass area I used equation 4.5:

$$F_{TGM} = -0.0063Eh_{Grass} - 0.06T_{Grass} + 0.0005SM_{Grass} + 4.84$$

Where T_{Forest} and T_{grass} were the hourly temperatures at the A – E soil horizon in the forest and grass area, respectively. I used these relationships to calculate hourly mean GEM flux values for the daylight hours of each day. With this method, I predicted an annual GEM emission of 5.3 µg m^{-2} y^{-1} from the forest area and 3.3 µg m^{-2} y^{-1} from the grass area.

The net annual fluxes were likely biased high because they were estimated from daytime fluxes only. Several studies have shown that GEM fluxes exhibited a diurnal pattern with maximum emission during the day and low emission or deposition during the night (Bash and Miller, 2009; Edwards et al., 2001; Fritsche et al., 2008c; Gustin et al., 2006; Gustin et al., 2008; Kim et al., 1995; Zhang et al., 2008). The annual GEM emission results were similar to other estimates of emission

for PRAAMS. For example, Bash (2010) used the CMAQ-Hg model with a new bi-directional Hg^0 module and predicted a net flux of 20 ng m^{-2} day^{-1} in the region. When scaled up to the annual time frame this daily flux equaled an emission of 7.3 µg m^{-2} y^{-1}. Choi and Holsen (2009) used their soil GEM flux measurements and empirical models to estimate a net emission of 7.0 µg m^{-2} y^{-1} from soils in an Adirondack forest. Hartman et al. (2009) used a regression tree based model to estimate a 2 – 3 µg m^{-2} y^{-1} emission from soils in the region. Since the estimates were biased high, it was possible that all model estimates of GEM emission for the area were also too high.

4.5 Conclusions

My results highlight the uncertainties in our understanding of the surface atmosphere exchange of GEM in background soils. The interactions of factors influencing the fluxes under field conditions make it difficult to determine the dominant factor(s) controlling the net GEM fluxes. At PRAAMS, I found that soil GEM fluxes vary significantly throughout the year. The study points to the potential importance of soil Eh as a factor influencing the surface atmosphere exchange of GEM. However, before I can draw any concrete conclusions about the influence of soil pore [TGM] concentrations on GEM fluxes more, finer scale TGM gradient measurements above and below the soil – atmosphere interface may be needed. The study also found that model estimates of GEM emission from my site may be too high. My results suggest that more long-term measurements of GEM fluxes at

background soil sites are needed to further elucidate the exact mechanism by which soil Eh may be controlling GEM fluxes.

Chapter 5: Modified Bowen Ratio Fluxes of Gaseous Elemental Mercury in Western Maryland

5.1 Abstract

The purpose of this study was to increase our understanding of the atmospheric exchange of gaseous elemental mercury (GEM, Hg^0) for background soils with low mercury concentrations. I measured GEM fluxes using the modified Bowen ratio (MBR) technique from 7/6/2009 to 7/6/2010 at the Piney Reservoir Ambient Air Monitoring Station (PRAAMS) in western Maryland. Annual hourly mean GEM flux was -0.63 ± 31.0 ng m^{-2} h^{-1} and was not significantly different among seasons. Using filtered data, GEM fluxes were not strongly correlated with atmospheric trace gases, aerosols, or meteorological variables. Separating filtered data into emissions and deposition allowed us to better understand the factors influencing these atmospheric exchanges. Annual mean GEM emission was 15.3 ± 27.9 ng m^{-2} h^{-1} and the annual mean GEM deposition was -14.6 ± 26.6 ng m^{-2} h^{-1}. Factors significantly correlated with emission and deposition were solar ultraviolet-B radiation (UV-B), wind speed (WS), ozone concentrations and relative humidity (RH). UV-B and ozone could oxidize GEM to gaseous oxidized mercury (GOM) near the soil surface. Wind and turbulence could transport GEM to or from the surface. Over the entire filtered data, annual net GEM flux was -3.33 µg m^{-2} y^{-1}. This was similar in magnitude to estimates of GOM dry deposition (2.5 to 3.2 µg m^{-2} y^{-1}) at PRAAMS. Total dry deposition (GEM + GOM, 5.8 to 6.5 µg m^{-2} y^{-1}) was

slightly less than the mean wet deposition (8 µg m^{-2} y^{-1}) of total mercury. Wet and dry deposition combined was about equal to the litterfall mercury deposition (15 µg m^{-2} y^{-1}) to the forest floor within the flux tower footprint. As a result, total (wet, dry and litterfall) mercury deposition within the flux tower footprint was almost 30 µg m^{-2} yr^{-1}. Dry deposition of GEM accounted for 11% of the total mercury deposition.

5.2 Introduction

Surface - atmosphere exchange of GEM can be important to the overall biogeochemical cycling of mercury (Gustin and Jaffe, 2010; Gustin et al., 2008; Lindberg et al., 2007). Studying this exchange is often difficult due to the relatively small concentration gradients, low surface - atmosphere fluxes, and rapid changes in the direction of the flux. GEM, which comprises up to 98% of total atmospheric gaseous mercury, can be emitted from and deposited to soils (Gustin and Jaffe, 2010; Poissant et al., 2005). This bi-directional movement can happen quickly, with a site switching between being a source and a sink of GEM within a few hours (Bash and Miller, 2008; Converse et al., 2010). This important flux has been measured with flux chambers and micrometeorological techniques. However, few studies have measured this flux for an entire year (Baya and Van Heyst, 2010; Converse et al., 2010). Due to the high variability of GEM fluxes, it is necessary to make long-term measurements in order to determine the factors controlling these fluxes (Gustin and Jaffe, 2010).

Many environmental parameters have been shown to influence this surface – atmosphere GEM exchange. Some of these factors include UV-B radiation, wind

speed, and ozone concentrations (Choi and Holsen, 2009a; Engle et al., 2005; Gustin et al., 1997; Moore and Carpi, 2005; Zhang et al., 2008). UV-B radiation is thought to increase the photoreduction of Hg^{2+} (gaseous oxidized mercury, GOM) to GEM in the shallow soil layers (Choi and Holsen, 2009a; Moore and Carpi, 2005). This GEM is volatile and may be readily emitted to the atmosphere. Therefore, increased UV-B radiation may lead to increased GEM emissions. Higher wind speeds and turbulence near the soil surface have also been shown to increase the turbulent transfer of GEM, leading to higher exchange at higher wind speeds (Kim et al., 1995; Schluter, 2000). Ambient air ozone may increase GEM deposition in some environments or increase GEM emissions in others. For example in Polar Regions, atmospheric mercury depletion events are believed to be caused by oxidation of GEM to GOM by species such as ozone or bromine (Brooks et al., 2011; Hall, 1995; Schroeder et al., 1998; Steffen et al., 2008). However, in one lab study with soils amended with Hg^0 and Hg^{2+}, oxidizers such as ozone were shown to increase the reduction of GOM to GEM and increase the volatilization of GEM from soils (Engle et al., 2005). The variability of these factors, that control GEM fluxes, together contribute to the bi - directional nature of the atmospheric fluxes.

Due to the variability of GEM fluxes and limited field measurements, little is known about long-term variations and the importance of this flux in mercury biogeochemical cycling at background sites. How different factors influence these fluxes is also not known. Therefore, one goal of this study was to continuously measure GEM fluxes for one year at a background site (soil bound mercury concentration less than 0.5 $\mu g\ g^{-1}$) in western Maryland. The second goal was to put

the annual GEM flux into perspective with other annual mercury fluxes measured at the same site.

5.3 Methods

5.3.1 Study Site

GEM fluxes were measured semi – continuously from 7/6/2009 to 7/6/2010 at PRAAMS in Garrett county Maryland (39°42'21.29"N, 79° 0'43.21"W). PRAAMS is located on a relatively flat, high elevation ridge top (781 m) adjacent to the Piney Creek Reservoir (Figure 5.1). In 2004, the ridge top was cleared, and now a diverse suite of atmospheric trace gases, aerosols and meteorological parameters is measured (Table 5.1). For this study, I also measured soil redox, soil temperature, soil

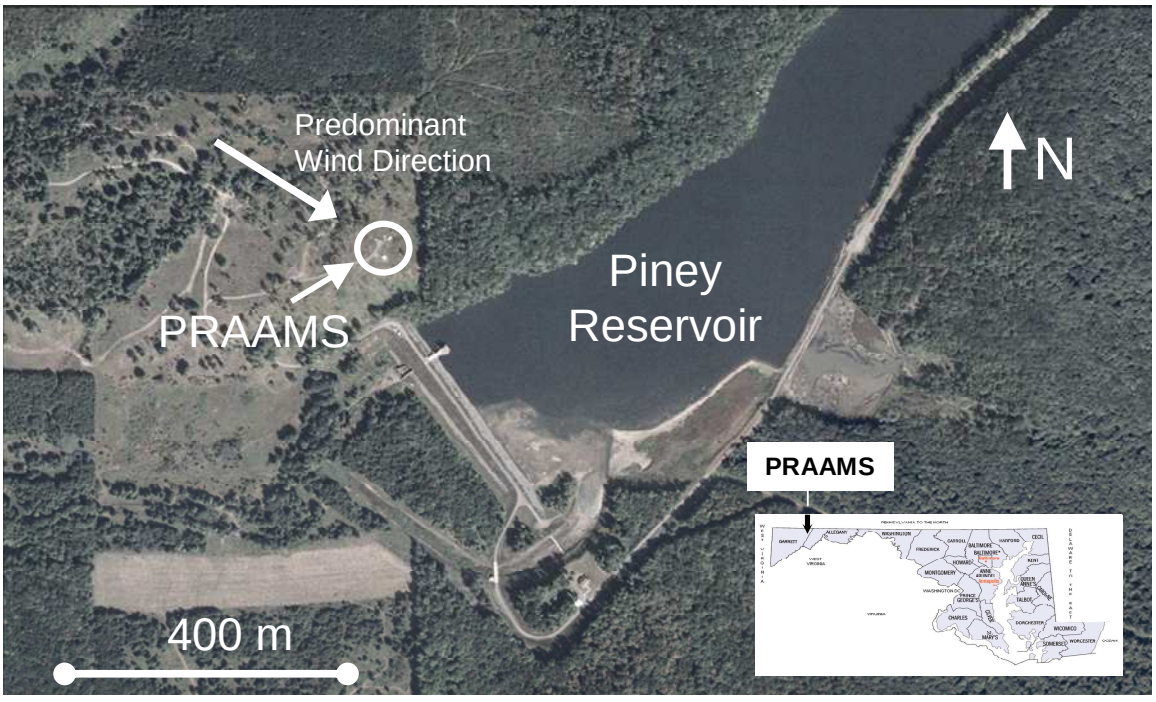

Figure 5.1. The Piney Reservoir Ambient Air Monitoring (PRAAMS) site.

Table 5.1. Means of each inlet during times of co-location.

	Start	End	Mean [GEM] Inlet 1 (ng m^{-3})	Mean [GEM] Inlet 2 (ng m^{-3})	Mean Difference	Maximum Gradient Magnitude	Minimum Gradient Magnitude
Collocated	6/26/2009	7/2/2009	1.199	1.190	0.009	0.086	0.000
Collocated	8/2/2009	8/9/2009	1.093	1.094	0.001	0.134	0.000
Collocated	8/29/2009	9/2/2009	1.024	1.008	0.016	0.125	0.000
Collocated	9/18/2009	9/23/2009	1.029	1.028	0.001	0.122	0.000
Collocated	11/6/2009	11/14/2009	1.532	1.534	0.008	0.110	0.000
Collocated	2/1/2010	2/5/2010	1.809	1.809	0.000	0.098	0.002
Separated (above 0.009 threshold)	7/2/2009	7/6/2010	-	-	-0.004	0.570	0.009

moisture, surface wetness, total UV, UV-B, net solar radiation, albedo, and wind speed and direction at 3 m. The flux tower was located 30 m to the west of the equipment shelters (Figure 5.1). I chose this location in order to have the most homogeneous fetch from west to north, which is the predominant wind sector. PRAAMS is also the location of MD08, a monitoring station in the National Atmospheric Deposition Program's National Trends Network, Mercury Deposition Network and Atmospheric Mercury Network.

Mean annual air temperature for the entire campaign was 8.5^{o}C, roughly equal to the long term (1972 – 2010) annual mean temperature of 8.8^{o}C (SERCC, 2010). For the measurement period, precipitation was 136.0 cm, the 5th highest since 1972 and snowfall was 260.9 cm, the 13th highest since 1972 (SERCC, 2010). PRAAMS was at least partially snow covered from 12/20/2009 to 3/25/2010. Soils were classified as Dekalb and Gilpin very stony loams (USDA, 2009) and had a mean total mercury concentration of 0.05 µg of mercury per g of soil (µg g^{-1}).

5.3.2 Modified Bowen Ratio

The MBR method was used to measure GEM fluxes (Converse et al., 2010; Fritsche et al., 2008b; Gustin et al., 1999; Kim et al., 1995; Lindberg et al., 1995). This is a micrometeorological technique that combines high speed eddy correlation measurements (10 Hz) with GEM concentration gradient measurements. The eddy correlation techniques were used to measure the kinematic heat flux with a 3D ultrasonic anemometer (R. M. Young 81000VRE). The ultrasonic anemometer was mounted at 2 m between two sets of thermistors that were mounted at 1 m and 3 m above the ground. I then used the kinematic heat flux and the temperature gradient measured between the aspirated thermistors at 1 and 3 m to calculate a vertical transport term (K) that was applied to the GEM gradient to determine the flux. In this way I was using heat as a reference scalar in order to determine the movement of GEM. By using heat as a reference scalar, I assumed that the mechanical vertical – air mixing transported heat from hot to cold and GEM from higher concentration to lower concentration with the same efficiency. I chose temperature and heat flux as the reference scalar instead of CO_2 or water vapor, to eliminate some of the problems experienced by others under dry and low CO_2 conditions (Converse et al., 2010). K was calculated with Equation 5.1:

$$K = \frac{w'T'}{\Delta T}$$

The GEM flux was then determined with Equation 5.2:

$$F_{GEM} = K\Delta C_{GEM}$$

Where w'T' was the kinematic heat flux (K m s^{-1}) and ΔT (K) was the hourly difference in temperature between 1 and 3 m, F_{GEM} was the GEM flux (ng m^{-2} h^{-1}), ΔC_{GEM} was the hourly GEM concentration gradient between 1 and 3 m. To determine hourly GEM and temperature gradients, the hourly mean at the lower height was subtracted from the hourly mean at the upper height. The dry deposition velocity (V_d) for GEM was then determined by Equation 5.3:

$$V_d = \frac{F_{GEM}}{C_{GEM}}$$

Where C_{GEM} is the concentration of GEM at the 3 m height.

GEM concentrations were measured with a Tekran 2537A Mercury Vapor Analyzer (2537A) located in a temperature controlled shed approximately 30 m from the flux tower. The 2537A continuously measured GEM concentrations by switching between two gold traps. Mercury was collected on one gold trap (A channel) for five minutes, then while the mercury was being desorbed and analyzed from the A channel, mercury was being collected by another gold trap (B channel). The 2537A had a detection limit of < 0.1 ng m^{-3} (Tekran, Inc.). To determine the GEM concentrations at 1 and 3 m, two identical length 3/16" ID Teflon lines, one from each height, were attached to a Tekran Model 1110 synchronized two port sampling system, which was attached to the 2537A. The 1110 automatically switched between the two inlets every 15 minutes (three 5 minute sampling periods). The first five minute sample was discarded during data analysis to prevent skewing of the data due to stagnant air in the 30 m Teflon line. Flows into the 2537A were maintained at 1.0 L min^{-1} and were checked monthly with a Bios DryCal Definer 220 flow meter.

The temperatures at each height were measured every minute with two 1000 Ω platinum resistance thermistors (PRT) inside Met One 076B aspirated shields. These shields produced consistent air flow across the PRTs and removed them from direct sunlight and precipitation. The precision of the PRTs was ± 0.01^{o}C. The temperature gradient was calculated by subtracting the hourly mean of the two PRTs at 3 m from the hourly mean of the two PRTs at 1 m.

5.3.3 QA/QC

The 2537A was automatically calibrated from an internal calibration system every 49 hours. The analyzer was closely monitored and taken offline or serviced if the difference between the gold traps (channels A and B) rose above 7.5%. The 2537A was offline 749 of 9234 hours over the annual measurement period for calibration, maintenance, power failures, or use on other projects. Twice during the year, the accuracy of the internal calibration source was examined by several injections of GEM from a Tekran 2505 mercury calibration unit and a digital syringe (1702RN, 25 µL, Hamilton Co., Reno, NV). Both times, the accuracy of internal calibration system was within the uncertainty of the permeation rate. The sample inlet on the back of the 2537A had a 2 µm Teflon filter which removed particles and gaseous oxidized mercury. Therefore, the only gaseous species of mercury that entered the analyzer was GEM.

To be certain I was measuring real GEM gradients with the flux tower, I set both sampling inlets at 1 m six times throughout the measurement campaign (Table 5.2). This allowed us to compare data from periods of collocated inlets to

Table 5.2. Means of each inlet during times of co-location.

	Start	End	Mean [GEM] Inlet 1 (ng m^{-3})	Mean [GEM] Inlet 2 (ng m^{-3})	Mean Difference	Maximum Gradient Magnitude	Minimum Gradient Magnitude
Collocated	6/26/2009	7/2/2009	1.199	1.190	0.009	0.086	0.000
Collocated	8/2/2009	8/9/2009	1.093	1.094	0.001	0.134	0.000
Collocated	8/29/2009	9/2/2009	1.024	1.008	0.016	0.125	0.000
Collocated	9/18/2009	9/23/2009	1.029	1.028	0.001	0.122	0.000
Collocated	11/6/2009	11/14/2009	1.532	1.534	0.008	0.110	0.000
Collocated	2/1/2010	2/5/2010	1.809	1.809	0.000	0.098	0.002
Separated (above 0.009 threshold)	7/2/2009	7/6/2010	-	-	-0.004	0.570	0.009

periods when inlets were separated by 2 m. This comparison was necessary in order to determine the GEM concentration gradient threshold that was caused by variation in the data and not measurement uncertainties. I also placed the PRTs at the same 1 m height during these six periods. By doing this, I was able to determine that one of the four PRTs was measuring 0.10^{o}C higher than the three other PRTs. Therefore, 0.1^{o}C was always subtracted from this PRT before any flux calculation.

5.3.4 Flux Footprint

The flux footprint was estimated with the model developed by Hsieh et al. (2000). This model had been widely used to estimate flux footprints (i.e. Oishi et al., 2008; Park et al., 2009; Wohlfahrt et al., 2009). This model was based on Lagrangian stochastic dispersion and similarity theory (Hsieh et al., 2000). The model used hourly measurements of sensible heat flux (H), air temperature, and friction velocity (u*). Canopy height, zero plane displacement, and momentum roughness were defined as 0.5 to 1.0 m (leaf off and leaf on, respectively), 0.335 m, and 0.05 m

respectively. Zero plane displacement and momentum roughness were estimated from Arya (2001a).

I used this model to calculate the direction and fetch where 80% of the GEM flux occurred (Hsieh et al., 2000). Only 80% of the flux footprint was modeled because the flux footprint follows an exponential decay function. The last 20% in the tail of the decay can extend for hundreds to thousands of meters with only a small contribution to the flux. The model results were then separated into periods of stable, neutral, and unstable atmospheric conditions. Unstable conditions were defined as Monin-Obukhov lengths ($z\ L^{-1}$) less than -0.02, stable conditions were $z\ L^{-1}$ greater than 0.02, and neutral conditions were the transition period between stable and unstable (Hsieh et al., 2000). The z is the measurement height and L is the Obukhov length (Arya, 2001b; Hsieh et al., 2000).

5.3.5 Statistical Analysis

All statistical analyses were performed in R Project (version 2.10.1) on hourly mean values. Pearson Product Moment correlations were reported as significant at the $\alpha = 0.05$ level. ANOVA was used to determine if there were significant differences in mean GEM fluxes by season and wind direction sector and the differences in mean emission and deposition by season. A Tukey's HSD test was used with the ANOVA results to test for significant differences among seasons. I used an ANOVA to determine significant differences by wind rose sector. I also used spectral and partial autocorrelation function analysis to evaluate the filtered GEM fluxes. Spectral analysis was used to identify any characteristic time frequency of variation in GEM fluxes. The partial autocorrelation function analysis was used to

determine if subsequent hours were correlated. In order to perform the spectral and partial autocorrelation function analysis, I performed linear interpolations to fill in missing data for 3975 hours out of the total sampling of 9234 hours. These data were missing due to the 2537A being offline for calibration periods, flow measurements, routine maintenance or when the weather prevented the ultrasonic anemometer from working properly.

5.4 Results and Discussion

5.4.1 GEM Flux Validation

In this section, I describe my rationale for removing some GEM fluxes that may have been caused by uncertainties in the measurements. The fluxes were calculated, in part, from the GEM concentration gradient between the 1 and 3 m measurement heights (Equation 5.2). I wanted to determine the concentration gradient threshold caused by real differences in GEM between the two heights. To do this, I examined the variation in the GEM concentration gradient when the two inlets were collocated at 1 m (Table 5.2). The overall mean for the collocated periods was 0.006 ng m^{-3} and the range was -0.004 to 0.016 ng m^{-3} (Table 5.2). From the mean gradients during collocation periods I selected two possible gradient thresholds, 0.009 ng m^{-3} and 0.016 ng m^{-3}.

To determine the more effective threshold, I examined the absolute value of the GEM concentration difference between the two inlets for the entire measurement campaign. By using the absolute value I avoided comparing mean GEM gradients

that could have been biased low by the many positive and negative values. To demonstrate this, the mean GEM gradient when the inlets were separated was -0.003 ± 0.045 ng m^{-3} and ranged from -0.281 to 0.570 ng m^{-3}. On the other hand, the mean absolute value for the same periods was 0.034 ± 0.029 ng m^{-3}. For the entire data set, there was no significant difference ($p = 0.5232$) between this mean absolute value and that during periods when the inlets were collocated at 1 m (0.035 ± 0.029 ng m^{-3}). When I removed concentration gradients smaller than 0.009 ng m^{-3}, the difference in mean absolute values became significant ($p = 6.83 \times 10^{-6}$). The mean GEM gradient during separated periods increased after filtering (0.040 ± 0.030 ng m^{-3}). As a result, all fluxes with concentration gradients less than 0.009 ng m^{-3} were removed from the data set (18% of total data). Filtering at a threshold of 0.016 ng m^{-3} also produced a significant difference between collocated and separated periods but would have removed 32% of the fluxes. The latter was not used because it removed more data than the 0.009 ng m^{-3} threshold.

I also wanted to be certain that the GEM fluxes were not simply random noise. To examine this, I performed a time series analysis on the filtered data. The partial autocorrelation function (PACF) of the annual time series revealed that the fluxes were correlated for five hours (Figure 5.2). This indicated that even though the

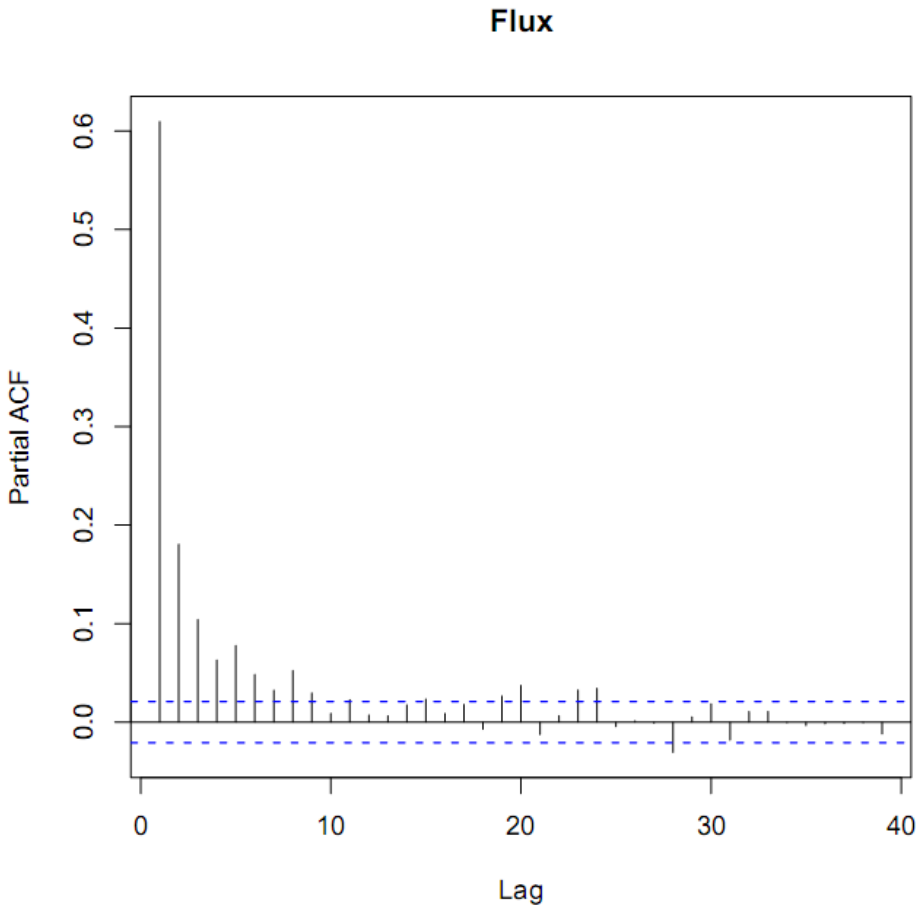

Figure 5.2. The partial autocorrelation function (ACF) diagram of hourly GEM fluxes for the entire campaign. The dotted lines indicate the 95% confidence interval above or below which hours are significantly correlated with hour zero. The time lag on the x axis is in units of hours and the Partial ACF on the y axis in units of percent (%).

fluxes oscillated between emission and deposition, subsequent hours, up to 5 hours, were correlated. If the fluxes had been noise alone, they would not have been autocorrelated. I also performed a spectral analysis on the fluxes. I did not find a characteristic frequency of variation, such as every 24 or 168 hours, that would

indicate a distinct daily or weekly variation. However, the spectrum was not a flat line, which would have indicated random noise. Collectively, the filtered data contained measurable fluxes generated by real differences in the GEM concentration gradient.

Finally, there were two buildings located 10 and 30 m east of the flux tower. I wanted to be certain that the buildings did not alter the GEM fluxes. To determine the effect of the buildings, I divided the fluxes into eight wind direction sectors (45 degree sections of the 360 degree wind rose). I looked for significant differences in the average flux for each sector. For the entire measurement campaign, GEM fluxes were not significantly different among the eight wind direction sectors. This indicated that the buildings did not artificially bias the GEM fluxes.

5.4.2 GEM Fluxes

Hourly GEM fluxes were highly variable, continuously switching between emission and deposition (Figure 5.3). Mean hourly GEM fluxes were -0.63 ± 31.0 ng m^{-2} h^{-1} (N = 5259). The mean GEM flux was consistent with fluxes from an upland

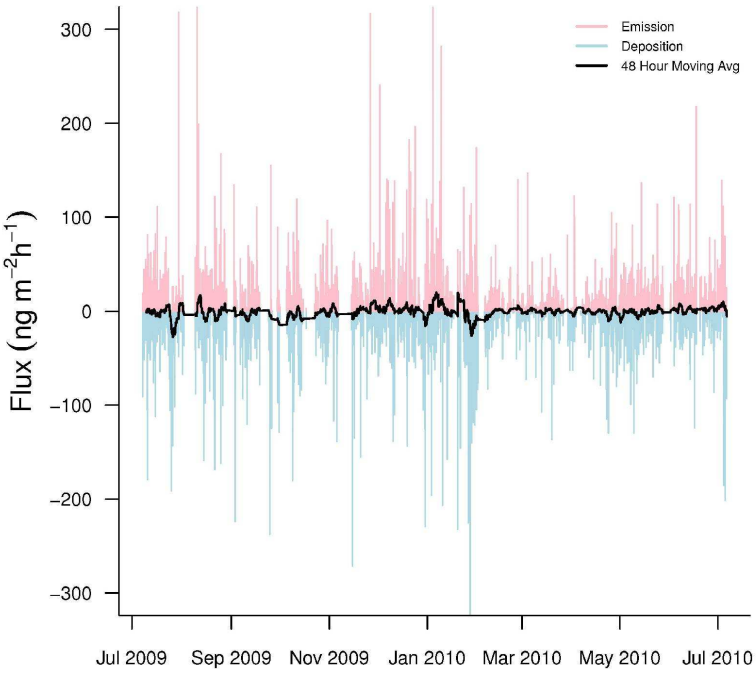

Figure 5.3. Hourly GEM fluxes from July 2009 to July 2010. Emissions are pink while depositions are light blue. The black line represents a 48 hour moving average of the hourly fluxes.

meadow in Shenandoah National Park, VA (Converse et al., 2010) (Table 5.3). The range of measured fluxes over the year (-346.1 to 379.8 ng m^{-2} h^{-1}) was much larger than other studies especially, in the winter (Table 5.3). The only other study

Table 5.3. A comparison of GEM fluxes measured at PRAAMS with those measured by other studies.

Mean TGM Flux ($ng\ m^{-2}\ hr^{-1}$)	Min Flux ($ng\ m^{-2}\ hr^{-1}$)	Max Flux ($ng\ m^{-2}\ hr^{-1}$)	Time of Year	Ecosystem	Study
PRAAMS:					
-1.41 ± 32.5	-224	353.6	Summer	Upland Meadow surrounded with deciduous forest	This study
0.32 ± 33.1	-271.3	316.8	Fall	Upland Meadow surrounded with deciduous forest	This study
-0.64 ± 34.4	-346.1	379.8	Winter	Upland Meadow surrounded with deciduous forest	This study
-0.62 ± 22.6	-129.7	217.7	Spring	Upland Meadow surrounded with deciduous forest	This study
Other Studies:					
2.5 ± 19.1	-124.8	82.4	Aug 6 - 12, 2009	High elevation meadow	Converse et al. 2010
0.3 ± 16.8	-77.1	67.6	Nov 7 - 14, 2008	High elevation meadow	Converse et al. 2010
4.1 ± 25.7	-112.0	119.1	Feb 11 - 17, 2009	High elevation meadow	Converse et al. 2010
-4.8 ± 25.5	-125.7	71.0	May 11 - 19, 2009	High elevation meadow	Converse et al. 2010
NR	-5.4	4.2	June 2 - 10, 1994	Forest Floor	Lindberg et al. 1998
-4.3 ± NR	-42.0	20.0	Aug 26 - Nov 23, 2005	Grassland	Fritsche et al. 2008a
-1.7 ± NR	-35.0	34.0	Mar 27 - Aug 30, 2006	Grassland	Fritsche et al. 2008a
0.3 ± NR	-34.0	29.0	Nov 24, 2005 - Mar 26, 2006	Grassland with snow	Fritsche et al. 2008a
9.67 ± NR	-91.7	190.5	May 7 - 14 and May 31 - June 8 , 2001	Agricultural Field	Cobos et al. 2002
-4.3 ± NR	-27.0	14.0	June 7 - July 20, 2006	Grassland	Fritsche et al. 2008b
-1.6 ± NR	-14.0	14.0	June 7 - July 20, 2006	Grassland	Fritsche et al. 2008b
-2.1 ± NR	-41.0	26.0	June 14 - 29, 2006	Grassland	Fritsche et al. 2008b
-0.5 ± NR	-76.0	37.0	June 14 - 29, 2006	Grassland	Fritsche et al. 2008b
0.2 ± NR	-33.0	29.0	Sep 14 -26, 2006	Managed Farmland	Fritsche et al. 2008b
0.3 ± NR	-18.0	30.0	Sep 14 -26, 2006	Managed Farmland	Fritsche et al. 2008b
32.1 ± 55.6	-110.0	278.0	Aug 23 - Sept 3, 2002	Wetlands, open water, mixed vegetation	Poissant et al.2004

with results similar to this range was over a mixed wetland, vegetation, and open water system in Quebec, Canada (Poissant et al., 2004). This could indicate that the vegetation, land cover (snow), UVB, wind speed, ozone, and RH within the flux footprint sporadically caused large spikes in the GEM fluxes. In addition, previous

studies with short measurement periods, may not have sampled enough duration to capture these extreme variations.

The net GEM flux for the year was -3.33 ug m^{-2} y^{-1} for the filtered fluxes. This estimate was made by summing the hourly filtered fluxes for the year. The net GEM flux for the unfiltered fluxes (all GEM gradients included) was -3.74 ug m^{-2} y^{-1}. This would indicate the removed fluxes made a small contribution to the overall net flux. Filtered GEM fluxes were not significantly different among seasons, but the flux patterns differed throughout the year. There were two periods in July 2009 when deposition was consistently -100 ng m^{-2} h^{-1} (Figure 5.3). In August 2009, the fluxes oscillated between -100 and 100 ng m^{-2} h^{-1} for a short period (Figure 5.3). In fall 2009, the GEM fluxes became less variable (Figure 5.3). Fluxes in winter became more variable until snow covered the site in early February. From February to early May 2010, fluxes were less erratic (Figure 5.3). From early May until early July 2010 the fluxes were as variable as in summer 2009 (Figure 5.3).

To determine the source area of the GEM flux measurements throughout the year, I examined the flux footprint model results. For the entire measurement campaign the atmospheric stability conditions were 25.8% unstable, 45.7% neutral and 28.6% stable. During unstable conditions, the mean footprint for 80% of the GEM flux was within 200 m of the flux tower. During neutral conditions, the mean footprint for 80% of the GEM flux was within 300 m of flux tower. During stable conditions, mean footprint for 80% of the GEM flux was within 2000 m from the flux tower. For 74.3% of the entire sampling campaign, 80% of the GEM flux was within

300 m of the tower. The vegetation within that 300 m was mostly grasses and brush with a few dispersed trees (Figure 5.1).

In order to put my study into perspective with others, I calculated the GEM V_d. The V_d is often used in by modelers to estimate atmospheric deposition of GEM (Zhang et al., 2009). The annual mean V_d was 0.33 ± 0.61 cm s^{-1} and ranged from 0 to 8.08 cm s^{-1}. The mean V_d was in agreement with the mean V_d reported for vegetated surfaces and wetlands (0.1 to 0.4 cm s^{-1}; Zhang et al. 2009). In spring, V_d (0.22 ± 0.33 cm s^{-1}) was significantly lower than summer (0.38 ± 0.71 cm s^{-1}), fall (0.38 ± 0.63 cm s^{-1}) and winter (0.31 ± 0.66 cm s^{-1}). Summer, fall and winter were not significantly different from each other. This pattern was also reported by Converse et al. (2010). The range of GEM fluxes at PRAAMS was also smaller in spring (Table 5.3). This indicated that there was less exchange of GEM between the surface and atmosphere during this season. The vegetation may have been less effective at removing GEM from the atmosphere during the onset of the growing season. The range of V_d values were also more consistent with the range of V_d for forest canopies (0.0003 to 1.88 cm s^{-1}) than bare background soil (0.002 to 0.064 cm s^{-1}) (Zhang et al., 2009). This could indicate that the forests at PRAAMS were important sinks for atmospheric GEM.

When analyzed in bulk, mean hourly GEM fluxes were slightly correlated ($r < 0.05$) with mean hourly NO_2, NO_y, soil redox at 5 cm into the E horizon and total UV. The fluxes were not related to any of the 25 other variables measured. Therefore, I was not able to identify any factors that consistently influenced the GEM fluxes.

5.4.3 GEM Emission and Deposition

Due to the low correlation coefficients between the GEM fluxes and all of the other measured variables, I examined the GEM emission and deposition separately, an approach also used by Kim et al. 1995. Annual mean GEM emission was 15.3 ± 27.9 ng m^{-2} h^{-1} (N = 2453). Emission in spring (12.9 ± 21.1 ng m^{-2} h^{-1}) was significantly lower than fall (17.8 ± 29.4 ng m^{-2} h^{-1}) but was not significantly different from summer (16.8 ± 29.8 ng m^{-2} h^{-1}) or winter (13.9 ± 29.8 ng m^{-2} h^{-1}). GEM emissions were also not significantly different among fall, summer, and winter. Among all seasons, GEM emissions were greater under unstable atmospheric conditions (23.8 ± 28.4 ng m^{-2} h^{-1}) than under neutral (21.5 ± 33.1 ng m^{-2} h^{-1}) or stable (3.00 ± 5.43 ng m^{-2} h^{-1}) conditions. This trend occurred in all seasons. The mean GEM emission was slightly higher than the emission (7.5 ± 7.0 ng m^{-2} h^{-1}) in the Walker Branch Watershed in Oak Ridge, TN (Kim et al., 1995). However, the Kim et al (1995) study was limited to short daytime sampling periods from May through November 1994.

Annual mean GEM deposition was -14.6 ± 26.6 ng m^{-2} h^{-1} (N = 2806). Mean GEM deposition in the spring (-11.4 ± 17.3 ng m^{-2} h^{-1}) was significantly lower than summer (-15.5 ± 27.3 ng m^{-2} h^{-1}), fall (-16.6 ± 21.1 ng m^{-2} h^{-1}) and winter (-15.2 ± 32.5 ng m^{-2} h^{-1}). Deposition for the year was also significantly higher under unstable atmospheric conditions (-23.0 ± 29.7 ng m^{-2} h^{-1}) than under neutral (-17.5 ± 29.3 ng m^{-2} h^{-1}) or stable (-3.3 ± 10.5 ng m^{-2} h^{-1}) atmospheric conditions. Deposition under unstable conditions was significantly higher within seasons. The GEM deposition

was also higher than the mean daytime GEM deposition (-2.2 ± 2.4 ng m^{-2} h^{-1}) at Walker Branch Watershed (Kim et al., 1995).

Separating the fluxes into emission and deposition revealed that several variables were influencing the fluxes. However, most of the correlation coefficients were still below 0.25 (Table 5.4). By looking at only the variables with the highest

Table 5.4. The variables most highly correlated with GEM emission and deposition separately. Only those variables with a correlation coefficient (r) greater than 0.25 are reported unless no variables were above 0.25 then only the variable with the highest r value is reported.

	Emission		Deposition	
Season	**Parameter**	**Correlation Coefficient**	**Parameters**	**Correlation Coefficient**
Summer			Relative Humidity	0.44
	UVB	0.47	WS (3 m)	-0.42
	Relative Humidity	-0.36	Ozone	-0.40
	Ozone	0.31	Total UV	-0.40
	WS (3 m)	0.27	UVB	-0.38
	Total UV	0.26	Surface Wetness	0.35
			Albedo	0.28
Fall	UVB	0.28	WS (3 m)	-0.29
Winter	WS (10 m)	0.24	WS (10 m)	-0.26
Spring			Net Solar Radiation	-0.47
	Net Solar Radiation	0.37	UVB	-0.41
	UVB	0.31	Total UV	-0.28
			WS (10 m)	-0.28
	Oe - A soil Horizon		WS (3 m)	-0.26
	Soil Temperature	0.30	Relative Humidity	0.25

correlation coefficients in each season, I was able to draw a few conclusions. UV-B was correlated with emission in summer, fall and spring and with deposition in

summer and spring (Table 5.4). Although more strongly related than other parameters, UV-B still only explained 22% of the variation of the GEM emissions (in summer) and 17% of the deposition (in spring). However, I did find that as UV-B increased, emissions increased and deposition decreased. This was consistent with the findings of others and may indicate that UV-B photo-reduction of GOM to GEM at the soil surface may have been influencing the GEM fluxes (Choi and Holsen, 2009a; Moore and Carpi, 2005; Xin et al., 2007). The importance of the conversion between GOM and GEM occurring at the soil surface was also supported by correlations with ambient air ozone concentrations in summer. As ozone concentrations increased, GEM emission increased and deposition decreased. This relationship was consistent with the findings of Engle et al (2005), who reported that GEM emissions increased from soils enriched in bound Hg^{2+} under higher ambient air ozone concentrations (up to ~ 70 ppb). Although they did not determine the exact mechanism, they speculated that the ozone was oxidizing sulfur species, such as HgS, and this oxidation was counterbalanced by reduction of Hg^{2+} (gaseous or bound) in the soil matrix to GEM. The GEM was then emitted to the atmosphere. It was possible that this process was occurring at PRAAMS. However, I could not rule out the fact that higher UV-B also produced more local ozone. Ozone can be produced in the troposphere from a photochemical reaction driven by UV-B radiation (Jacob et al., 1995).

There were also higher GEM emissions and lower GEM deposition at higher wind speed. The influence of wind speed on GEM fluxes could indicate that air turbulence was physically moving the GEM from the shallow soil layers into the

atmosphere. This would agree with my findings that both emissions and deposition were higher under unstable atmospheric conditions. As turbulence near the surface increased, the physical movement of the GEM increased. This indicated that pressure fluctuations at the surface move gases in and out of the soil pore spaces. This further emphasized the importance of the soil surface even during periods when UV-B and ozone were lower, such as in the fall and winter.

RH appeared to be a factor controlling emission and deposition during the warmer spring and summer months. Higher RH led to lower emissions and higher deposition. This was similar to that seen by other studies (Boudala et al., 2000; Converse et al., 2010; Ericksen et al., 2006; Poissant and Casimir, 1998). This relationship may indicate that increased moisture in the air could facilitate the oxidation of GEM to GOM and increase deposition.

5.4.4 Comparison with other measurements at PRAAMS

The MBR measurements of GEM flux were part of a larger study to better understand the atmospheric mercury cycle at PRAAMS. Other studies measured GEM fluxes with dynamic flux chambers (Moore et al., 2011b), GOM deposition with ion exchange membranes (Castro et al., 2011), total mercury in litterfall deposition (USGS, 2010), and total mercury in wet deposition (NADP, 2010). One of the projects also modeled GOM deposition (Castro et al., 2011). Here, I present a comparison of the two GEM flux measurement campaigns (dynamic flux chambers vs MBR), and then I put these fluxes into perspective with the other mercury measurements made at PRAAMS.

The net annual GEM flux estimates were different between the dynamic flux chambers and MBR methods (Moore et al. 2011). With the flux chambers I estimated a net daytime emission of 2.0 to 5.3 µg m^{-2} y^{-1}. With the MBR method, I estimated a net deposition of 3.3 µg m^{-2} y^{-1} for both all periods. When only the daytime MBR fluxes were included the net deposition was only slightly lower (2.4 µg m^{-2} y^{-1}). This emphasized the differences between the measurement techniques. Fluxes measured with the MBR method were representative of large footprint areas from 300 to 2000 m^2. The MBR fluxes were also a summation of the soil, vegetation, and snow surfaces, and each surface may have had different factors controlling the GEM fluxes. The chambers measured fluxes over a much smaller area (< 0.5 m^2) and only during daytime hours. This could have biased the flux chamber estimates high, due to the missing deposition that may occur at night. Also, there were periods when the soils beneath the chambers would switch from source to sink of GEM. This indicated that the landscape consisted of spatially variable and highly dynamic GEM fluxes, which could not be captured with flux chamber measurements. Therefore, we must be careful when scaling up fluxes measured with flux chambers to be representative of a large area. My efforts verify the findings of others that micrometeorological and chamber fluxes do not typically agree (Gustin et al., 1999).

The annual estimate of GOM deposition measured with ion exchange membranes was 2.5 µg m^{-2} y^{-1} (Castro et al., 2011). The GOM deposition modeled using a multi-layer inferential model of GOM dry deposition velocities was 3.2 µg m^{-2} y^{-1} (Castro et al., 2011). These two estimates were very similar in magnitude to the net GEM flux measured with the flux tower. This would indicate that dry

deposition of GEM was as important as GOM deposition at PRAAMS. GEM was thought to have a much smaller deposition velocity than GOM and was often not included in many deposition estimates (Lyman et al., 2007; Ryaboshapko et al., 2007). Other models estimated that GEM deposition could be roughly equal to GOM deposition (Miller et al., 2005). My findings strengthen this estimation. However, the measured dry deposition was slightly lower than the 12 to 15 $\mu g\ m^{-2}\ y^{-1}$ that had been modeled for PRAAMS (Miller et al., 2005).

The dry deposition estimates (5.8 to 6.5 $\mu g\ m^{-2}\ y^{-1}$) were roughly equal to the mean mercury wet deposition (7.6 $\mu g\ m^{-2}\ y^{-1}$) from 2004 to 2009 (NADP, 2010). Other modeling and measurement studies have estimated that wet and dry deposition could be roughly equal (Engle et al., 2010; Miller et al., 2005). My studies verify this assumption. The wet and dry deposition estimates, however, were much lower than the litterfall mercury input (15 $ug\ m^{-2}\ y^{-1}$) measured in 2008 (USGS, 2010). Although there is likely some annual variation in the litterfall input of mercury, this confirms the importance of this component of total mercury deposition (Rea et al., 1996; Rea et al., 2001). Since there are both grass and forest areas at PRAAMS litterfall plays an important role in mercury biogeochemical cycling.

5.5 Conclusions

In bulk, GEM fluxes at PRAAMS were very dynamic and not strongly correlated with any of the atmospheric trace gases, aerosols, or meteorological variables. After separating the fluxes into periods of emission and deposition, I was

able to determine that UV-B, ozone, wind speed and relative humidity influenced the GEM fluxes. However, even these relationships explained less than 22% of the variation in GEM fluxes. This could indicate that parameters other than those measured were influencing GEM fluxes at PRAAMS. These factors could include biological processes, variables that change on a shorter than one hour time scale, or variables that change substantially within the footprint of the flux tower. The few correlations could also indicate that it might be beneficial to have higher resolution measurements of the possible GEM flux controls within the MBR flux footprint. The comprehensive studies of mercury cycling at PRAAMS indicated that GEM deposition was as large as GOM deposition and GEM deposition was 11% of total mercury deposition.

I suggest that future work at background sites focus on improving our understanding of the role of ozone in GEM deposition and the importance of humidity in GEM atmospheric dynamics. I would also suggest that future work focus on the variability of the factors controlling the GEM fluxes in the MBR footprint.

Chapter 6: Conclusions

The toxicity and mobility of mercury has stimulated new, detailed research on all aspects of the mercury biogeochemical cycle. Gaseous elemental mercury (GEM) constitutes more than 95% of the 5 gigagram global atmospheric mercury pool (Mason and Sheu, 2002). The interaction of GEM between the atmosphere and the 1 teragram terrestrial mercury pool may involve the movement of as much as several gigagrams of mercury per year. This global movement of large quantities of mercury was the reason that we attempted to measure and estimate the uncertainties associated with the surface – atmosphere exchange of GEM. Three areas that needed careful study were measurement based estimates of the annual net exchange of GEM in western Maryland, the environmental factors affecting the net exchange of GEM and the factors affecting the soil pore air gaseous mercury concentrations. Actual long term measurements of GEM exchange have been limited, with most current estimates of mercury dynamics based on model projections (Bash et al., 2004; Bullock and Brehme, 2002; Cohen et al., 2004; Marsik et al., 2007; Zhang et al., 2009). These models are usually based on environmental variables correlated with mercury movement that are more easily determined than direct estimates of GEM exchange. Therefore, efforts to verify the utility of models of GEM exchange and/or the identification of more robust variables for estimating exchange rates are essential for defining mercury dynamics in the environment. In addition, by making direct measurements of GEM exchange, we hope to improve our ability to predict the consequences of limiting future anthropogenic emissions of mercury or allowing emissions to continue un-regulated.

The bi-directional nature of GEM fluxes means that despite the global potential for the movement of gigagrams of mercury there may actually be zero net exchange between terrestrial surfaces and the atmosphere over a year. This possibility for zero net exchange is enhanced at background sites that are far from point sources of mercury pollution, that have been affected only by atmospheric deposition and have low soil mercury concentrations (< 0.5 μg of Hg per g of soil). At PRAAMS in western Maryland, I quantified the GEM exchange on two different scales with flux chambers and micrometeorological techniques. Also, a new method for measuring TGM in soil pore air was developed that improved on previous designs by increasing sample sizes, reducing flow rates to remove ambient air contamination issues, and removed container wall effects by collecting on gold coated quartz sand traps. With these techniques, I was able to study the three areas of GEM surface - atmosphere exchange mentioned earlier.

One important finding from the project was that soil Eh was a dominant factor controlling soil total gaseous mercury dynamics, including both soil pore air TGM concentrations and surface atmosphere fluxes of GEM. Another important finding was that the net GEM exchange at PRAAMS was a deposition of 3.3 $\mu g\ m^{-2}\ yr^{-1}$. These results allowed me to provide quantitative estimates in the conceptual diagram of GEM exchange at PRAAMS presented in the introduction (Figure 6.1). GEM deposition at

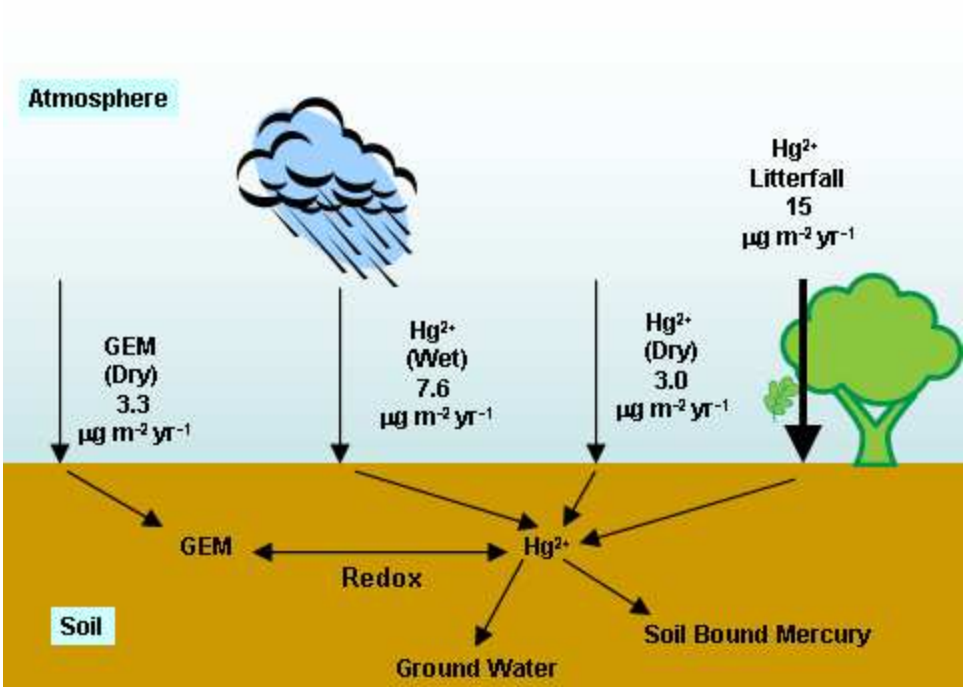

Figure 6.1. The final conceptual model of the surface atmosphere exchange of mercury at PRAAMS with all components complete.

PRAAMS was as high as gaseous oxidized mercury (GOM) deposition. This finding is important because GOM deposition was traditionally thought to be the major form of gaseous mercury deposition, while GEM has traditionally been predicted to have a net emission from background sites. The finding of soil redox as a control of GEM dynamics and the net deposition measured at PRAAMS meant that current models detailing the surface atmosphere exchange of mercury and the emissions of mercury from background soils may need to be re-evaluated. Also, those same models may need to be re-parameterized to include bulk changes in soil Eh among land cover types.

The findings of this study also show how difficult it will be to measure the environmental benefits of limiting anthropogenic mercury emissions. For instance, the total amount of mercury contained in a 1 square meter, 25 cm depth block of soil in the forest area is 14.6 mg and in the grass area is 10.1 mg (Appendix 4). Currently all forms of mercury deposition add up to 29 $\mu g\ m^{-2}\ yr^{-1}$ (Figure 6.1). The net inputs are currently 500 times smaller than the soil mercury pool at PRAAMS. The discrepancy between the GEM flux and pool sizes indicates that small changes in mercury deposition may take thousands of years to affect the soil mercury pool. This slow change coupled with lower atmospheric deposition of mercury may mean that significant stores of mercury will be retained or "tied up" in the soil matrix keeping them from cycling through aquatic systems. Less mobile mercury would also mean that fewer humans fewer humans are affected. However, only through studies like this one, that actually make the long term GEM exchange measurements, can we track the changes in deposition and soil mercury cycling.

Several important areas of the mercury biogeochemical cycle must be monitored to understand how changes in anthropogenic mercury emissions will alter the atmospheric and terrestrial mercury pools. Those areas can be expanded beyond what was measured in this study. First, and always with any study, additional, longer term measurements are highly desirable. One year of continuous measurements was beneficial, but at least 5 years of measurements would be needed to estimate longer term net exchange. Longer term measurements would also allow me to more precisely track how the exchange changes as new regulations are implemented. Also, my study was concentrated at one site, but the inclusion of other sites, measured

simultaneously, would let me evaluate how the net exchange and environmental controls vary across different land cover types. It would also be beneficial to perform a detailed fine-scale analysis of the measurements in the current study, focusing on short one to two week periods that are more similar to other short term studies than the annual measurement period in this study. This fine scale examination may more clearly reveal the factors controlling the highly variable GEM fluxes at PRAAMS.

Future studies of the surface atmosphere exchange of gaseous mercury should focus on improving our measurement techniques for both GEM and GOM. Measurement techniques for quantifying GEM and GOM fluxes have advanced little in the past 20 years. More research needs to be completed in order to make reliable, real time measurements of GEM. Only by making sub-second measurements will we be able to study this very dynamic, quickly changing exchange with actual eddy correlation techniques. GOM deposition measurements could be relatively easily and cheaply conducted at a network of sites similar to the NADP MDN or AMNET measurement programs. We are currently in a very exciting time for mercury research with many areas of the biogeochemical cycle in need of study. The benefits of such studies have already been realized to some extent through the implementation of regulations, however, we must continue the quest to monitor and understand the fruits of our labor.

Appendix 1: Supporting Information for Chapter 3

Chapter 3 was submitted to *Environmental Science & Technology* (ES&T). ES&T publications are short (less than 7000 words) and often have Support Information Sections that are published online. This Appendix is that supporting information.

Soil Pore TGM Sampling information

Each time I sampled, I randomly selected one area on the first day then sampled the other area on the next sampling day. Within a day, I sampled twice for 1.5 to 3 hours. The main factor that would require the 1.5 hour sample periods was the forecast of rain. During the second sampling of the day, one of the two plots pumped during the first period was re-sampled. This pattern allowed replication of one plot on each sampling day.

I also randomly selected the order in which the plots would be pumped on each day to prevent a sampling bias. However, in the forest area on 1/6/2010 and 1/28/2010, there was only one pumping of the funnels due to heavy snow and limited daylight. This meant that one of the three plots was not sampled and there was no replicate plot sampling. On 1/9/2010 and 1/29/2010 in the grass area, not all funnels were sampled due to some of the funnels having ice in them. This caused the replication at some of the depths to be limited during these samplings. Although samples were collected twice on each sampling day, there were no significant differences between the first and second samplings for either area. This confirms that I did not alter the soil TGM pool with our sampling.

Table A1.1. A comparison of the soil pore air [TGM] measured at PRAAMS with other studies.

Soil Pore [TGM] (ng m^{-3})	Maximum (ng m^{-3})	Minimum (ng m^{-3})	Depth	Ecosystem	Study
At PRAAMS:					
4.11 ± 2.04	8.36	1.50	Oe - A soil horizon interface	Deciduous forest	This study
1.60 ± 0.97	4.62	0.29	A - E soil horizon interface	Deciduous forest	This study
1.57 ± 0.89	4.30	0.61	5 cm into the E soil horizon	Deciduous forest	This study
1.30 ± 0.68	3.35	0.61	10 cm into the E soil horizon	Deciduous forest	This study
1.53 ± 1.53	5.86	0.52	Oe - A soil horizon interface	Grass	This study
1.23 ± 0.97	4.17	0.29	A - E soil horizon interface	Grass	This study
1.33 ± 0.89	3.56	0.47	5 cm into the E soil horizon	Grass	This study
1.63 ± 1.09	4.23	0.44	10 cm into the E soil horizon	Grass	This study
Other Studies:					
1 to 2*	NR	NR	2 cm	Mixed Deciduous and Evergreen Forest	Siger and Lee 2003
3.5 to 6*	NR	NR	5 cm	Mixed Deciduous and Evergreen Forest	Sigler and Lee 2003
0.25 to 2.5*	NR	NR	20 cm	Mixed Deciduous and Evergreen Forest	Sigler and Lee 2003
0.75 to 2	NR	NR	50 cm	Mixed Deciduous and Evergreen Forest	Sigler and Lee 2003
275 to 310*	NR	NR	20 cm	In ECOCELL, Hg enriched soil, before replanting	Johnson et al. 2003
330 to 360*	NR	NR	40 cm	In ECOCELL, Hg enriched soil, before replanting	Johnson et al. 2003
125 to 175*	600*	100*	20 cm	In ECOCELL, Hg enriched soil, after replanting	Johnson et al. 2003
175*	600*	100*	40 cm	In ECOCELL, Hg enriched soil, after replanting	Johnson et al. 2003
137 ± 37	BDL	200	NR	Hg enriched floodplain soils	Wallschlager et al. 2002
NR	4800*	1200*	50 - 70 cm	In Pb-Zn vein type deposits	Kromer et al. 1981

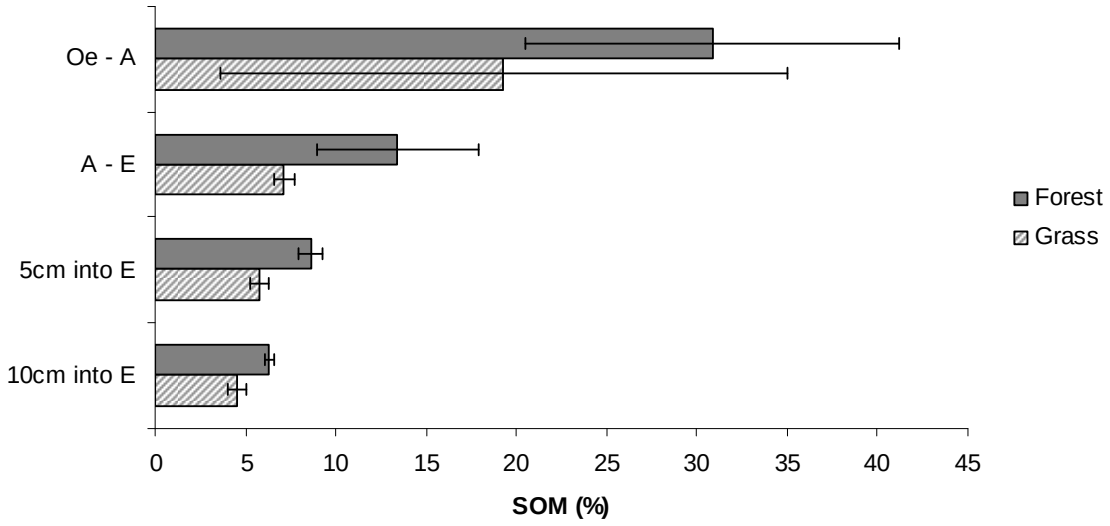

Figure A1.1. Mean soil organic matter (SOM) content at each depth where soil pore [TGM] was measured. Error bars represent one standard deviation from the mean.

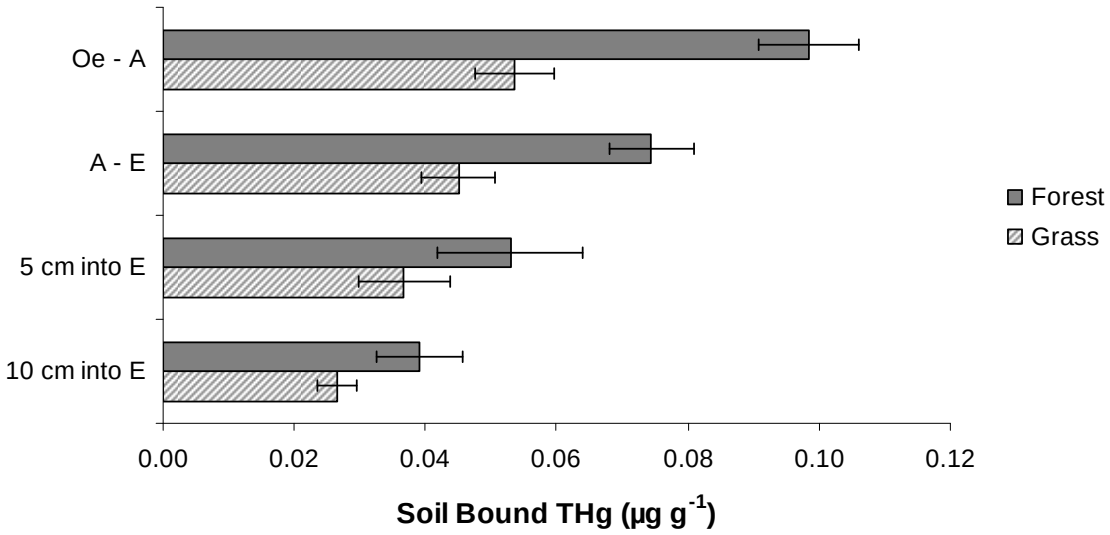

Figure A1.2. Mean soil bound [THg] at each depth where soil pore [TGM] was measured. Error bars represent one standard deviation from the mean.

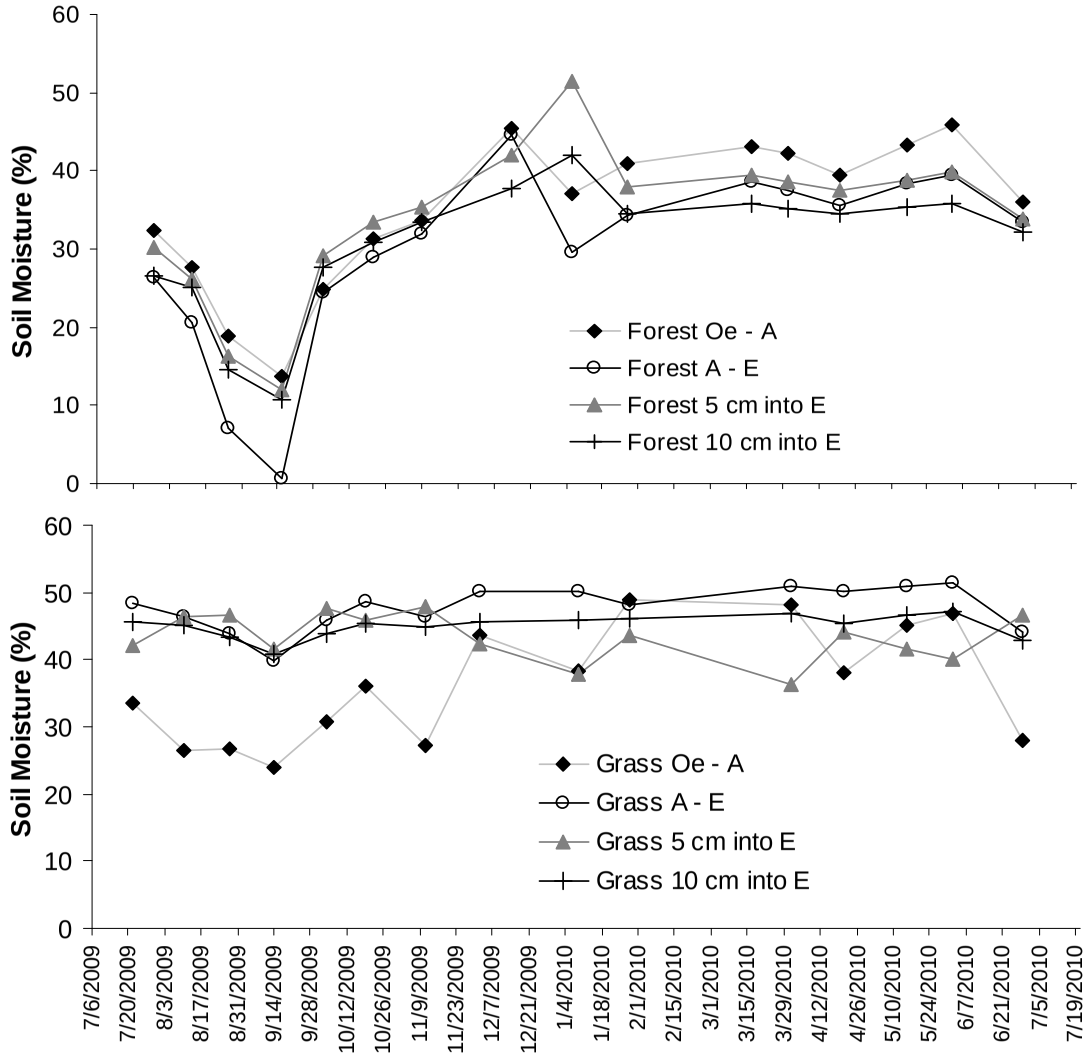

Figure A1.3. Mean soil moisture at all depths in the forest (top) and grass (bottom) areas during the times of soil pore air [TGM] sampling at PRAAMS.

Appendix 2: Soil Redox Probe Construction

Materials:

10 ga insulated copper wire

- I used 10-2 indoor wire from Lowes

0.5mm dia Premion 99.997% platinum wire

Epoxy (need specs)

Black shrink tubing (need specs)

Light solution

Saturated Quinhydrone solution

600 grit sandpaper

Equipment:

Jewelers drill press 1mm drill bit

Wire strippers

Heat gun

20mL disposable syringes

Grinding stone

Dremel

Procedure:

1) If 10-2 copper wire is used, strip outer plastic from wire to expose the inner single strand insulated copper wire.
2) Cut wire to length of the probe with wire cutters. Length should be at least 15 to 20cm. Probe length should be kept at a minimum as the longer they are the

more chance they will bend. I cut approximately 10 – 15 at a time and prepared them to be put on the wheel for epoxy.

3) Grind one end of the length of copper wire to make a completely flat surface for drilling.

Figure A2.1 Grinding stone for grinding end of copper wire.

4) Drill a lmm diameter hole approximately 3mm into the ground end of the wire.

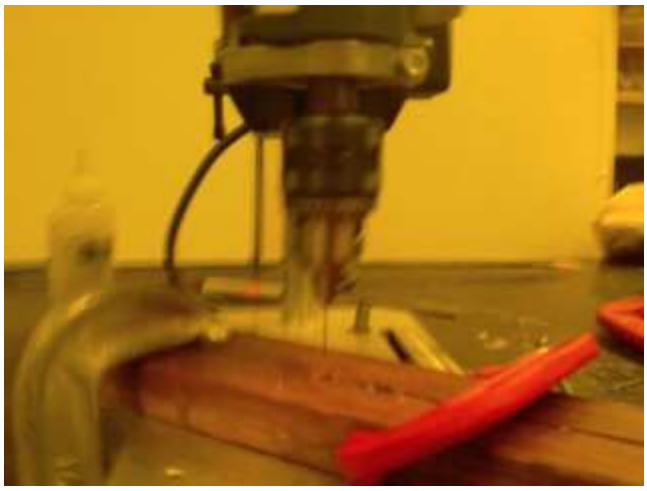

Figure A2.2. Jewelers drill press for drilling hole in end of copper wire.

5) Strip 1 cm of insulation from the end with the hole drilled into it.
6) Cut 1.5 cm of platinum wire and drop it into the hole drilled in the end of the copper wire.
7) Place approximately 5 mm of the copper wire in a small vise and crimp the platinum wire into the end of the copper wire. This produces are very strong connection. Pull on the platinum to be sure the connection is good.
8) Use a Dremel tool to sharpen the end of the copper wire like a pencil around the Pt wire. This is done because when the epoxy is applied it tends to pull back from the tip of the copper. The sharper the tip on the copper the less likely the epoxy will shrink back and expose some of the copper during drying. If a small amount of copper is exposed during curing this will be fixed in a later step.
9) Mix the epoxy in a small disposable weighing dish. Mix the epoxy and hardener by weight. Place the epoxy on one side of the dish and the hardener on the other in case some has to be removed to obtain the proper mix. The easiest way to pull the epoxy and hardener out of the container is a disposable pipette.

Figure A2.3. Syringe for applying epoxy.

10) Rinse the end of the probes with ethanol.

11) Mix the epoxy with the hardener with a new clean pipette. Once the two have been mixed there is 20 to 30 minutes before it becomes too set up to apply to the end of the probe.

12) Spread the epoxy resin on the tip of the probe. Apply starting approximately 2 cm onto the insulation toward the tip of the copper. Try to bunch as much of the epoxy toward tip of the copper possible without getting epoxy on the platinum. A small amount of epoxy at the base of the Pt is inevitable. Continuously turn the probe during application to avoid dripping. Place the probe on a foam wheel that is turned by a slow rotating electrical motor. The one that was used is typically used to apply epoxy to fishing rods. The foam wheel could hold 17 probes a time. Probes were inserted while the wheel was turning. While these probes are turning more can be made and prepared for epoxy.

Figure A2.4. Set up for rotation of redox electrodes to prevent epoxy from just running off the tip of electrode.

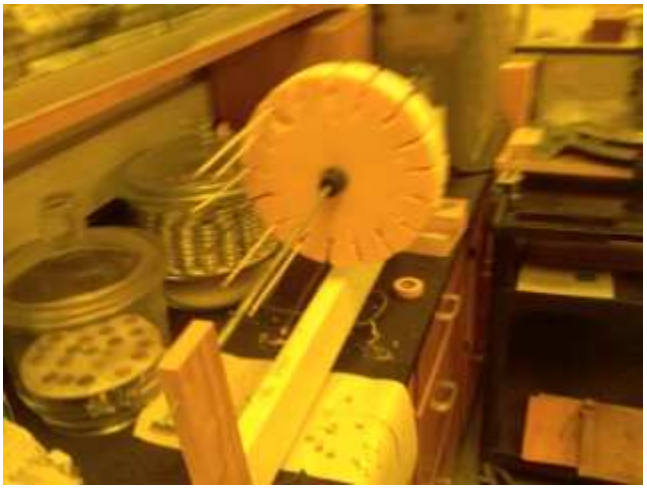

Figure A2.5. Alternate view of rotation set up.

13) Allow probes to turn for 4 to 5 hours. After 4 to 5 hours the epoxy is dry enough so that it will not run. However, probes should be laid on the edge of a bench top with the ends hanging over for at least 12 hours before the epoxy is cured enough to be ground with the Dremel.

14) When the epoxy has cured cut approximately 4 cm of black heat shrink tubing and slide it onto the probe. It is easiest to slide the tubing onto the end opposite the Pt wire.

Figure A2.6. End of electrode before grinding and heat shrink tubing addition.

15) Grind the epoxy with the Dremel just enough so that the heat shrink will slide up to the Pt wire.

Figure A2.7. Epoxy and tip after using the Dremel tool on it.

16) Slide the heat shrink tubing up so that only about 3 – 4 mm of Pt is sticking beyond the heat shrink. Use a heat gun to shrink the tubing up to the base of the bulb produced by the epoxy. Leave the end of the heat shrink open so that more epoxy can be injected later.

17) Tape the probes upright along the edge of a bench. Mix up epoxy and put it in the back side of a disposable syringe. Inject the epoxy into the end of the heat shrink tubing until the epoxy forms a dome shape at the top of the tubing. Roll the tip of the tubing with fingers to work out as many large air pockets as possible. Air makes weak spots in the electrode and may cause them to fail later. If this process causes the epoxy to settle add more to the top.

Figure A2.8. Electrodes taped top up to add the final injection of epoxy.

18) Allow the probes to cure for 12 hours.

19) When the probes are ready to be tested polish the Pt tip with some 600 grit sandpaper until shiny.

20) Rinse the probes with distilled water.

21) Set up reference electrode and instrumentation that will be used to read the probes.

22) Place reference probe and 10 – 15 probes in a Ferrous – Ferric redox solution and read each probe. This solution is heavily poised and all readings should be within 2 mV.

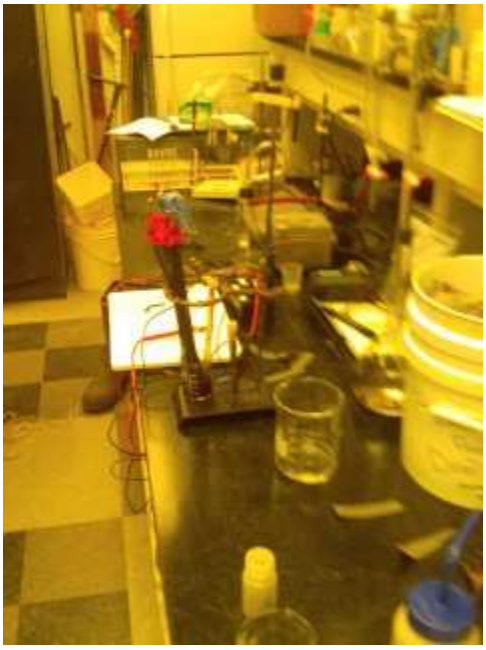

Figure A2.9. Electrodes in reference solution for testing.

23) Rinse the probes and reference electrode and place in a saturated quinhydrone in pH 4.0 buffer solution. This solution is not as poised and tends to be more similar to soils. This solution should produce a 300mV response. However, each group of 15 will be slightly different. Acceptable variation is 20mV.

24) Calculation of eh for a Ag/AgCl electrode mV reading + 199, for a calomel electrode mV reading + 244.

Table A2.1. Example redox probe testing.

Redox Probe Testing

Probe	mV Solution 1	mV of Solution 2	
1	446	266	
2	447	270	
3	447	266	
4	447	265	
5	446	258	Changed from a Calomel electrode
6	484	328	to our Ag/AgCl electrode
7	484	317	
8	484	314	
9	484	326	
10	484	325	
11	484	315	
12	484	324	
13	485	320	
14	484	305	
15	483	316	
16	484	317	
17	484	312	
18	485	317	
19	485	309	
20	484	304	
21	474	312	
22	476	314	
23	476	310	
24	476	309	
25	474	319	
26	476	311	
27	475	332	
28	474	315	
29	476	316	
30	476	323	
31	475	322	
32	474	325	
33	475	308	
34	475	325	
35	476	304	
36	476	309	
37	476	310	
38	476	332	
39	476	313	
40	476	316	
41	476	308	

42	476	316	
43	476	314	
44	476	308	
45	476	316	
46	476	312	
47	476	315	
48	476	311	
49	476	309	
50	476	319	Switched from Rabenhorst meter to our pH meter
51	462	333	
52	464	323	
53	464	320	
54	464	320	
55	466	329	
56	465	329	
57	464	326	
58	464	335	
59	465	317	
60	465	333	
61	464	340	
62	463	324	
63	462	319	
64	458	346	
65	462	335	
66	462	332	
67	461	334	
68	464	333	
69	459	334	
70	460	323	
71	465	324	
72	479	295	
73	479	291	
74	479	291	
75	479	291	
76	479	300	
77	479	294	
78	479	293	
79	479	297	
80	479	294	
81	479	296	
82	479	299	
83	479	291	
84	479	289	
85	479	291	

Appendix 3: Soil Moisture Probe Calibration

Calibration Method (Adapted from Application Note: Calibrating ECH2O Soil Moisture Sensors by Douglas R. Cobos, Decagon Devices).

The calibration generally follows the standard procedure for calibrating capacitance probes outlined by Starr and Palineanu (2002).

A3.1. Equipment

A3.1.1. Shovel and for each type of soil a 5 gallon bucket.

A1.2. Calibration containers large enough to pack the soil back to approximate field bulk density while maintaining at least 5 cm of soil depth. I used roughly 2 gallon planters from the greenhouse.

A3.1.3. 5TE probe and data acquisition system (1 each)

A3.1.3.1. 5TE probe output does not vary among probes of the same type. Calibration was carried out with a single probe and the calibration was applied to all other probes.

A3.1.3.2. I attached a Campbell Scientific CR10X similar to those to be used in the field.

A3.1.4. Volumetric soil sampler (1)

A3.1.4.1. I sampler out of PVC. The sampler was 60cm high and 50.9 cm (2 inches) in diameter with a volume of 122.2 cm^3.

A3.1.5. Soil drying containers

A3.1.5.1. 125mL IChem Jars. Five per soil type.

A3.1.5.2. The mass was determined for each clean, dry soil drying container before adding soil to them.

A3.1.6. Balance with a resolution of 0.0001 g for best possible soil specific calibration.

A3.1.7. Drying oven at 70^{o}C.

A3.2. Soil Preparation

A3.2.1. The soil was air dried in thin layers on large plastic flat pans for 48 to 72 hours.

A2.2.2. Large objects were removed from the soil by running through a 1mm sieve.

A3.3. Calibration

A3.3.1. The soil was packed into the calibration container at approximately the field bulk density.

A3.3.2. The 5TE probe was inserted vertically (including the black plastic base) into the soil trying to avoid any air gaps between the tines and soil. The probe was surrounded by continuous soil for a radius of at least 5 cm from the flat sensing portion of the probe.

A3.3.3. A mV response was recorded from the CR10X.

A3.3.4. A volumetric soil sample was collected without removing the 5TE probe, the volumetric soil sampler was inserted fully into the undisturbed soil near the probe. The sampler was removed, making sure that the soil core inside is intact. The excess soil was shaved from the end(s) with a flat edge, and any small voids were refilled. The entire core was placed in a drying container and immediately weighed.

A3.3.5. 300 – 500 mL of water was then added to the calibration soil and the soil was mixed until the mixture was homogeneous and 3.1 – 3.4 repeated.

A3.3.6. This was repeated 5 times for each sample until the soil approached saturation. Two random lab blanks were taken for each soil sample.

A3.3.7. The tightly capped already-weighed, moist samples were placed in the an oven at 70^{o}C oven for at least 48 hours.

A3.3.8. The dry soil was removed from the oven and allowed to cool, capped inside a desiccator. The containers without lids were weighed.

A3.4. Calculations

The volumetric water content is defined as the volume of water per volume of bulk soil:

$$\theta = Vw/Vt \qquad (1)$$

Where θ is volumetric water content (cm3/cm3), Vw is the volume of water (cm3) and Vt is the total volume of bulk soil sample (cm3). To find Vw, I calculated the volume of the water that is lost from the soil sample during oven drying:

$$mw = mwet - mdry \qquad (2)$$

$$Vw = mw/\rho w \qquad (3)$$

Where mw is the mass of water, mwet is the mass of moist soil (g), mdry is the mass of the dry soil, and ρw is the density of water (1 g/cm3). In addition to the volumetric water content, the bulk density of the soil sample was also calculated. Bulk density (ρb) is defined as the density of dry soil (g/cm3):

$$\rho b = mdry/Vsoil \qquad (4)$$

A3.5. Finding and using the calibration function

I made a scatter plot with the mV probe output on the X-axis, and the calculated VWC on the Y-axis (Figure 1). Then I used a curve fitting function to construct a mathematical model of the relationship. This relationship was best fit with a quadratic equation. The relationship was used to convert the raw output to a volumetric water content.

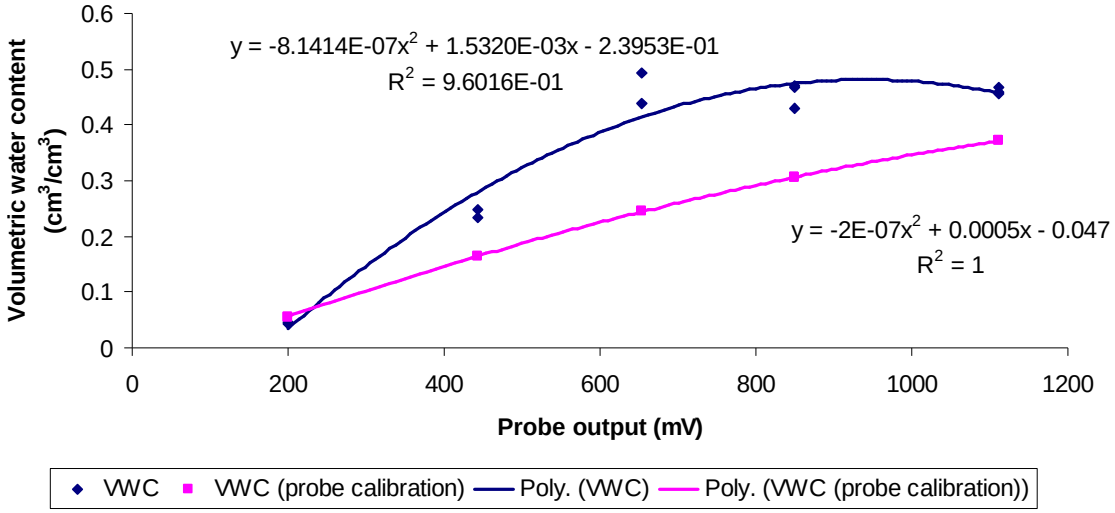

Figure A3.1. Response to added water input in the grass area E horizon.

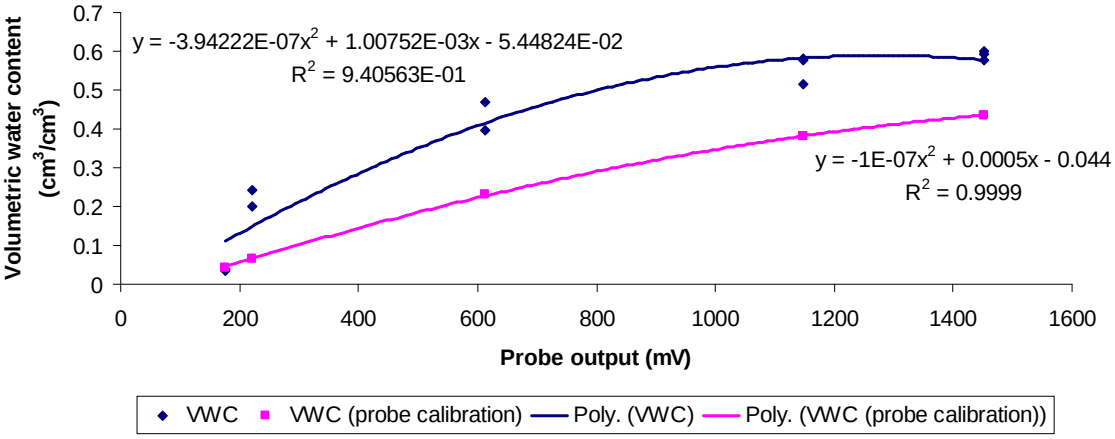

Figure A3.2. Response to added water input in the grass area A horizon.

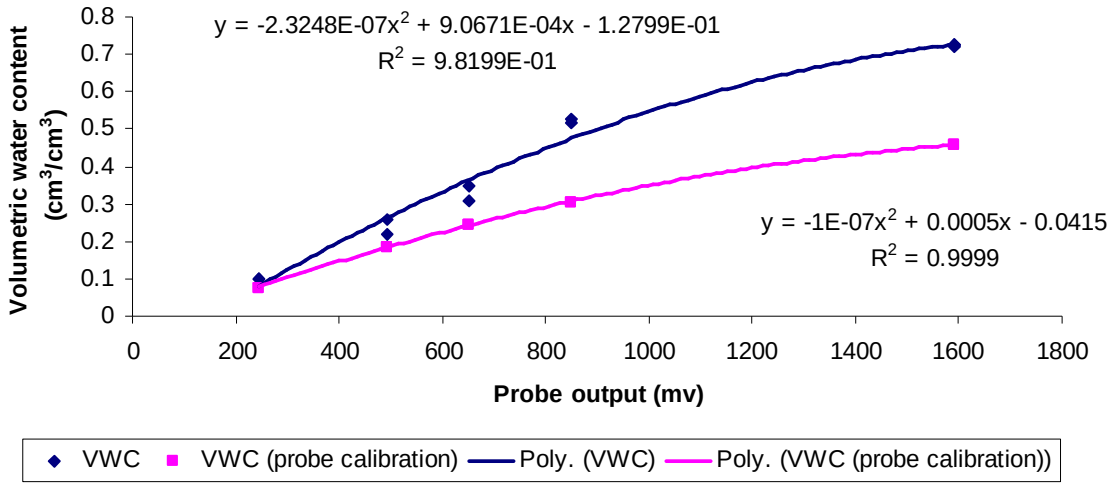

Figure A3.3. Response to added water input in the grass area O horizon.

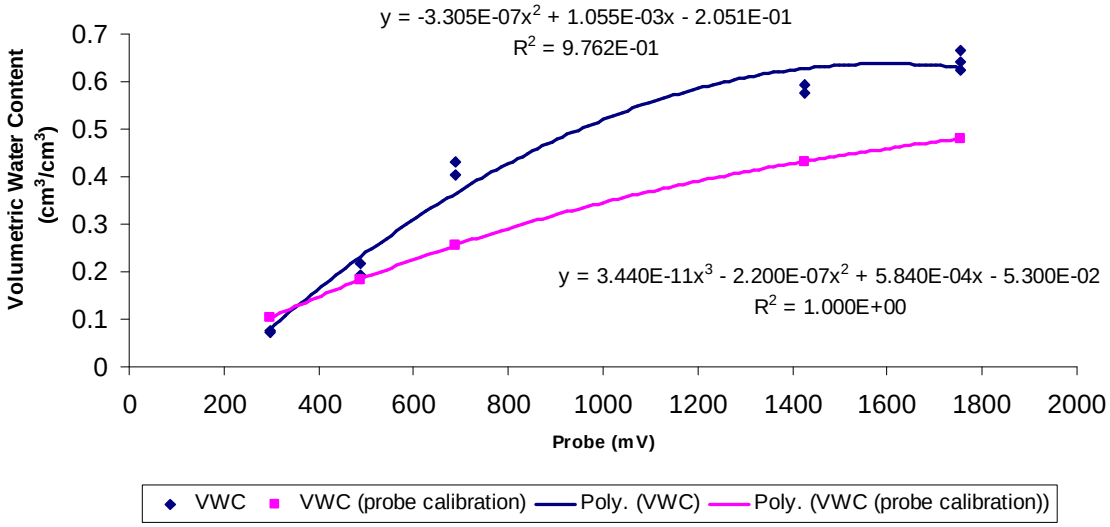

Figure A3.4. Response to added water input in the forest area E horizon.

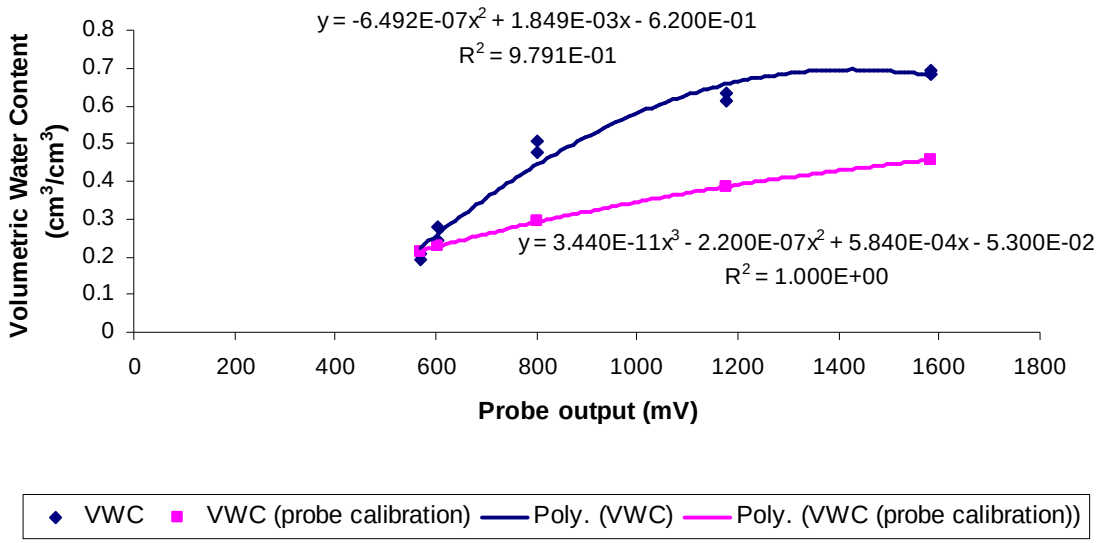

Figure A3.5 Response to added water input in the forest area A horizon.

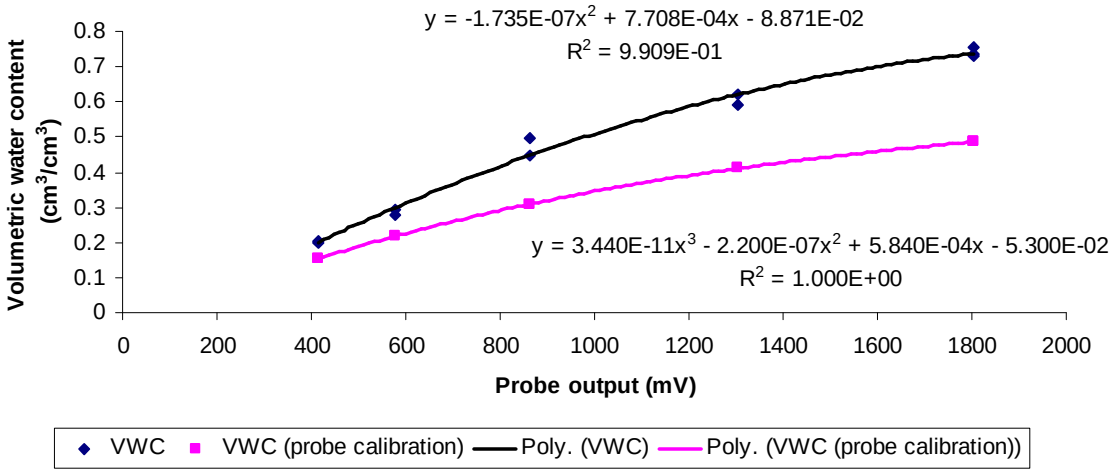

Figure A3.6. Response to added water input in the forest area O horizon.

Appendix 4: Total Mercury Inputs to PRAAMS

The study was part of a larger comprehensive study of atmospheric mercury exchange at PRAAMS. These studies provided me with a unique opportunity to examine the inputs and the retention of mercury for our soils. The mean soil bound total mercury concentrations in the top 25 cm of soil in the grass area were 0.04 $\mu g\ g^{-1}$. The mean bulk density was 1.01 $g\ cm^{-3}$. Therefore, a 1 m^2, 25 cm deep section of soil in the grass area contained 10.1 mg of mercury. In the forest area, the top 25 cm of soil had a mean bulk density of 0.83 $g\ cm^3$ and a mean bound total mercury concentration of 0.07 $\mu g\ g^{-1}$. The 25 cm deep, 1 m^2 volume of soil in the forest had 14.5 mg of mercury. This accumulation of THg in soils at PRAAMS was slightly more than the 8 $mg\ m^{-2}$ reported by Lindquist et al (1991) for upland soils in north – temperate areas in Sweden.

For PRAAMS, the wet deposition was 8 $\mu g\ m^{-2}\ y^{-1}$, estimated GEM deposition was 3 $\mu g\ m^{-2}\ y^{-1}$, GOM deposition was 2.5 to 3.2 $\mu g\ m^{-2}\ y^{-1}$, and litterfall deposition was 15 $\mu g\ m^{-2}\ y^{-1}$ (Castro et al., 2011; NADP, 2010; USGS, 2010). Combined there was a total deposition of 28.8 to 29.5 $\mu g\ m^{-2}\ y^{-1}$ to PRAAMS. According to Grigal (2002) only about 20% of the total deposited mercury is sequestered in the soils (Grigal 2002). Therefore, almost 24 $\mu g\ m^{-2}\ y^{-1}$ of mercury is incorporated into ground water or surface water runoff.

The differences in accumulation between the forest and grass areas also pointed to the importance of the litterfall input to a site. The grass area was cleared 5 years before the beginning of this study. Prior to 2004, it was similar to the forested

area. After clearing there was no longer the 15 $\mu g\, m^{-2}\, y^{-1}$ input of mercury from litterfall. Also after clearing there must have been a large initial flux of mercury from the soil and vegetation that left the grass area lower in SOM, soil bound [THg] and soil pore [TGM]. Only a few short years therefore, was enough to see a measurable change in the mercury cycling.

Bibliography

Clean Air Partners (2010). http://www.cleanairpartners.net/index.cfm, Washington, DC.

Akerblom S, Meili M, Bringmark L, Johansson K, Kleja DB, Bergkvist B. Partitioning of Hg between solid and dissolved organic matter in the humus layer of boreal forests. Water Air and Soil Pollution 2008; 189: 239-252.

Andersson A. Mercury in soils. In: Nriagu JO, editor. The Biogeochemistry of Mercury in the Environment. Elsevier/North Holland Biomedical Press, Amsterdam, 1979, pp. 79 - 122.

Arya SP. Introduction to Micrometeorology. San Diego: Academic Press, 2001a.

Arya SP. Introduction to Micrometeorology. San Diego: Academic Press, 2001b.

Bahlmann E, Ebinghaus R. Process studies on mercury fluxes over different soils with a Laboratory Flux Measurement System (LFMS). Journal De Physique Iv 2003; 107: 99-102.

Baldi F. Microbial transformation of mercury species and their importance in the biogeochemical cycle of mercury. Metal Ions in Biological Systems, Vol 34 1997; 34: 213-257.

Bash JO, Miller DR. A relaxed eddy accumulation system for measuring surface fluxes of total gaseous mercury. Journal of Atmospheric and Oceanic Technology 2008; 25: 244-257.

Bash JO, Miller DR. Growing season total gaseous mercury (TGM) flux measurements over an Acer rubrum L. stand. ATMOSPHERIC ENVIRONMENT 2009; 43: 5953-5961.

Bash JO, Miller DR, Meyer TH, Bresnahan PA. Northeast United States and Southeast Canada natural mercury emissions estimated with a surface emission model. Atmospheric Environment 2004; 38: 5683-5692.

Baya AP, Van Heyst B. Assessing the trends and effects of environmental parameters on the behaviour of mercury in the lower atmosphere over cropped land over four seasons. Atmos. Chem. Phys. 2010; 10: 8617-8628.

Boudala FS, Folkins I, Beauchamp S, Tordon R, Neima J, Johnson B. Mercury flux measurements over air and water in Kejimkujik National Park, Nova Scotia. Water Air and Soil Pollution 2000; 122: 183-202.

Brooks S, Moore C, Lew D, Lefer B, Huey G, Tanner D. Temperature and sunlight sontrols of mercury oxidation and deposition atop the Greenland ice sheet Atmospheric Chemistry and Physics. In Revision 2011.

Bullock OR, Brehme KA. Atmospheric mercury simulation using the CMAQ model: formulation description and analysis of wet deposition results. Atmospheric Environment 2002; 36: 2135-2146.

Carpi A, Lindberg SE. Application of a Teflon (TM) dynamic flux chamber for quantifying soil mercury flux: Tests and results over background soil. Atmospheric Environment 1998; 32: 873-882.

Castro MS, Moore CW, Sherwell JS, Brooks SB. Dry Deposition of Gaseous Oxidized Mercury. In Preparation. 2011.

Choi HD, Holsen TM. Gaseous mercury emissions from unsterilized and sterilized soils: The effect of temperature and UV radiation. ENVIRONMENTAL POLLUTION 2009a; 157: 1673-1678.
Choi HD, Holsen TM. Gaseous mercury fluxes from the forest floor of the Adirondacks. ENVIRONMENTAL POLLUTION 2009b; 157: 592-600.
Cohen M, Artz R, Draxler R, Miller P, Poissant L, Niemi D, et al. Modeling the atmospheric transport and deposition of mercury to the Great Lakes. Environmental Research 2004; 95: 247-265.
Converse AD, Riscassi AL, Scanlon TM. Seasonal variability in gaseous mercury fluxes measured in a high-elevation meadow. ATMOSPHERIC ENVIRONMENT 2010; 44: 2176-2185.
Demers JD, Driscoll CT, Fahey TJ, Yavitt JB. Mercury cycling in litter and soil in different forest types in the Adirondack region, New York, USA. Ecological Applications 2007; 17: 1341-1351.
Edwards GC, Rasmussen PE, Schroeder WH, Kemp RJ, Dias GM, Fitzgerald-Hubble CR, et al. Sources of variability in mercury flux measurements. Journal of Geophysical Research-Atmospheres 2001; 106: 5421-5435.
Engle MA, Gustin MS, Lindberg SE, Gertler AW, Ariya PA. The influence of ozone on atmospheric emissions of gaseous elemental mercury and reactive gaseous mercury from substrates. Atmospheric Environment 2005; 39: 7506-7517.
Engle MA, Tate MT, Krabbenhoft DP, Schauer JJ, Kolker A, Shanley JB, et al. Comparison of atmospheric mercury speciation and deposition at nine sites across central and eastern North America. J. Geophys. Res. 2010; 115: D18306.
Ericksen JA, Gustin MS, Xin M, Weisberg PJ, Fernandez GCJ. Air-soil exchange of mercury from background soils in the United States. Science of The Total Environment 2006; 366: 851-863.
Fang C, Moncrieff JB. Simple and fast technique to measure CO2 profiles in soil. Soil Biol. Biochem. 1998; 30: 2107-2112.
Fritsche J, Obrist D, Alewell C. Evidence of microbial control of Hg-0 emissions from uncontaminated terrestrial soils. Journal of Plant Nutrition and Soil Science-Zeitschrift Fur Pflanzenernahrung Und Bodenkunde 2008a; 171: 200-209.
Fritsche J, Obrist D, Zeeman MJ, Conen F, Eugster W, Alewell C. Elemental mercury fluxes over a sub-alpine grassland determined with two micrometeorological methods. Atmospheric Environment 2008b; 42: 2922-2933.
Fritsche J, Wohlfahrt G, Ammann C, Zeeman M, Hammerle A, Obrist D, et al. Summertime elemental mercury exchange of temperate grasslands on an ecosystem-scale. Atmospheric Chemistry and Physics 2008c; 8: 7709-7722.
Gabriel MC, Williamson DG. Principal biogeochemical factors affecting the speciation and transport of mercury through the terrestrial environment. Environmental Geochemistry and Health 2004; 26: 421-434.
Gillis AA, Miller DR. Some local environmental effects on mercury emission and absorption at a soil surface. Science of the Total Environment 2000; 260: 191-200.

Grigal DF. Mercury sequestration in forests and peatlands: A review. Journal of Environmental Quality 2003; 32: 393-405.
Gustin M, Jaffe D. Reducing the Uncertainty in Measurement and Understanding of Mercury in the Atmosphere. Environmental Science & Technology 2010; 44: 2222-2227.
Gustin MS, Engle M, Ericksen J, Lyman S, Stamenkovic J, Xin M. Mercury exchange between the atmosphere and low mercury containing substrates. Applied Geochemistry 2006; 21: 1913-1923.
Gustin MS, Ericksen JA, Schorran DE, Johnson DW, Lindberg SE, Coleman JS. Application of controlled mesocosms for understanding mercury air-soil-plant exchange. Environmental Science & Technology 2004; 38: 6044-6050.
Gustin MS, Lindberg S, Marsik F, Casimir A, Ebinghaus R, Edwards G, et al. Nevada STORMS project: Measurement of mercury emissions from naturally enriched surfaces. Journal of Geophysical Research-Atmospheres 1999; 104: 21831-21844.
Gustin MS, Lindberg SE, Weisberg PJ. An update on the natural sources and sinks of atmospheric mercury. Applied Geochemistry 2008; 23: 482-493.
Gustin MS, Stamenkovic J. Effect of watering and soil moisture on mercury emissions from soils. Biogeochemistry 2005; 76: 215-232.
Gustin MS, Taylor GE, Maxey RA. Effect of temperature and air movement on the flux of elemental mercury from substrate to the atmosphere. Journal of Geophysical Research-Atmospheres 1997; 102: 3891-3898.
Hall B. The Gas-Phase Oxidation of Elemental Mercury by Ozone. Water Air and Soil Pollution 1995; 80: 301-315.
Hartman JS, Weisberg PJ, Pillai R, Ericksen JA, Kuiken T, Lindberg SE, et al. Application of a Rule-Based Model to Estimate Mercury Exchange for Three Background Biomes in the Continental United States. ENVIRONMENTAL SCIENCE & TECHNOLOGY 2009; 43: 4989-4994.
Hsieh C-I, Katul G, Chi T-w. An approximate analytical model for footprint estimation of scalar fluxes in thermally stratified atmospheric flows. Advances in Water Resources 2000; 23: 765-772.
Jacob DJ, Horowitz LW, Munger JW, Heikes BG, Dickerson RR, Artz RS, et al. Seasonal Transition from Nox- to Hydrocarbon-Limited Conditions for Ozone Production over the Eastern United-States in September. JOURNAL OF GEOPHYSICAL RESEARCH-ATMOSPHERES 1995; 100: 9315-9324.
Johansson K, Aastrup M, Andersson A, Bringmark L, Iverfeldt A. Mercury in Swedish Forest Soils and Waters - Assessment of Critical Load. Water Air and Soil Pollution 1991; 56: 267-281.
Johnson DW, Benesch JA, Gustin MS, Schorran DS, Lindberg SE, Coleman JS. Experimental evidence against diffusion control of Hg evasion from soils. Science of the Total Environment 2003; 304: 175-184.
Johnson DW, Lindberg SE. The Biogeochemical Cycling of Hg in Forests - Alternative Methods for Quantifying Total Deposition and Soil Emission. Water Air and Soil Pollution 1995; 80: 1069-1077.

Kim KH, Lindberg SE, Meyers TP. Micrometeorological Measurements of Mercury-Vapor Fluxes over Background Forest Soils in Eastern Tennessee. Atmospheric Environment 1995; 29: 267-282.
Kritee K, Blum JD, Barkay T. Mercury Stable Isotope Fractionation during Reduction of Hg(II) by Different Microbial Pathways. Environmental Science & Technology 2008; 42: 9171-9177.
Kromer E, Friedrich G, Wallner P. Mercury and mercury - compounds in the surface, air, soil gas, soils, and rocks Journal of Geochemical Exploration 1981; 15: 51-62.
Kuiken T, Zhang H, Gustin M, Lindberg S. Mercury emission from terrestrial background surfaces in the eastern USA. Part I: Air/surface exchange of mercury within a southeastern deciduous forest (Tennessee) over one year. Applied Geochemistry 2008; 23: 345-355.
Light TS. Standard Solution for Redox Potential Measurements. Analytical Chemistry 1972; 44: 1038-&-1038-&.
Lin CJ, Gustin MS, Singhasuk P, Eckley C, Miller M. Empirical Models for Estimating Mercury Flux from Soils. ENVIRONMENTAL SCIENCE & TECHNOLOGY 2010; 44: 8522-8528.
Lindberg S, Bullock R, Ebinghaus R, Engstrom D, Feng XB, Fitzgerald W, et al. A synthesis of progress and uncertainties in attributing the sources of mercury in deposition. Ambio 2007; 36: 19-32.
Lindberg SE, Kim KH, Meyers TP, Owens JG. Micrometeorological Gradient Approach for Quantifying Air-Surface Exchange of Mercury-Vapor - Tests over Contaminated Soils. Environmental Science & Technology 1995; 29: 126-135.
Lindberg SE, Zhang H. Air/water exchange of mercury in the Everglades II: measuring and modeling evasion of mercury from surface waters in the Everglades Nutrient Removal Project. Science of the Total Environment 2000; 259: 135-143.
Lindberg SE, Zhang H, Gustin M, Vette A, Marsik F, Owens J, et al. Increases in mercury emissions from desert soils in response to rainfall and irrigation. Journal of Geophysical Research-Atmospheres 1999; 104: 21879-21888.
Lindqvist O, Johansson K, Aastrup M, Andersson A, Bringmark L, Hovsenius G, et al. Mercury in the Swedish Environment - Recent Research on Causes, Consequences and Corrective Methods. Water Air and Soil Pollution 1991; 55: R11-&-R11-&.
Lyman SN, Gustin MS, Prestbo EM, Marsik FJ. Estimation of dry deposition of atmospheric mercury in Nevada by direct and indirect methods. Environmental Science & Technology 2007; 41: 1970-1976.
Marsik FJ, Keeler GJ, Landis MS. The dry-deposition of speciated mercury to the Florida Everglades: Measurements and modeling. Atmospheric Environment 2007; 41: 136-149.
Mason RP, Laporte JM, Andres S. Factors controlling the bioaccumulation of mercury, methylmercury, arsenic, selenium, and cadmium by freshwater invertebrates and fish. Archives of Environmental Contamination and Toxicology 2000; 38: 283-297.

Mason RP, Sheu GR. Role of the ocean in the global mercury cycle. Global Biogeochemical Cycles 2002; 16.
Meili M. The Coupling of Mercury and Organic-Matter in the Biogeochemical Cycle - Towards a Mechanistic Model for the Boreal Forest Zone. WATER AIR AND SOIL POLLUTION 1991; 56: 333-347.
Miller EK, Vanarsdale A, Keeler GJ, Chalmers A, Poissant L, Kamman NC, et al. Estimation and mapping of wet and dry mercury deposition across northeastern North America. Ecotoxicology 2005; 14: 53-70.
Moore C, Carpi A. Mechanisms of the emission of mercury from soil: Role of UV radiation. Journal of Geophysical Research-Atmospheres 2005; 110: ---.
Moore CW, Castro MS, Brooks SB. A Simple and Accurate Method to Measure Total Gaseous Mercury Concentrations in Unsaturated Soils
WATER AIR AND SOIL POLLUTION 2010; In Press.
Moore CW, Castro MS, Brooks SB. A Simple and Accurate Method to Measure Total Gaseous Mercury Concentrations in Unsaturated Soils
Water Air and Soil Pollution 2011a; In Press.
Moore CW, Castro MS, Heyes A. Factors Influencing Gaseous Mercury Fluxes in Background Soils of Western Maryland. The Science of the Total Environment: Submitted 2011b.
NADP. *National Atmospheric Deposition Program 2008 Annual Summary.* NADP Data Report 2009-01. Illinois State
Water Survey, University of Illinois at Urbana-Champaign, Champaign, IL. 2009.
NADP. *National Atmospheric Deposition Program 2009 Annual Summary.* NADP Data Report 2009-01. Illinois State
Water Survey, University of Illinois at Urbana-Champaign, Champaign, IL. 2010.
Nelson DW, Sommers LE. Loss-On-Ignition Method. In: Sparks DL, editor. Methods of Soil Analysis Part 3. Chemical Methods. SSSA Book Series 5. SSSA Madison, WI, 1996, pp. 1004 -1005.
Norrstrom AC. Field-Measured Redox Potentials in Soils at the Groundwater Surface-Water Interface. European Journal of Soil Science 1994; 45: 31-36.
Obrist D, Fain X, Berger C. Gaseous elemental mercury emissions and CO2 respiration rates in terrestrial soils under controlled aerobic and anaerobic laboratory conditions. SCIENCE OF THE TOTAL ENVIRONMENT 2010; 408: 1691-1700.
Obrist D, Gustin MS, Arnone JA, Johnson DW, Schorran DE, Verburg PSJ. Measurements of gaseous elemental mercury fluxes over intact tallgrass prairie monoliths during one full year. Atmospheric Environment 2005; 39: 957-965.
Obrist D, Johnson DW, Lindberg SE. Mercury concentrations and pools in four Sierra Nevada forest sites, and relationships to organic carbon and nitrogen. Biogeosciences 2009; 6: 765-777.
Obrist D, Johnson DW, Lindberg SE, Luo Y, Hararuk O, Bracho R, et al. Mercury Distribution Across 14 U.S. Forests. Part I: Spatial Patterns of Concentrations in Biomass, Litter, and Soils. ENVIRONMENTAL SCIENCE & TECHNOLOGY 2011.

Oishi AC, Oren R, Stoy PC. Estimating components of forest evapotranspiration: A footprint approach for scaling sap flux measurements. Agricultural and Forest Meteorology 2008; 148: 1719-1732.
Park SJ, Park SU, Ho CH, Mahrt L. Flux-gradient relationship of water vapor in the surface layer obtained from CASES-99 experiment. Journal of Geophysical Research-Atmospheres 2009; 114: -.
Poissant L, Casimir A. Water-air and soil-air exchange rate of total gaseous mercury measured at background sites. Atmospheric Environment 1998; 32: 883-893.
Poissant L, Pilote M, Beauvais C, Constant P, Zhang HH. A year of continuous measurements of three atmospheric mercury species (GEM, RGM and Hgp) in southern Quebec, Canada. Atmospheric Environment 2005; 39: 1275-1287.
Poissant L, Pilote M, Constant P, Beauvais C, Zhang HH, Xu XH. Mercury gas exchanges over selected bare soil and flooded sites in the bay St. Francois wetlands (Quebec, Canada). Atmospheric Environment 2004; 38: 4205-4214.
Ponnamperum FN. The Chemistry of Submerged Soils: Academic Press, Inc., 1972.
Rabenhorst AC, Hively WD, James BR. Measurements of Soil Redox Potential. SOIL SCIENCE SOCIETY OF AMERICA JOURNAL 2009; 73: 668-674.
Rea AW, Keeler GJ, Scherbatskoy T. The deposition of mercury in throughfall and litterfall in the lake champlain watershed: A short-term study. Atmospheric Environment 1996; 30: 3257-3263.
Rea AW, Lindberg SE, Keeler GJ. Dry deposition and foliar leaching of mercury and selected trace elements in deciduous forest throughfall. Atmospheric Environment 2001; 35: 3453-3462.
Ryaboshapko A, Bullock OR, Christensen J, Cohen M, Dastoor A, Ilyin I, et al. Intercomparison study of atmospheric mercury models: 1. Comparison of models with short-term measurements. Science of the Total Environment 2007; 376: 228-240.
Schluter K. Review: evaporation of mercury from soils. An integration and synthesis of current knowledge. Environmental Geology 2000; 39: 249-271.
Scholtz MT, Van Heyst BJ, Schroeder W. Modelling of mercury emissions from background soils. Science of the Total Environment 2003; 304: 185-207.
Schroeder WH, Anlauf KG, Barrie LA, Lu JY, Steffen A, Schneeberger DR, et al. Arctic springtime depletion of mercury. Nature 1998; 394: 331-332.
Schroeder WH, Munthe J. Atmospheric mercury - An overview. Atmospheric Environment 1998; 32: 809-822.
Schuster E. The Behavior of Mercury in the Soil with Special Emphasis on Complexation and Adsorption Processes - a Review of the Literature. Water Air and Soil Pollution 1991; 56: 667-680.
SERCC. Southeastern Regional Climate Center. http://www.sercc.com/climateinfo/historical/historical_md.html, 2010.
Sigler JM, Lee X. Gaseous mercury in background forest soil in the northeastern United States. Journal of Geophysical Research - Biogeosciences 2006; 111.
Skogerboe RK, Wilson SA. Reduction of Ionic Species by Fulvic-Acid. Analytical Chemistry 1981; 53: 228-232.
Song XX, Van Heyst B. Volatilization of mercury from soils in response to simulated precipitation. Atmospheric Environment 2005; 39: 7494-7505.

Southworth G, Lindberg S, Hintelmann H, Amyot M, Poulain A, Bogle M, et al. Evasion of added isotopic mercury from a northern temperate lake. Environmental Toxicology and Chemistry 2007; 26: 53-60.
Steffen A, Douglas T, Amyot M, Ariya P, Aspmo K, Berg T, et al. A synthesis of atmospheric mercury depletion event chemistry in the atmosphere and snow. Atmospheric Chemistry and Physics 2008; 8: 1445-1482.
Tsiros IX. Modeling assessment of air emission flux of mercury from soils in terrestrial landscape components: Model tests and sensitivities. Journal of the Air & Waste Management Association 2002; 52: 339-348.
USDA. Web Soil Survey. http://websoilsurvey.nrcs.usda.gov/app/WebSoilSurvey.aspx, 2009.
USEPA. Method 1631, Revision E: Mercury in Water by Oxidation, Purge, and Trap, and Cold Vapor Atomic Fluorescence Spectrometry. 2002.
USGS. Mercury in Litterfall at NADP sites. 2010.
van Bochove E, Beauchemin S, Theriault G. Continuous multiple measurement of soil redox potential using platinum microelectrodes. Soil Sci. Soc. Am. J. 2002; 66: 1813-1820.
Wafer CC, Richards JB, Osmond DL. Construction of platinum-tipped redox probes for determining soil redox potential. Journal of Environmental Quality 2004; 33: 2375-2379.
Wallschläger D, Kock HH, Schroeder WH, Lindberg SE, Ebinghaus R, Wilken R-D. Estimating Gaseous Mercury Emissions from Contaminated Floodplain Soils to the Atmosphere with Simple Field Measurement Techniques. Water, Air, & Soil Pollution 2002; 135: 39-54.
Wallschlager D, Kock HH, Schroeder WH, Lindberg SE, Ebinghaus R, Wilken RD. Mechanism and significance of mercury volatilization from contaminated floodplains of the German river Elbe. Atmospheric Environment 2000; 34: 3745-3755.
Wohlfahrt G, Hortnagl L, Hammerle A, Graus M, Hansel A. Measuring eddy covariance fluxes of ozone with a slow-response analyser. Atmospheric Environment 2009; 43: 4570-4576.
Xiao ZF, Munthe J, Schroeder WH, Lindqvist O. Vertical Fluxes of Volatile Mercury over Forest Soil and Lake Surfaces in Sweden. Tellus Series B-Chemical and Physical Meteorology 1991; 43: 267-279.
Xin M, Gustin M, Johnson D. Laboratory investigation of the potential for re-emission of atmospherically derived Hg from soils. Environmental Science & Technology 2007; 41: 4946-4951.
Yin YJ, Allen HE, Huang CP, Sparks DL, Sanders PF. Kinetics of mercury(II) adsorption and desorption on soil. Environmental Science & Technology 1997; 31: 496-503.
Zarate-Valdez JL, Zasoski RJ, Lauchli A. Short-term effects of moisture content on soil solution pH and soil Eh. Soil Science 2006; 171: 423-431.
Zhang H, Lindberg SE. Processes influencing the emission of mercury from soils: A conceptual model. Journal of Geophysical Research-Atmospheres 1999; 104: 21889-21896.

Zhang H, Lindberg SE, Kuiken T. Mysterious diel cycles of mercury emission from soils held in the dark at constant temperature. ATMOSPHERIC ENVIRONMENT 2008; 42: 5424-5433.
Zhang H, Lindberg SE, Marsik FJ, Keeler GJ. Mercury air/surface exchange kinetics of background soils of the Tahquamenon River watershed in the Michigan Upper Peninsula. Water Air and Soil Pollution 2001; 126: 151-169.
Zhang LM, Wright LP, Blanchard P. A review of current knowledge concerning dry deposition of atmospheric mercury. ATMOSPHERIC ENVIRONMENT 2009; 43: 5853-5864.